7-17-2015 12:00 AM

The CTCF Chromatin Organizer is Required for Hindlimb Development

Katherine L. Rabicki, *The University of Western Ontario*

Supervisor: Drs. Frank Beier, *The University of Western Ontario*
Joint Supervisor: Nathalie Berube, *The University of Western Ontario*
A thesis submitted in partial fulfillment of the requirements for the Master of Science degree in Physiology and Pharmacology
© Katherine L. Rabicki 2015

Recommended Citation

THE CTCF CHROMATIN ORGANIZER IS REQUIRED FOR HINDLIMB DEVELOPMENT

(Thesis Format: Monograph)

By

Katherine Lee <u>Rabicki</u>

**Graduate Program in Physiology and Pharmacology
Collaborative Program in Developmental Biology**

**A thesis submitted in partial fulfillment
of the requirements for the degree of
Master of Science**

**The School of Graduate and Postdoctoral Studies
Western University
London, Ontario, Canada**

ABSTRACT

Mutations in chromatin organizer CTCF were identified in patients with intellectual disability and skeletal defects. Previous studies demonstrated that depletion of CTCF in murine limb mesenchyme results in apoptosis in the forelimb. The role of CTCF in the hindlimb, however, is unknown. My objective was to investigate effects of CTCF deletion on chondrogenesis and skeletal development in the hindlimb. *In vitro* wild-type micromass cultures demonstrate that chondrocyte-specific gene expression is delayed in the hindlimb when compared to forelimbs. Embryonic *Ctcf^{Fl/Fl};Prx1Cre* mice were investigated, and qRT-PCR and histology were performed on limb buds and long bones. Results show that E12.5 mutant hindlimb buds have increased apoptosis, but no change in proliferation. Later time points reveal growth plate defects, and delayed cartilage mineralization in mutant tibiae. Furthermore, mutant mice have skull defects, shortened long bones and oligodactyly. Overall, data suggest that CTCF is a key regulator of endochondral/intramembranous ossification and hindlimb development.

Key Words: CTCF, chondrocytes, hindlimb, micromass cultures, hypertrophy, differentiation

CONTRIBUTORS

The mice used for analysis in this thesis were bred from the colonies of Dr. Jason Bush of the Beier Lab. Additional colonies bred were maintained and harvested by Katherine Rabicki.

Immunofluorescent staining for CTCF was performed by Adrienne Elbert, an MD/PhD student of the Bérubé Lab. Analysis of the data as presented in this thesis was performed by Katherine Rabicki.

ACKNOWLEDGEMENTS

First and foremost, I am infinitely thankful to my wonderful family for their love, encouragement, good humour, and support over the last two years (and my whole life). Mom, thank-you for being my indomitable role model, steadfast supporter, and biggest fan. Your tenacity, positivity, and passion for learning motivates me every single day, and I am proud to be your daughter. Dad, thank-you for your endless patience and willingness to listen during Sunday morning brunch, and for always making me laugh, especially when I'm frustrated. I admire your hard work, dedication, and commitment to serving others, and I am proud to be your daughter. Alex, thank-you for always showing up to lab with coffee, for being genuinely interested in my work, and most importantly, for inspiring me to be a good role model. I am proud to be your sister. Mom, Dad, brother - thank-you for believing in me, this one's for you.

A million thank-you's to my other family: the Beier Empire. Dr. Frank Beier, thank-you for the opportunity to be part of your lab. I am grateful every day to be your student, and I appreciate your compassion, encouragement, and support. My Masters degree has been an education in both science and character-building, and I could not have asked for a better mentor. Thank-you for being patient and kind, and for trusting me to work independently while always being available for help. Thank-you, also, for the opportunity to present my work at conferences - those meetings were invaluable for building my confidence and research skills.

My sincerest thanks also go to Dr. Nathalie Bérubé, you have been a tremendous help throughout my Masters and a wonderful co-supervisor. Thank-you for making me feel welcome in your lab, for all your advice and editing genius, and for always encouraging me to increase my knowledge. I am very grateful for your kindness and guidance.

whose patience, wisdom, and support has been invaluable throughout this journey - you are wonderful.

Finally, a shout-out to all my other friends, for being an unfailing source of love and laughter. Alexandra, facing all the challenges and victories science brings has been so much fun with you, #stayfresh. Anita and Elaine, thank-you for having faith in me and for always having my back, even from beautiful BC. Darcy, thank-you for always having a hilarious story to cheer me up, and for reminding me to never give up. Lastly, Carly, thank-you for being my family and my best friend, I could not have done it without you.

TABLE OF CONTENTS

VIII

LIST OF TABLES

2.0 MATERIALS & METHODS   **Page**

LIST OF FIGURES

X

LIST OF APPENDICES

LIST OF ABBREVIATIONS

ACAN	Aggrecan
APP	Amyloid β-protein precursor
BMP	Bone morphogenic protein
CCD	Cleidocranial dysplasia
CD	Campomelic dysplasia
CDH-2	Cadherin-2; N-cadherin
CDH-11	Cadherin-11
CdLS	Cornelia de Lange syndrome
CFTR	Cystic fibrosis transmembrane conductance regulator
ChIP-seq	Chromatin immunoprecipitation-sequencing
COLI	Collagen I
COLIX	Collagen IX
COLXI	Collagen XI
COL2A1	Collagen II
COL10A1	Collagen X
CTCF	CCCTC-binding factor

DAB	3,3'-Diaminobenzidine
DDX5	DEAD-box RNA helicase p68
DMEM	Dulbecco's modified eagles medium
DNMT1	DNA (cytosine-5)-methyltransferase 1
ECM	Extracellular matrix
EDTA	Ethylenediaminetetraacetic acid
FGFR	Fibroblast growth factor receptor
HOX	Homeobox
ICR	Imprinting control region
IF	Immunofluorescence
IHC	Immunohistochemistry
IHH	Indian hedgehog
KO	Knockout
lncRNA	Long non-coding RNA
MMP-9	Matrix metalloproteinase-9
MMP-13	Matrix metalloproteinase-13
O.C.T	Optimal Cutting Temperature

OSX	Osterix
PARP1	Poly(ADP-ribose) polymerase 1
PBS	Phosphate buffered saline
PBST	Phosphate buffered saline and 0.1% Tween
PcG	Polycomb group
PCNA	Proliferating cell nuclear antigen
PCR	Polymerase chain reaction
PFA	Paraformaldehyde
POC	Primary ossification centre
PSA	Puck's saline solution A
PTHrP	Parathyroid hormone-related protein
PUMA	p53 upregulated modulator of apoptosis
RNA-seq	RNA-sequencing
RT-PCR	Real-time polymerase chain reaction
RUNX2	Runt related gene 2
SCX	Scleraxis
SEM	Standard error of mean

SHH	Sonic hedgehog
SNP	Single nucleotide polymorphism
SRA	Steroid receptor RNA activator
SRY	Sex determining region Y
SOC	Secondary ossification centre
SOX	SRY box
SUMO	Small ubiquitin-like modifier protein
TAD	Topologically associated domain
TGFβ	Transforming growth factor beta
VEGF	Vascular endothelial growth factor
3C	Chromosome conformation capture
4C	Circularized chromosome conformation capture

1.0 INTRODUCTION

1.1   Skeletal Development

The human skeleton is a remarkable organ composed of over 200 fused and individual bones that provide coordinated structure, anchor muscles, and protect essential organs[1]. Skeletal development is highly regulated, and any disruption in the process can result in severe and sometimes life-threatening malformations. The two major routes of bone formation, or osteogenesis, are intramembranous and endochondral ossification, both of which involve the transformation of mesenchyme into mineralized bone. Intramembranous ossification occurs in the developing clavicle, portions of the facial skeleton, and the flat bones of the skull, and involves direct formation of bone from mesenchymal cells[2]. In contrast, endochondral ossification is characteristic of the majority of bones in the axial and appendicular skeleton and involves a cartilaginous precursor to mineralized bone[3].

1.1.1   *Intramembranous Ossification*

The calvariae of the skull, clavicle, mandible, and frontal region of the facial skeleton are all formed through intramembranous ossification, a process that is also critical to certain types of bone repair[4]. Intramembranous ossification commences when cranial neural crest and mesoderm-derived mesenchymal cells proliferate and then condense into nodules[4]. Some of these mesenchymal cells then differentiate into bone-forming osteoblasts and secrete an extracellular matrix (ECM) called osteoid that is rich in collagen type I (COLI)[5]. The osteoid matrix is calcified through the binding of calcium salts, and bony spicules form and radiate outwards from the start point of ossification[5]. Compact mesenchymal cells then surround the developing bone to form a membrane known as the periosteum[5]. The innermost periosteum cells

then develop into osteoblasts and continue secreting osteoid matrix, thus enabling the development of many calcified bone layers[5].

1.1.2 Endochondral Ossification

The majority of the human skeleton, and particularly the long bones in the developing limbs, is formed through endochondral ossification. Endochondral ossification is an osteogenic process in which an anlage composed of chondrocytes and a cartilage-specific ECM is deposited and subsequently replaced by mineralized bone **(Figure 1.1)**[3,5]. Like other developmental processes, endochondral ossification involves numerous growth factors, transcriptional regulators, and signaling molecules, and is tightly regulated.

Endochondral ossification commences with the commitment of mesodermal cells to the cartilage lineage. Mesenchymal cells express the transcription factors PAX1 and Scleraxis (SCX), which are believed to activate cartilage-specific genes, before condensing into nodules[7,8]. The precartilaginous condensations then express various growth factors and associated receptors, including sonic hedgehog (SHH), bone morphogenic proteins (BMP), and fibroblast growth factor receptor (FGFR), as well as runt-related transcription factor 2 (RUNX2)[9]. The adhesion molecules N-cadherin (Cadherin-2; CDH-2), Cadherin-11 (CDH-11), and N-CAM are important for stabilizing these condensations, which then enables peripheral mesenchymal cells to flatten and elongate forming the rudimentary perichondrium[10,11]. The first condensations occur in humans at 6.5 weeks of development and in mice at embryonic day 10.5 (E10.5)[12].

Next, expression of SOX9, the master chondrogenic transcription factor, in the condensations leads to the differentiation of these cells into chondrocytes[13]. SOX9 is a DNA-binding protein that, together with L-SOX5 and SOX6, regulates the chondrocyte-specific genes

Figure 1.1 Schematic representation of endochondral ossification.

Endochondral ossification involves mesenchymal cells condensing and differentiating into chondrocytes. Chondrocytes express *SOX9*, leading to activation of *COL2A1* and *ACAN* which are critical for the cartilaginous ECM. The chondrocytes line up in characteristic zones known as the growth plate and undergo rapid proliferation before becoming hypertrophic, characterized by the expression of *COL10A1* and *VEGF*. The hypertrophic chondrocytes then attract invading vasculature and bone-forming osteoblasts before undergoing apoptosis or becoming osteoblasts or osteocytes. Mineralized bone forms in the middle, appropriately known as the primary ossification centre and as the bone grows outward secondary ossification centres form on either end. This figure has been modified from Solomon, *et al.*, 2008[6].

Mesenchymal Condensation

Sox9

2° Ossification Centre

Resting Chondrocytes

Proliferating Chondrocytes
Sox9, Sox5/6, ColII, Aggrecan

1° Ossification Centre

Hypertrophic Chondrocytes
ColX, VEGF
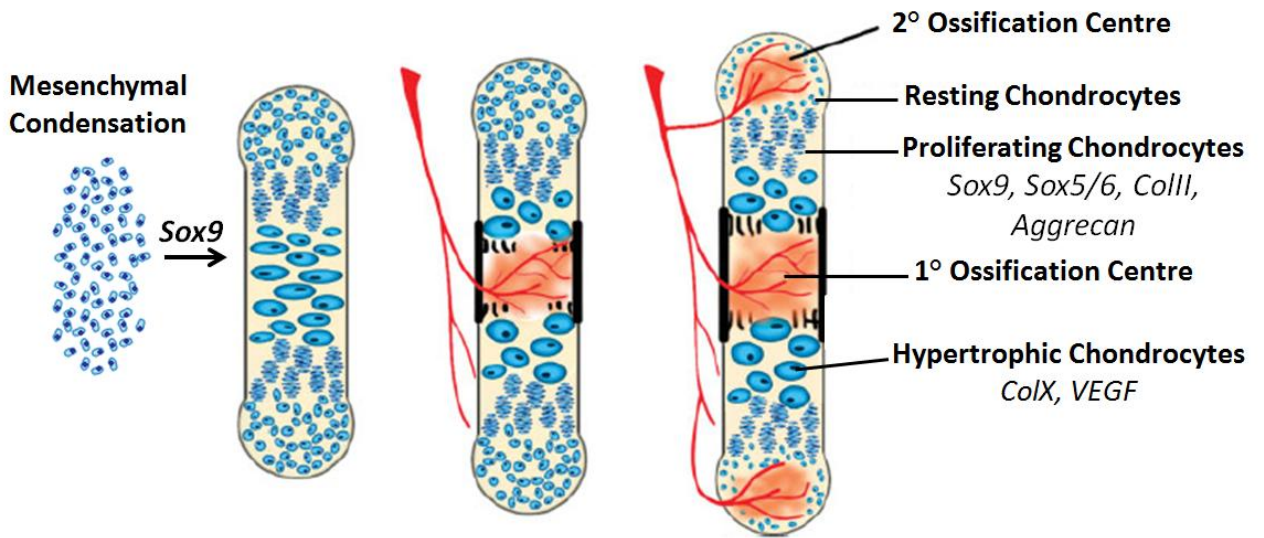
collagen type II (COL2A1), *collagen type IX (COLIX)*, *collagen type XI* (COLXI), and *aggrecan (ACAN)*[14–17]. The chondrocytes then undergo a number of maturation steps involving proliferation and hypertrophy. Developing cartilage forms a number of characteristic zones known as the growth plate[18]. Chondrocytes at the outermost edge of the growth plate are considered resting chondrocytes, and are small and round in morphology[19]. The resting zone chondrocytes proliferate at a slower rate than the neighbouring proliferating zone, but continue to express high levels of *COL2A1* and *ACAN*[19]. Adjacent to the resting zone, is the proliferative zone, in which chondrocytes divide at a rapid rate. The proliferating chondrocytes are flattened or discoidal in morphology, and form characteristic longitudinal columns[20]. The proliferating chondrocytes then exit the cell cycle and increase their volume, becoming prehypertrophic.

Prehypertrophic chondrocytes express genes related to both proliferating and hypertrophic chondrocytes, and differentiation into hypertrophic chondrocytes is governed by the Indian hedgehog/Parathyroid hormone-related protein (IHH/PTHrP) negative feedback loop[21–23]. IHH regulates cell cycle progression and stimulates PTHrP secretion from both proliferating chondrocytes and perichondrial cells, which inhibits the onset of hypertrophy. An increase in chondrocyte hypertrophy is accompanied by increased IHH/PTHrP signaling, thus maintaining the proliferative pool of chondrocytes. Hypertrophic chondrocytes are round to cuboidal in shape and up-regulate the expression of *RUNX2*, which triggers the secretion of a matrix rich in collagen type X (COL10A1)[18]. The cell volume increase during hypertrophy is considered a major determinant of bone length and growth. Hypertrophic chondrocytes release osteopontin and the extracellular matrix remodeling proteins matrix metalloproteinase-9 (MMP-9), matrix metalloproteinase-13 (MMP-13) and the aggrecanases ADAMTS4 and ADAMTS5[24–27]. Additionally, cleavage of the collagen ECM by MMP-9 causes the release of vascular

endothelial growth factor (VEGF) [24]. At the same time as hypertrophy begins, the cells of the perichondrium also differentiate into osteoblasts, which enables the formation of the mineralized bone collar, or periosteum, around the developing skeletal element[28]. While some hypertrophic chondrocytes undergo apoptosis, new evidence suggests that some hypertrophic chondrocytes trans-differentiate into osteoblasts[6,29].

Capillaries are recruited into the cartilage anlage from surrounding tissues and the perichondrium, through a VEGF-dependent pathway[28,30]. The invading vasculature is accompanied by osteoclasts, which act to resorb the ECM while the osteoblasts lay down mineralized bone[30]. The first region in a long bone to become mineralized is considered the primary ossification centre (POC) and forms in the centre of the bone, also known as the diaphysis. As the developing bone lengthens, secondary ossification centres (SOC) form at either end, also known as the epiphyses. In humans, the growth plates between the diaphyses and epiphyses disappears after skeletal maturity is reached, between ages 18 to 25, while in mice a growth plate is visible in the long bones throughout the entire life of the animal[5].

1.1.3 Transcription Factors, Growth Factors, and Signaling Molecules Regulating Endochondral Ossification

While there are many regulatory factors involved in chondrogenesis, members of the sex determining region Y (SRY) box (SOX) family, specifically SOX9, L-SOX5, and SOX6, are of particular importance[31]. SOX9 is considered the master transcription factor of chondrogenesis and regulates the differentiation of mesenchymal cells to chondrocytes[32]. *SOX9* expression is restricted to all chondroprogenitors and differentiated chondrocytes, and is not expressed in hypertrophic chondrocytes[17]. Initial studies on mouse embryo chimeras from *Sox9*-null

embryonic stem cells demonstrated that mutant cells were absent from mesenchymal condensations and failed to express chondrogenic markers including *Col2a1* and *Acan*[32]. Furthermore, limb-specific *Sox9*-null mice display a complete absence of cartilage and bone in the developing limb, and cartilage-specific *Sox9*-null mice present with severe generalized chondrodysplasia and lack *L-Sox5* and *Sox6* expression[17]. Interestingly, the *SOX9* gene locus has a complex regulatory region spanning approximately 3Mb upstream and downstream of the coding region that is highly conserved between humans and mice[33]. This regulatory region was first identified in patients with Campomelic Dysplasia (discussed below) when translocations upstream of the coding region caused reduced *SOX9* transcription and severe skeletal defects[34]. The regulatory region is flanked by two genes with no known function in chondrogenesis, *KCNJ2* and *SLC39A11*, and is devoid of other protein-coding genes. This aptly named gene desert does, however, encode the two long non-coding RNAs *BC006965* and *D17RIK*, both of which have unknown functions. Overall, data indicate complex regulation of the *SOX9* locus, however, the details are not well understood. The relatively long distance between some regulatory elements and the coding regions suggest that DNA looping may be important in the control of *SOX9* transcription.

L-SOX5 and SOX6 are co-expressed with *SOX9* in chondroprogenitors and differentiated chondrocytes, and act cooperatively with SOX9 to activate *COL2A1* expression via the *COL2A1* enhancer[15]. Mice null for either *L-Sox5* or *Sox6* died of neonatal respiratory distress and both had only a small subset of endochondral elements affected[14]. *L-Sox5*$^{-/-}$ mice present with cleft palate and shortened ribs, as well as delayed mineralization of vertebral bodies and nasal bones[14]. *Sox6*$^{-/-}$ mice also die in the perinatal period and develop severe dwarfism[14]. Interestingly, *L-Sox5*

and *Sox6* double mutants have chondrocytes which fail to produce a typical proteoglycan-rich ECM, and never form growth plates[14,15].

A recent study screened the genomic region upstream of the *SOX9* gene and reported three enhancers primarily active in chondrocytes[35]. These enhancers affect gene expression in chondrocytes at different stages of their life cycle, including condensed prechondrocytes, proliferating chondrocytes, and all differentiated chondrocytes[35]. While the SOX9 protein has been shown to activate previously reported enhancers by itself, it requires both L-SOX5 and SOX6 proteins as well as additional factors to robustly activate these enhancers[35]. Therefore, evidence demonstrates an elegant synergistic regulation of chondrogenic genes by the SOX trio of transcription factors.

Another important transcription factor in skeletal development is RUNX2. Formerly known as CBFA1, RUNX2 is an important regulator of chondrocyte and osteoblast differentiation[36,37]. RUNX2 is expressed at a high level in prehypertrophic and hypertrophic chondrocytes, as well as perichondrial cells, and osteoblasts[37]. The developing bones in *Runx2*-null mice show decreased chondrocyte maturation and fail to develop osteoblasts, thus they do not undergo ossification[37]. RUNX2 is therefore necessary for proper chondrocyte differentiation and osteogenesis.

Finally, cell cycle machinery and cyclin-dependent kinases have been demonstrated to control cell proliferation[18]. Responsible for controlling cell cycle exit and differentiation into prehypertrophic chondrocytes, p57 is a cyclin-dependent kinase inhibitor of the Kip family[38]. p57 functions to inhibit the G1-S phase cyclin-dependent kinases and is expressed at very high levels in prehypertrophic and hypertrophic chondrocytes[38]. *p57*-null mice display shortened,

thick bones with thinner hypertrophic zones and reduced *Col10a1* expression[38]. p57 is therefore critical for regulating chondrocyte differentiation and cell cycle exit.

1.1.4   Skeletal Dysplasias

The group of genetic conditions known as skeletal dysplasias encompasses over 200 phenotypes identified in humans, ranging in severity from profound truncations to subtle alterations in length. Patients affected by skeletal dysplasia have impaired bone growth and abnormal cartilage, and are often very short in stature. More specifically, the subset of over 150 skeletal disorders affecting cartilage growth and development are termed chondrodysplasias. The most common form of chondrodysplasia is achondroplasia, caused by a heterozygous gain-of-function mutation in the *FGFR3* gene[39]. Achondroplasia is a type of short-limbed dwarfism in which patients also present with short digits, trident hand, megalencephaly, spinal curvature, and limitation of elbow extension[39].   Interestingly, the growth plates of patients with achondroplasia have shortened proliferating zones, but do not appear otherwise disorganized as in other chondrodysplasias[39].

Another significant skeletal disorder is campomelic dysplasia (CD), a form of dwarfism in which the patients suffer from congenital bowing and angulation of the long bones[40]. CD is an autosomal dominant disorder caused by loss-of-function mutations in a single allele of the *SOX9* gene, leading to haploinsufficiency[34,41]. Importantly, mutations are reported not only within the coding region for *SOX9*, but also in the region upstream[42]. Patients with CD also often present with genital ambiguities, 46 XY sex reversal, cleft palate, micrognathia, facial abnormalities, and only 11 sets of ribs[40,43]. Ribcage defects lead to respiratory distress during the perinatal period, accounting for the high mortality rate[40]. Heterozygous *Sox9* mutant mice have been generated

and are considered a model of CD, as they recapitulate most of the skeletal abnormalities including bowing of the long bones, cleft palate, hypoplasia, and ribcage defects[44].

Other skeletal dysplasias exist and are can be caused by mutations in ECM-related genes. For example, Schmid metaphyseal dysplasia is caused by mutations in the *COL10A1* gene and results in shortened stature, bowed legs, and irregular growth plates[45]. Additionally, haploinsuffiency of RUNX2 causes the autosomal dominant skeletal dysplasia cleidocranial dysplasia (CCD)[46]. Patients with CCD also present with short stature, decreased *COL10A1* expression, and diminished hypertrophic zones in their growth plates. While all of these conditions severely impact a patient's quality of life, there are also high mortality rates associated with skeletal disorders. The use of model systems to deeply investigate endochondral ossification is therefore an important step in identifying the specific causes of skeletal dysplasia.

1.2   CCCTC-Binding Factor

The large size and complexity of higher eukaryotic genomes necessitates the sophisticated and dynamic packaging of DNA into stratified levels of organization. DNA is wrapped around histones to form nucleosomes, which are subsequently looped into higher-order structures and ultimately form chromosomes residing in defined nuclear territories. Chromatin acts in a dynamic manner, condensing and de-condensing as a cause and consequence of transcriptional activity[47]. There exists an extensive nuclear network aptly nicknamed the "loopome" or "interactome," in which local and long-range intra- and interchromosomal loops form contacts[47]. While some of these *cis-* and *trans-* contacts are stochastic, others appear highly regulated and have been associated with specific biological processes including X chromosome inactivation, monoallelic gene expression, and transcription during development[48–50]. Thus,

accumulating evidence over the past decade suggests that chromatin structure and the stability of its 3D architecture significantly affect nuclear functions including transcription, replication, DNA repair, and mitosis[51].

CCCTC-binding factor, commonly known as CTCF, is a highly-conserved transcription factor that has been heralded as "the master weaver of the genome."[47] Evidence demonstrates a role for CTCF in regulating higher-order chromatin structure and influencing many processes including X chromosome inactivation, genomic imprinting, long-range interactions, and transcriptional regulation **(Figure 1.2)**. Currently there are no reported/published studies investigating the role of CTCF in cartilage development.

1.2.1   *Structure and Regulation*

The name CCCTC-binding factor, shortened to CTCF, was determined based on the initial discovery of CTCF binding to three regularly spaced repeats of the core sequence CCCTC approximately 200 bp upstream of the transcriptional start site of the chicken c-*myc* oncogene's[52,53]. CTCF is a ubiquitously expressed 82-kDa protein containing 11-zinc finger motifs[54,55]. CTCF is highly conserved in most eukaryotes, displaying a 93% identity between avian and human amino acid sequences, however it is not conserved in yeast and plants[55,56]. A study by Klenova *et al*. reported four CTCF RNA species and six differentially expressed forms of CTCF protein with molecular masses ranging from 55-130 kDa[54]. The authors speculated that alternative mRNA processing was involved in the generation of multiple isoforms of mRNAs and multiple forms of proteins, and proposed that some forms of the CTCF protein may act predominantly as repressors or activators with different characteristics[54].

Figure 1.2 Schematic representation of CTCF-mediated chromatin looping

CTCF has been shown to form chromatin loops between genes and their associated enhancers. These loops can either promote gene expression (left) or prevent the enhancer's association with genes, thereby inhibiting expression (right).
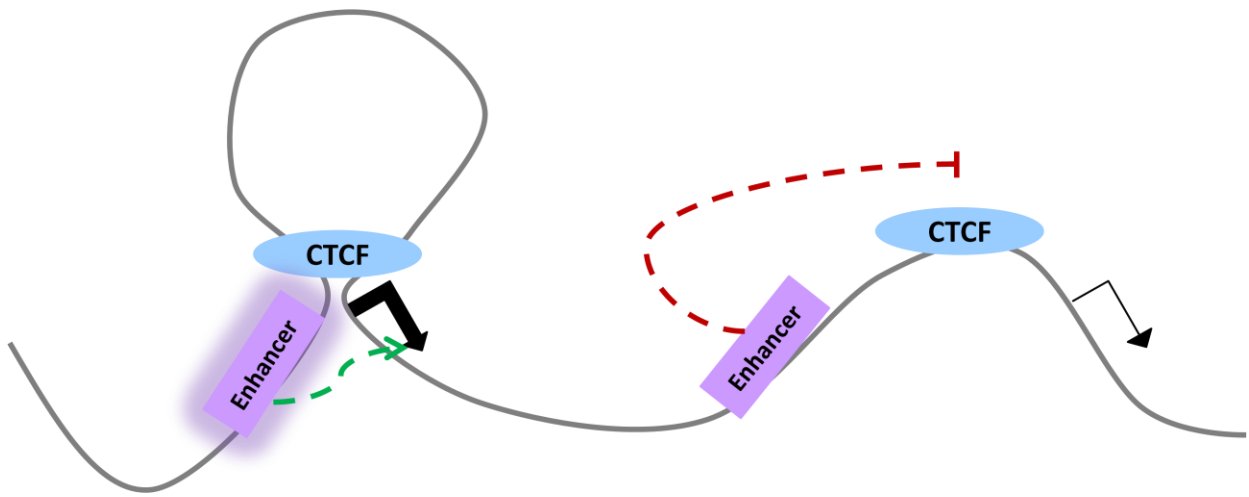
The structure of CTCF involves three distinct domains: an N-terminal domain, a C-terminal domain, and the central 11-zinc finger domain[55]. The central zinc finger domain is particularly highly conserved, which underscores its importance[55]. CTCF is regulated, in part, by distinct modifications of each domain. CTCF can be post-translationally modified by phosphorylation, poly(ADP-ribosy)lation, and SUMOylation. All strong phosphorylation sites in CTCF have been mapped to the C-terminal domain and studies have demonstrated that CTCF can be phosphorylated by protein kinase CK2, leading to abrogation of its repressive activity at the c-*myc* promoter[57,58]. Another group reported poly(ADP-ribosy)lation *in vivo,* and data from *in vitro* studies in breast cancer cells have shown that proper poly(ADP-ribosy)lation is required for CTCF to associate with and activate the *CDKN2A* tumour suppressor gene[59,60]. Finally, CTCF can be modified at one site in each of the C-terminal domain and the N-terminal domain by small ubiquitin-like modifier proteins (SUMO). In contrast to phosphorylation, SUMOylation of CTCF is important for maintaining the repressive activity of CTCF on the c-*myc* promoter[61].

CTCF function is also regulated through other processes including DNA methylation, interactions with other proteins, and even interactions with RNAs. In particular, DNA methylation plays a critical role in regulating CTCF function, as both cause and consequence. A study by Wang *et al.* found that 41% of cell-type-specific CTCF-binding sites are associated with differential DNA methylation at two specific positions within the CTCF recognition sequence[62]. A key example is that of the imprinted *H19/IGF2* locus, where the *H19* and *IGF2* genes are separated by an imprinting control region (ICR). When the ICR is conditionally methylated on the paternal allele, CTCF cannot bind and the promoter of *IGF2* is activated by a distal enhancer. Conversely, when the ICR is unmethylated, CTCF binds and the enhancer

activates the *H19* promoter[63]. CTCF has also been shown to form a complex with poly(ADP-ribose) polymerase 1 (PARP1) and DNA (cytosine-5)-methyltransferase 1 (DNMT1) to maintain methyl-free CpGs in certain CTCF-bound regions throughout the genome[64].

In addition to PARP1, CTCF interacts with other proteins, which provides another level of complexity to its regulation. In particular, the interaction between CTCF and the multiprotein cohesin complex has been well-studied. The cohesin complex is ring-shaped and composed of 4 subunits: SMC1, SMC3, RAD21, and SA1/SA2[65]. Cohesin is known for providing sister chromatid cohesion during DNA replication and until cell division, but also has roles in postmitotic cells[65]. The cohesin complex does not bind DNA directly, but the SCC3 subunit associates with C-terminal domain of CTCF. Cohesin is present at 50-80% of CTCF-binding sites, depending on the cell type, and multiple studies have demonstrated that a down-regulation of cohesin leads to disturbance of the chromatin structure at certain loci, such as the Cystic Fibrosis Transmembrane Conductance Regulator (CFTR) locus[66–69]. Cohesin is also required for the insulator function of CTCF, particularly at the *H19/IGF2* locus as discussed in detail below[70]. Overall, CTCF is necessary to enrich cohesin binding at specific sites, and cohesin is necessary to mediate CTCF's insulator activity.[70]

Finally, in mammalian cells CTCF was shown to form a complex with DEAD-box RNA helicase p68 (DDX5) and its associated non-coding RNA, steroid receptor RNA activator (SRA)[71]. This complex is necessary for stabilizing the cohesin-CTCF interaction at the ICR that allows for proper imprinted expression of the *H19/IGF2* locus, and provides evidence for an interaction between CTCF and RNAs[71].

1.2.2 *Function and Roles*

As previously mentioned, CTCF is ubiquitously expressed and binds 55,000-65,000 sites in mammalian genomes[72]. Of these binding sites, approximately 5,000 are conserved between species and tissues, and ~30-60% of binding sites are cell-type-specific[73–75]. Studies demonstrate that approximately ~50% of CTCF-binding sites are in intergenic regions, ~15% are proximal to promoters, and ~35% are intragenic[72,74]. Described as a "multivalent factor," CTCF exerts combinatorial control over its different zinc fingers to bind to a wide range of variant sequences[55]. For example, zinc fingers 2-7 are utilized in CTCF binding to the chicken c-*myc* site, whereas fingers 3-11 are utilized in binding at the human *C-MYC* site[55]. This structural feature of CTCF enables it to serve a diverse set of roles in genome regulation, largely through altering the genome's topology and 3D architecture. The importance of CTCF in multiple biological processes is further underscored by CTCF homozygous knockout mice exhibiting early embryonic lethality prior to implantation[76].

Of all the functions assigned to CTCF, its classical role is as an insulator protein; however, newer evidence suggests insulation is a minor role compared to CTCF's involvement in regulating chromatin loops in megabase-scale topologically associated domains (TADs). Insulators are DNA elements that function to block genes from the action of *cis*-acting elements, such as enhancers. The well-characterized *H19/IGF2* locus discussed above serves as evidence for CTCF as an insulator[63]. This locus also provides evidence of CTCF operating by mediating long-range chromatin interactions. When CTCF binds the ICR, it forms a loop with *IGF2* and blocks enhancers from activating the *IGF2* promoter in *cis*[63]. Another important piece of evidence for CTCF as an insulator protein and chromatin looping mediator involves the chicken *β-globin* locus, which was shown to contain an insulator sequence[77]. CTCF binds to the insulator and forms a chromatin loop encompassing the *β-globin* gene and locus control region,

positioning the elements in such a way that blocks enhancer signals and represses transcription[78].

Beyond its role as an insulator protein, studies have shown CTCF functions as a context-dependent promoter activator and repressor. The original studies on CTCF and the chicken c-*myc* gene demonstrated through reporter assays that CTCF is a transcriptional repressor[52]. In these experiments, deletion of the CTCF binding sequence led to a 4 to 8-fold increase in transcription of c-*myc* fusion constructs, thereby providing evidence of repressive activity by CTCF[52]. A later study also reported that CTCF binds to and acts as a transcriptional repressor at the amyloid β-protein precursor (APP) gene promoter[79]. Interestingly, the APP gene transcript level is increased in Down's syndrome and in certain brain regions of patients with Alzheimer's disease, potentially linking CTCF to these neurological pathologies[79].

One of the most important processes during development is the precise expression of *Homeobox* (HOX) gene clusters. The *HOX* genes are a group of highly-conserved transcription factors required for cells to maintain their relative position in the developing embryo, and are partitioned transcriptionally into discrete clusters. Mammals have 39 *HOX* genes in four clusters, *A-D*, each on a different chromosome[80]. The *HOX* genes pattern the anterior-posterior axis of the body, and are also critical to limb and genitalia formation. Interestingly, the 5'-end *HOX* genes *A7-13* are repressed by Polycomb group (PcG) proteins, which utilize repressive post-translational histone modification H3K27me3, until the correct developmental timepoint[80,81]. Evidence also demonstrates that the *HOX* clusters are organized into multiple chromatin loops which are dependent on transcription activity[80]. In order to understand the proper temporal and spatial expression of the *HOX* gene clusters, CTCF was investigated as a candidate regulatory protein in the process. A highly-conserved binding site for CTCF exists between genes in the *HOXD* clusters in human cells, so the role of CTCF as an insulator for the

HOX gene clusters was investigated[82]. Narendra *et al*. deleted the CTCF binding sites and showed the expansion of active chromatin into the adjacent repressive domain of the *HOXA* cluster in motor neuron progenitor cells[81]. The study concluded that CTCF partitions the *HOX* clusters into architectural domains[81]. These domains are then acted upon by Trithorax and Polycomb proteins to establish discrete transcriptional proteins[81]. Therefore, CTCF is required to insulate heterochromatin from adjacent euchromatin and to facilitate proper gene expression patterns of the *HOX* genes.

This study is in contrast with experiments performed by Soshnikova *et al*. involving conditional inactivation of *Ctcf* in the developing limbs using the *Prx1*-Cre driver. The mice had severe developmental defects, including a complete lack of forelimbs[83]. The authors also noted that the hindlimb was malformed and had oligodactyly, but did not investigate the hindlimb in any detail[83]. In the mutant forelimbs, expression patterns of *Hoxa13* and *Hoxa11* were not different from controls, and there was no induction of *Hoxb* or *Hoxc* genes in mutant mesenchyme[83]. The limbs did show weakened *Shh* gene expression, which may have affected *Fgf4* expression and the absolute amount of *Hoxd* transcripts; however the authors felt that this explanation did not account for the whole effect[83]. Rather, the investigation showed massive cell death caused by the impairment of mitochondrial processes and attributed the phenotype to this effect[83].

CTCF has also been implicated in neuroprogenitor differentiation and survival in the developing mouse brain. A study by Watson *et al.* elegantly showed that CTCF is required in the developing telencephalon to prevent massive apoptosis and regulate differentiation and proliferation of neuroprogenitors[84]. This study also indicated that the loss of CTCF contributed to a depletion of the neuroprogenitor pool early in development[84]. These data provide new

evidence for the relationship between CTCF-depletion and intellectual disability pathology discussed below.

Although emerging evidence suggests an important role for CTCF in many tissues and cell types, little evidence linking CTCF to the developing skeleton has been produced. Notably, however, was the discovery by Schaub *et al.* that many CTCF binding sites overlap single nucleotide polymorphisms (SNP) associated with human height[85]. Their analysis found that 15 of the 39 SNPs associated with height overlap a ChIP-seq peak for CTCF[85]. This finding suggests a possible link between human height, which is partially dependent on proper skeletal growth, and CTCF. Additionally, recent unpublished data from our laboratory by Bush *et al*. demonstrate that the conditional knockout of CTCF in developing cartilage, using the *Col2a1-*Cre driver, severely affects cartilage development. Mutant mice are neonatal lethal and die from respiratory distress caused by ribcage defects. These animals also demonstrate severely malformed limbs and bowing of the long bones. This phenotype resembles that of patients with CD and the current mouse model of the disease. Furthermore, the *Ctcf$^{Fl/Fl}$;Prx1Cre* mice present with a slight but significant reduction in *Sox9* gene expression and SOX9 protein levels. The growth plates were also affected in the knockout animals, showing a shortened hypertrophic zone with fewer and smaller hypertrophic chondrocytes. Together these data suggest that CTCF is critical for normal cartilage development, potentially through the regulation of *Sox9* gene expression

1.2.3 *Pathologies*

As the study of epigenetics and chromatin structure grows, so too does the number of genes implicated in developmental pathologies. A recent article by Gregor and colleagues

identified de novo mutations in *CTCF* in four individuals presenting with intellectual disability[86]. The mutations varied between individuals, although all were heterozygous. Individuals one and two had frameshift mutations in exon three and exon six of *CTCF*, which corresponds to the N-terminal region and fifth zinc finger, respectively. Individual three presented with a missense mutation in exon nine, which corresponds to the eleventh zinc finger. Finally individual four had a large deletion containing *CTCF* and seven additional genes. All four individuals suffered from developmental delay, and two of the individuals presented with cryptorchidism (undescended testicles). Interestingly, individuals one, two, and four all had reduced expression of *CTCF,* which suggested that haploinsufficiency can cause the intellectual disability phenotype. Conversely, individual three had unaltered *CTCF* mRNA and CTCF protein levels, but modeling programs indicate that the amino acid substitution may affect DNA binding affinity and specificity. Of particular interest, all four individuals presented with short stature and two patients had digit abnormalities, suggesting that hypomorphic mutations in *CTCF* also affect proper skeletal development.

Gene mutations in the cohesin network also leads to a family of rare human diseases known as cohesinopathies. The two cohesinopathies that have been studied in depth are Cornelia de Lange syndrome (CdLS) and Roberts syndrome. CdLS is an autosomal dominant neurodevelopmental disorder most commonly caused by mutations in the gene encoding *NIPBL*[87]. While not a subunit of cohesin, NIPBL is required to load cohesin onto chromatin[87]. Patients with CdLS are characterized by intellectual disability, facial dysmorphism, upper limb abnormalities, and growth retardation, however the disease is thought to result from transcriptional alterations, not from problems in sister chromatid cohesion[87]. Roberts syndrome is phenotypically related to CdLS, however it is autosomal recessive and caused by mutations in

the gene encoding *ESCO2*, another cohesin-associated protein required for the establishment of cohesion between sister chromatids following DNA replication[87]. Roberts syndrome is extremely rare and severe, patients also present with craniofacial abnormalities, limb reduction, and growth retardation[87]. In patients with Roberts syndrome, both sister chromatin cohesion and mitosis are affected. All these conditions, therefore, underscore the importance of proper epigenetic regulation and chromatin cohesion via the cohesin complex during skeletal development.

1.3   Governing Rationale and Objectives

Emerging evidence shows that CTCF is critical for the proper regulation of multiple cell and tissue types. However, the role of CTCF in the developing hindlimb and skeleton has never before been investigated. Studies show a role for CTCF in regulating the *HOX* gene clusters, which are critical for limb development, and other studies have demonstrated that CTCF is required to prevent massive apoptosis in the developing forelimb[81,83]. Furthermore, our unpublished research reveals that CTCF is required for the maintenance of *Sox9* expression in developing cartilage and that loss of CTCF in cartilage causes campomelia. Thus, both these CTCF-deficient animal models and *de novo* human *CTCF* mutations suggest that CTCF regulates limb and cartilage development. Given that CTCF deletion in the forelimb of mice using the *Prx1*-Cre driver line caused excessive apoptosis and loss of tissue, **my objective was to investigate the effects of CTCF deletion on chondrogenesis and skeletal development in the hindlimb of *Ctcf$^{Fl/Fl}$;Prx1Cre* mice**. The *Ctcf$^{Fl/Fl}$;Prx1Cre* hindlimb presents an intermediate phenotype that falls in between the completely abrogated *Ctcf$^{Fl/Fl}$;Prx1Cre* forelimb, and the slightly bowed *Ctcf$^{Fl/Fl}$;Col2Cre* hindlimb. My first objective was to

investigate differences in the onset of chondrogenic gene expression in micromass cultures established from wild-type forelimbs versus hindlimbs. Secondly, I assessed gene expression differences and alterations in development of the hindlimbs and long bones of the $Ctcf^{Fl/Fl}$;*Prx1Cre* mice. This thesis, to the best of my knowledge, represents the first in-depth characterization of the role of CTCF in the developing hindlimb of $Ctcf^{Fl/Fl}$;*Prx1Cre* mice.

2.0 MATERIALS & METHODS

2.1 Timed Pregnant CD1 Mice

Timed pregnant CD1 mice were purchased from Charles River Laboratories (Sherbrooke, Quebec) and were sacrificed for experimentation by carbon dioxide asphyxiation. The use of animals for experimentation was approved by Animal Care and Veterinary Services at Western University.

2.2 Murine Micromass Cultures

Micromass cultures were prepared as described with minor modifications[88,89]. Forelimb and hindlimb buds of up to 12 embryonic day 10.5 (E10.5) CD1 mouse embryos were dissected in Puck's Saline Solution A buffer (PSA) and diced using a sterile razor blade. The limb buds were then digested in 10 mg/ml dispase (Roche Molecular Biochemicals, Indianapolis, IN, USA) solution containing 10% fetal bovine serum (FBS; Sigma-Aldrich, Oakville, ON, Canada)/PSA for 2 hours at 37°C and shaken at 100 rpm, with vortexing every 15 minutes. After digestion, the enzymatic reaction was neutralized with 2:3 Dulbecco's Modified Eagles Medium (DMEM):F12 media (Sigma-Aldrich) containing 10% FBS, 0.25% Penicillin (10,000 units/ml; Sigma-Aldrich)/Streptomycin (10,000 μg/ml; Sigma-Aldrich), and 0.25% L-glutamine (200mM; Sigma-Aldrich). Digested tissue was passed through a 40 μm cell strainer (Falcon, Lincoln Park, NJ) before centrifugation for 5 minutes at 23°C and 1000 rpm. Cells were then re-suspended in DMEM:F12 media containing 10% FBS, 0.25% Penicillin/Streptomycin, and 0.25% L-glutamine, and counted using a haemocytometer (Hausser Scientific Partnership, Horsham, PA, catalogue number 3200). Cells were then centrifuged again for 5 minutes at 23°C and 1000 rpm, re-suspended at a final concentration of 2.5×10^7 cells/ml, and plated in eight 10 μl droplets per well in a six-well NUNC delta surface cell culture plate (Thermo Scientific, Burlington, ON, Canada). Cells adhered to the plate during a 1-hour incubation period at 37°C and 5% CO_2.

Finally, 2 ml of 2:3 DMEM:F12 media containing 10% FBS, 0.25% Penicillin/Streptomycin, and 0.25% L-glutamate was added to each well. Micromass cultures were grown for up to 60 hours with media changed every 24 hours.

2.3 *Ctcf$^{Fl/Fl}$;Prx1Cre* Mice

All studies were conducted in accordance with the policies and guidelines set forth by the Canadian Council on Animal Care and were approved by the Animal Use Subcommittee of Western University. Mice were housed in Animal Care and Veterinary Services facilities at Western University and cared for according to protocol number 2007-045 (Appendix A). Mice were housed in standard cages and maintained on a 12-hour light/dark cycle, with rodent chow and water available *ad libitum*. Timed matings involved one male *Ctcf$^{Fl/+}$;Prx1Cre* and one female *Ctcf$^{Fl/Fl}$* mouse per cage, placed together at 5:00 pm and separated the following morning at 9:00 am **(Figure 2.1)**. Pregnant females were sacrificed and embryos were collected at embryonic day 12.5 (E12.5), 13.5 (E13.5), 15.5 (E15.5), and 18.5 (E18.5). Pups were also collected at post-natal day 0 (P0). Litters containing a wild-type, heterozygote, and homozygote conditional knockout mouse were considered one trial (N=1). Euthanasia was performed on the pregnant dames by carbon dioxide asphyxiation or lethal injection of 270 µg Euthanyl/g body weight (Animal Health Inc.) for P0 pups.

Tissue for genotyping was collected from tail clippings of euthanized embryos and pups. Clippings were digested in Eppendorf tubes with 100 µl of Solution A (25 mM NaOH, 0.5 M EDTA at pH 6.0) for 1 hour at 95°C before 100 µl of Solution B (40 mM Tris-HCL at pH 6.0) was added. Polymerase chain reaction (PCR) was performed using oligonucleotides *Ctcf* forward primer (5'- CTAGGAGTGTAGTTCAGTGAG -3'), *Ctcf* reverse primer (5'- GCTCTAAAGAAGGTTGTGAGT -3') and *Cre* forward primer

Figure 2.1 Schematic representation of mouse breeding strategy.

The Cre/loxP recombination system was utilized in C57BL/6 mice to produce conditional *Ctcf*
knockout animals. Female mice homogenous for the floxed *Ctcf* locus were bred with male mice
heterogeneous for the floxed *Ctcf* locus and expressing Cre recombinase under the control of the
Prx1 enhancer. After Cre-mediated recombination, *Ctcf*-null pups were produced (KO) and
compared to littermates lacking Cre as controls.

$CTCF^{Fl/Fl}$ $CTCF^{Fl/+}; Prx1Cre^{+/-}$

$CTCF^{Fl/Fl}; Prx1Cre^{+/-}$
knockout

$CTCF^{Fl/+}$
or
$CTCF^{Fl/Fl}$
control

$CTCF^{Fl/+}; Prx1Cre^{+/-}$
heterozygote
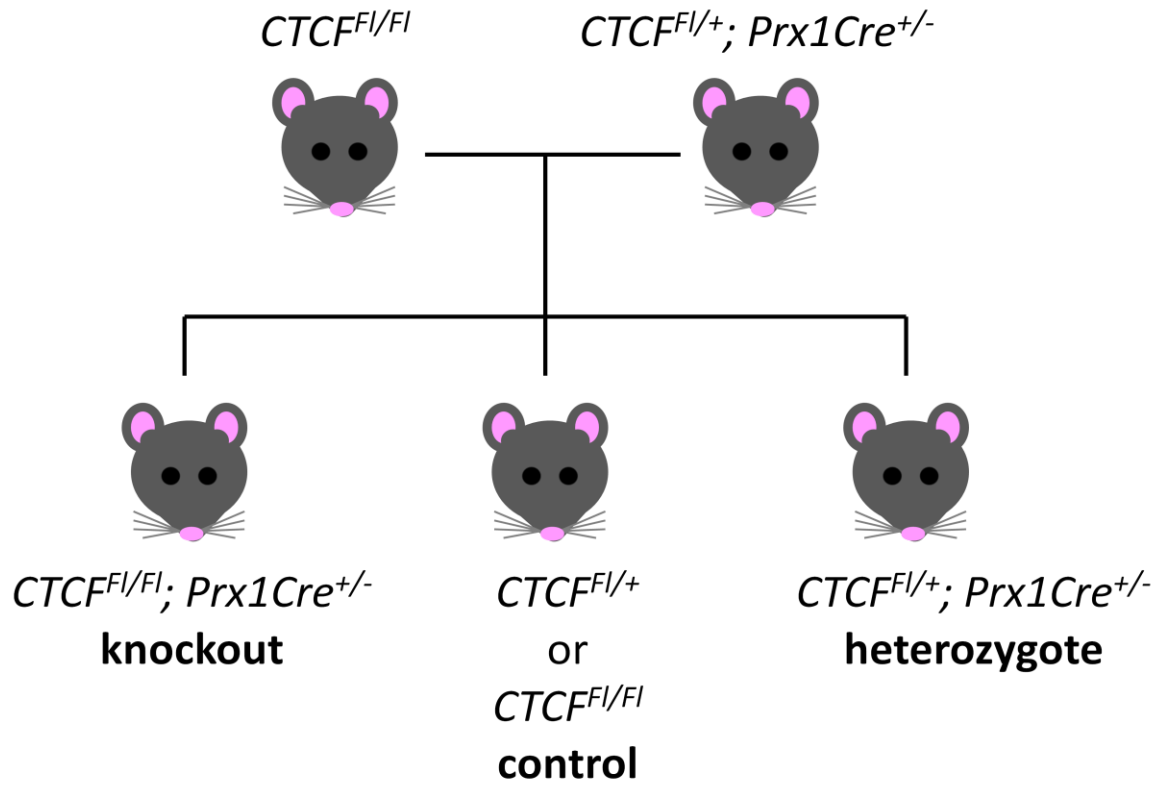
(5'-CCTGGAAAATGCTTCTGTCCG -3'), *Cre* reverse primer (5'-CAGGGTGTTATAACAATCCC. -3') for amplification. All oligonucleotides were purchased from Sigma-Aldrich and all additional genotyping reagents were purchased from Roche. Samples were run in a MyCycler™ thermal cycler (Bio-Rad, Mississauga, ON, Canada). PCR protocol included a 3-minute denaturing step at 95°C, followed by 34 cycles of 95°C for 45 seconds, 58°C for 30 seconds, and 72°C for one minute, before a 10-minute incubation at 72°C. PCR products were run on a 1.5% agarose (Bio-Shop, Burlington, ON, Canada), 0.005% Ethidium bromide (Sigma-Aldrich) gel at 120 V for 1 hour. Bands were visualized using a Gel Doc™ EZ System (Bio-Rad).

2.4 Skeletal Preparation

Following euthanasia, P0 mice were skinned, eviscerated, and fixed in 70% ethanol for 24 hours at room temperature. The solution was then changed to acetone for 24 hours at room temperature before the bodies were placed in staining solution (0.05% Alizarin Red (Sigma-Aldrich), 0.015% Alcian Blue (Sigma-Aldrich), 5% Acetic Acid and 70% ethanol) for five days. Upon removal of staining solution, soft tissue was digested by graded potassium hydroxide solutions placed on a rocker at room temperature. Finally, clean skeletons were stored in a 1:1 Glycerol:70% ethanol solution.

Skeletons were visualized using a Leica S6D Stereomicroscope with a 0.63x de-magnifying lens and images were taken using a Leica EC3 digital camera. Total long bone length and mineralized zone length were measured using the Leica Application Suite software.

2.5 Tissue Processing

Following euthanasia, the skulls, forelimb and hindlimb buds of E12.5 wild-type mice were microdissected in phosphate buffered saline (PBS) and fixed in 4.0% paraformaldehyde (PFA) for 15 minutes. Following fixation, tissues were submerged in a 30% sucrose in PBS solution and kept for 24 hours at 4°C. Tissues were then embedded in Tissue-Tek® O.C.T (Optimal Cutting Temperature; VWR International, Mississauga, ON, Canada) compound and stored at -80°C until cryosectioning was completed at the Molecular Pathology Core Facility, Robarts Research Institute (London, ON, Canada).

Additionally, following euthanasia, tibiae were dissected from E15.5 conditional knockout mice and controls in PBS and fixed in 4.0% PFA for 24 hours. Following fixation, the solution was replaced with 70% ethanol, and bones were labeled using 2% Mercurochrome (Fisher Scientific, Toronto, ON, Canada) before being sent to the Molecular Pathology Core Facility, Robarts Research Institute, for tissue processing, paraffin embedding, and sectioning.

2.6   Histology

Paraffin sections were de-waxed in xylene and rehydrated for staining in graded series of ethanol solutions (100%, 100%, 95%, 70%) and then water. Histological staining was performed on sections of E15.5 tibiae using Safranin-O/Fast Green, and von Kossa staining. For Safranin-O/Fast Green staining of proteoglycans, sections were incubated in Hematoxylin (Fisher Scientific) for 2 minutes, then washed in running tap water for 10 minutes. Slides were then incubated in 0.01% Fast Green (Fisher Scientific) for 25 minutes, dipped in 1% Acetic Acid five times, and incubated in 0.1% Safranin-O (Fisher Scientific) for 7 minutes. Slides were then dehydrated and cover slips were applied using SHUR/Mount™ Liquid Mounting Medium (VWR). Representative images of tibia sections were taken using a Leica DM1000 microscope.

Sections processed for von Kossa staining were incubated with 5% silver nitrate solution under light for 1 hour, then were washed with water and incubated in 5% sodium thiosulfate for 5 minutes. Slides were then rinsed in distilled water, counterstained with Methyl Green (Fisher Scientific), dehydrated and cover slips were applied using SHUR/Mount^{TM} Liquid Mounting Medium (VWR). Representative images of tibia sections were taken using a Leica DM1000 microscope.

2.7   Immunohistochemistry and Immunofluorescence

Immunohistochemistry (IHC) was performed on E15.5 tibiae using antibodies against p57 (Santa Cruz Biotechnology, Dallas, TX, USA). Sections were de-waxed and rehydrated in xylenes and a graded series of ethanol, then incubated in 3% hydrogen peroxide in methanol for 15 minutes at room temperature. Antigen retrieval was performed by incubating sections in 0.1% Triton-X (Sigma-Aldrich) at room temperature for 13 minutes before sections were blocked in 5% goat serum in PBS-0.1% Tween (PBST; Sigma-Aldrich) for 1 hour at room temperature. Primary antibody against p57 was diluted in blocking solution according to its optimized concentration of 1:200. Sections were incubated with the primary antibody overnight in a humidified chamber at 4°C before being washed in dH$_2$0 the following day. Sections were then incubated in horseradish peroxidase (HRP)-conjugated goat anti-rabbit IgG secondary antibody (Santa Cruz Biotechnology) diluted 1:200 in PBS for 1 hour at room temperature. Visualization was performed using 3,3'-Diaminobenzidine (DAB) substrate solution (Dako, Burlington, ON, Canada) before being counterstained with Methyl Green (Fisher-Scientific) in 0.1 mM sodium acetate buffer for 10 minutes. Sections were then dehydrated and cover slips were applied using SHUR/Mount^{TM} Liquid Mounting Medium (VWR). Representative images

of tibia sections were taken using a Leica DM1000 microscope and Leica Application Suite was used for measurements of the unstained resting and proliferating chondrocyte zones.

Immunofluorescence (IF) was performed on frozen E12.5 hindlimb bud sections for CTCF, SOX9, and proliferating cell nuclear antigen (PCNA). Sections were thawed at room temperature for 1 hour, baked at 42°C for 30 minutes, then rehydrated in PBS at room temperature for 5 minutes. Antigen retrieval was performed by incubating slides in 10 mM sodium citrate, pH 6, at 95°C for 10 minutes, then cooled for 20 minutes before blocking with 5% donkey serum or goat serum in PBST for 1 hour at room temperature. Primary antibody against CTCF (rabbit anti-CTCF; Cell Signaling Technologies, Danvers, MA, USA) was diluted in blocking solution according to its optimized concentration of 1:400. Primary antibody against SOX9 (goat anti-SOX9; R&D Systems, Minneapolis, MN, USA) was diluted in blocking solution according to its optimized concentration of 1:300. Primary antibody against PCNA (mouse anti-PCNA; Cell Signaling Technologies) was diluted in blocking solution according to its optimized concentration of 1:400. Sections were incubated with the primary antibody overnight in a humidified chamber at 4°C before being washed in dH_20 the following day. Sections were then incubated with donkey anti-goat IgG (Life Technologies, Burlington, ON, Canada) or goat anti-mouse IgG (Life Technologies) secondary antibody diluted 1:200 in PBS for 1 hour at room temperature, prior to applying cover slips with VECTASHIELD Mounting Medium with DAPI (Vector Laboratories, Burlington, ON, Canada). Images of CTCF staining were captured with a digital camera (ORCA-ER; Hamamatsu, Middlesex, NJ, USA) on a Leica DMI 6000b microscope. Open-Lab imaging software (PerkinElmer, Waltham, MA, USA) was used for image capture, and processing was performed using Volocity software (PerkinElmer). Images of SOX9 and PCNA staining were captured with a Leica DMRA2 fluorescence

microscope. SOX9- and PCNA-positive cells were counted in a region of interest using ImageJ software (National Institutes of Health, Bethesda, MD, USA), and the positively stained cells were taken as a percentage of the total cells (DAPI-positive cells) in the area.

2.8   TUNEL Staining

TUNEL staining was performed on E12.5 hindlimb bud sections using the In Situ Cell Death Detection Kit, Fluorescin (Roche) according to the manufacturer's instructions. Cover slips were then applied using VECTASHIELD Mounting Medium with DAPI (Vector), and representative images were visualized with a Leica DMRA2 fluorescence microscope. TUNEL-positive cells were counted in a region of interest using ImageJ software (National Institutes of Health), and the positively stained cells were taken as a percentage of the total cells in the area.

2.9   RNA Isolation and Quantitative Real-Time Polymerase Chain Reaction

Total RNA was isolated from wild-type limb bud micromass cultures at 0, 12, 24, 36, 48, and 60 hours after plating. Total RNA was also isolated from whole E12.5 and E13.5 hindlimb buds of conditional knockout embryos and control littermates. In both cases, TRIzol reagent (Life Technologies) was used to extract RNA according to the manufacturer's instructions. A NanoDrop 2000 spectrophotometer (Thermo Scientific) was used to quantify RNA. 500 ng of RNA were reverse transcribed into complementary DNA (cDNA) using the iScript cDNA Synthesis kit (Bio-Rad) according to the manufacturer's instructions.

Gene expression was assessed by real-time PCR using a Bio-Rad CFX384 RT-PCR system. PCR reactions were run in triplicate, using 0.4 μl of cDNA per reaction and 0.1 μl forward and reverse primers (100 μM). PCR parameters involved an initial denaturing step at 95°C for 3 minutes, followed by 40 cycles of denaturing at 95°C for 10 seconds, and annealing/elongating at 58°C for 20 seconds. Relative gene expression was calculated using the

$\Delta\Delta C_t$ normalized for input using β-*actin* and expressed relative to the 0 h time point in micromass cultures, or E12.5 control in hindlimb buds.

Relative gene expression was determined for *Ctcf*, type II collagen (*Col2a1*), the proteoglycan aggrecan (*Acan*), the *Sox* trio (*Sox9*, *Sox5*, *Sox6*), long non-coding RNAs *BC006965* and *D17Rik*, the two genes bordering the *Sox9* locus: *Kcnj2* and *Slc39a11*, N-cadherin (*Cdh2*) and cadherin-11 (*Cdh11*; **Table 2.1**). Standard curves were generated to control for primer efficiency, and the specificity of the primers was determined by melt curve analysis (0.5°C/5 seconds).

2.10   Statistical Analysis

All data collected were from a minimum of three independent trials. Data were expressed as mean ± SD. P values less than 0.05 were considered significant (*). Statistical significance was determined with a t-test, one-way ANOVA, or two-way ANOVA followed by a Tukey's multiple comparison test using GraphPad Prism version 6.0 (GraphPad Software, San Diego, CA, USA).

Table 2.1 Primers for Quantitative Real-Time PCR

NCBI Gene Symbol	Primer Sequence 5' » 3'
β-actin Fwd	CTGTCGAGTCGCGTCCACCC
β-actin Rev	ACATGCCGGAGCCGTTGTCG
Ctcf Fwd	GAGCCTGCTGTAGAAATTGAA
Ctcf Rev	CCAATAGTCCTGGTGCCGAGCAAGGCCCC
Sox9 Fwd	CTCTGGGCAAGCTCTGGA
Sox9 Rev	GTCGGTTTTGGGAGTGGTG
Sox5 Fwd	CCTGAAGCAGAGGAAGATGG
Sox5 Rev	CTCCTTCTCAGCGAGGCTCT
Sox6 Fwd	CTGAGCAACTGAGGACTGA
Sox6 Rev	AGCCATTCATTGCTTTGCTT
Col2a1 Fwd	AAGGGTCACAGAGGTTACCC
Col2a1 Rev	GTCCTCTCTCACCAGGCAG
Acan Fwd	GCTGCAGTGATCTCAGAAGAAG
Acan Rev	CACCAGCAGTACCACCTCCT
BC006965 Fwd	GTCAAGTCTTGGGCCTGATG
BC006965 Rev	CGCACAGAAACGTACCATTG
D17Rik Fwd	CGCACAGAAACGTACCATTG
D17Rik Rev	CTTGCTCTTGTTCCATGCAG
Kcnj2 Fwd	TAATCCCCACTTCCACTCCA
Kcnj2 Rev	TCGGTGAAGACACACCAAAA
Slc39a11 Fwd	TTCCAGAGGGTCTTGCTGTT
Slc39a11 Rev	GCTCAGCTGTCCATACCAGA
Cdh2 Fwd	TGCCAGAAAACTCCAGAGGA
Cdh2 Rev	TCGATCCAGAGGCTTTGTGA
Cdh11 Fwd	GACACAGCCAATGGACCAAG
Cdh11 Rev	ACGTCGGGCATATACTCCTG

3.0 RESULTS

3.1 Micromass cultures from wild-type forelimb and hindlimb buds showed patterns of increasing chondrogenic gene expression over 60 hours post-plating.

$Ctcf^{Fl/Fl}$;*Prx1Cre* mice were originally described by Soshnikova *et al.* in 2010 during a study on CTCF and *Hox* gene regulation. This study described the mutant mice as having truncated forelimbs and a milder hindlimb phenotype: shortened long bones and oligodactyly (reduced number of digits). Given the startling difference between the forelimb and hindlimb phenotypes, I began my investigation by examining key chondrogenic genes in wild-type micromass cultures from E10.5 forelimb and hindlimb buds. Micromass cultures replicate early chondrogenesis *in vitro*, thus I explored the possibility of differential gene expression between limbs as a contributor to phenotypic severity. RNA was collected from micromass cultures every 12 hours post-plating, and qRT-PCR was utilized to examine gene expression changes. I first set out to examine expression differences in the *Sox* gene trio because of their critical role in differentiation of mesenchymal cells into chondrocytes. *Sox9* gene expression in the forelimb showed a significant 3.5-fold and 4-fold increase at 48 hours and 60 hours post-plating, while expression showed a trend in increasing expression in the hindlimb, although the increase was not statistically significant **(Figure 3.1A)**. The increase in *Sox9* expression was also steeper in the forelimb than in hindlimb micromass cultures, particularly between 12-24 hours post-plating **(Figure 3.1A)**. *Sox5* transcript levels showed a pattern of increasing expression in forelimb micromass cultures until 24 hours, then maintained steady expression levels until 36 hours before declining back to baseline levels by 60 hours post-plating **(Figure 3.1B)**. Conversely, *Sox5* expression in hindlimb micromass cultures increased slightly until 24 hours, plateaued until 48 hours, and then increased again at 60 hours post-plating **(Figure 3.1B)**. However, trends seen in *Sox5* expression in both forelimb and hindlimb cultures were not statistically significant.

Figure 3.1 *Sox9*, *Sox5*, **and** *Sox6* **gene expression in micromass cultures from wild-type forelimbs and hindlimbs.**

Micromass cultures from E10.5 forelimb buds and hindlimb buds were plated and collected at 12-hour intervals. RNA from the cultures was used to perform qRT-PCR reactions to examine *Sox9, Sox5,* and *Sox6* gene expression. **A.** Forelimb micromass cultures demonstrated a significant increase in *Sox9* expression at 48 hours and 60 hours post-plating. Although there was no significant difference in *Sox9* transcript in the hindlimb, data suggest a trend showing a steady increase in expression in both cultures after 12 hours. **B.** There was no significant difference in *Sox5* gene expression in either forelimb or hindlimb micromass cultures over time; however, a trend suggests increasing *Sox5* expression in hindlimb micromass cultures. *Sox5* expression in forelimb micromass cultures appeared to increase immediately after plating then decreases after 36 hours**. C.** Although there was no significant difference in *Sox6* transcript levels in either forelimb or hindlimb micromass cultures over time, data suggest a trend showing a steady increase in expression in both cultures after 0 hours. All data represented are mean ± SD; * = $P < 0.05$. N=3 for forelimb, N=6 for hindlimb.

A. *Sox9* (Forelimb) / *Sox9* (Hindlimb)

B. *Sox5* (Forelimb) / *Sox5* (Hindlimb)

C. *Sox6* (Forelimb) / *Sox6* (Hindlimb)
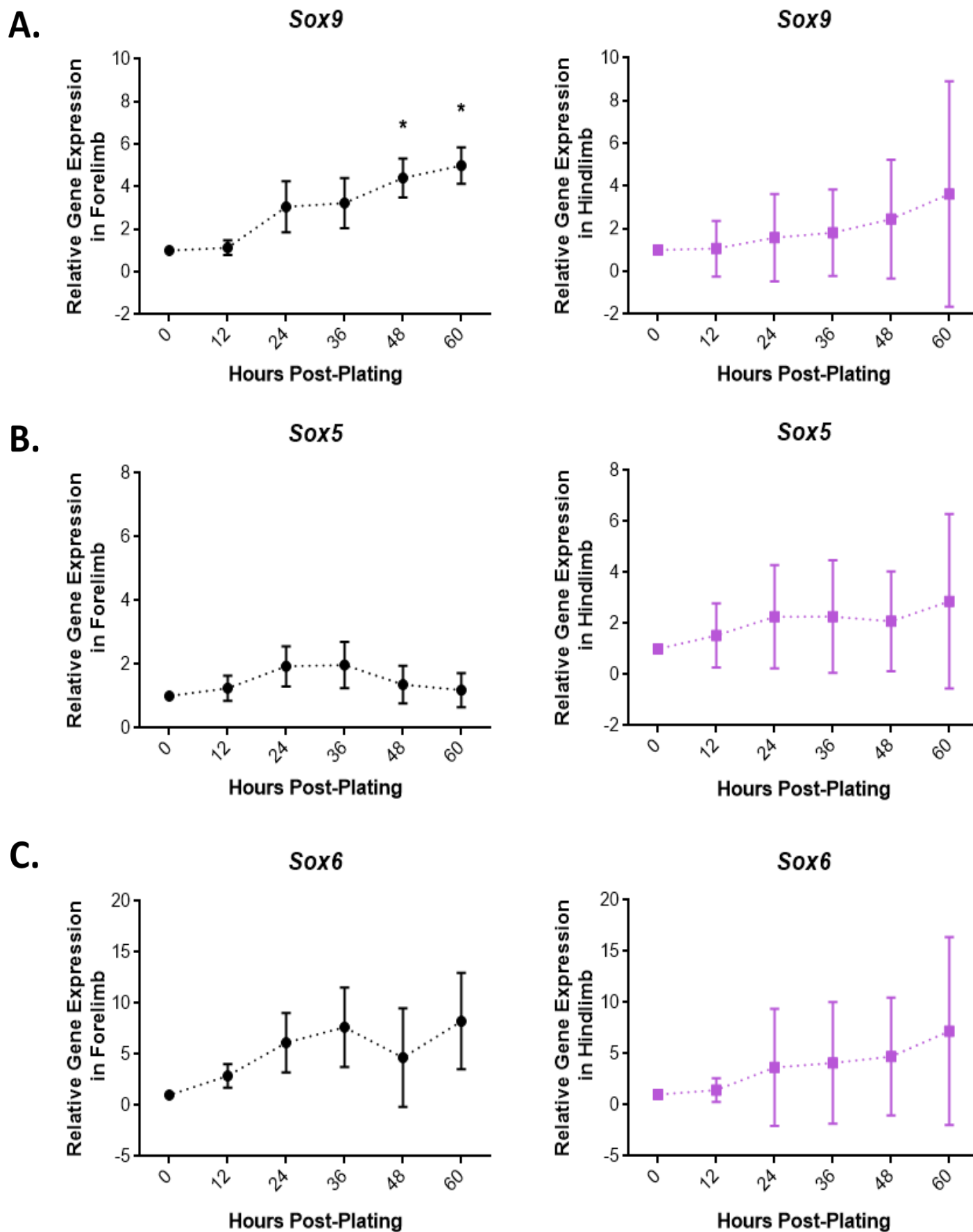
Finally, *Sox6* expression showed a trend of increasing expression in both forelimb and hindlimb micromass cultures, but while forelimb cultures showed a decrease in expression from 36-48 hours before increasing again by 60 hours, hindlimb micromass cultures demonstrated a relatively steady increase in transcript expression over the time course **(Figure 3.1C)**. These results indicate that the overall patterns of *Sox* trio gene expression are similar between forelimb and hindlimb, although *Sox9* expression increased more rapidly in the forelimb micromass cultures which suggests chondrogenesis is occurring more rapidly.

To investigate potential differences between limbs in chondrogenic genes downstream of the *Sox* trio, transcript levels of the cartilaginous ECM genes *Acan* and *Col2a1* were analyzed. Expression profiles of forelimb micromass cultures showed a robust and steady increase in *Acan* expression that reached a significant 50-fold increase at 60 hours post-plating, when compared to 0 hours **(Figure 3.2A)**. *Acan* expression levels in hindlimb micromass cultures also increased approximately 4-fold over 60 hours, although these results did not reach significance **(Figure 3.2A)**. Moreover, *Col2a1* transcript levels showed a significant 180-fold increase at 60 hours post-plating in the forelimb micromass cultures **(Figure 3.2B)**. Hindlimb micromass cultures also showed a significant increase in *Col2a1* expression, although the increase was approximately 75-fold **(Figure 3.2B)**. Taken together, these results demonstrate that forelimb and hindlimb micromass cultures show similar overall patterns of cartilaginous ECM gene expression, although the fold-change appears to be higher, and the time course faster, in forelimb micromass cultures than in hindlimb.

Given our lab's unpublished data suggesting a role for CTCF in regulating gene expression at the *Sox9* locus, I set out to investigate expression of the long non-coding RNA *BC006965*, whose gene is located directly upstream of the *Sox9* gene, overlapping with genomic

Figure 3.2   Relative *Acan* and *Col2a1* expression in wild-type micromass cultures from forelimbs and hindlimbs.

Micromass cultures from E10.5 forelimb buds and hindlimb buds were plated and collected at 12-hour intervals. RNA from the cultures was used to perform qRT-PCR reactions to examine *Acan* and *Col2a1* gene expression. **A.** *Acan* expression showed a steady and significant increase in forelimb micromass cultures 60 hours post-plating when compared to expression levels at 0 hours. Hindlimb micromass cultures showed no significant differences, however data show a trend indicating an increase in *Acan* expression over the time course. **B.** *Col2a1* gene expression was significantly increased in forelimb and hindlimb micromass cultures at 60 hours post-plating when compared to 0 hours. All data represented are mean $\pm$ SD; * = $P < 0.05$. N=3 for forelimb, N=6 for hindlimb.

A. *Acan* (Forelimb and Hindlimb panels) — Relative Gene Expression in Forelimb and in Hindlimb versus Hours Post-Plating.

B. *Col2a1* (Forelimb and Hindlimb panels) — Relative Gene Expression in Forelimb and in Hindlimb versus Hours Post-Plating.
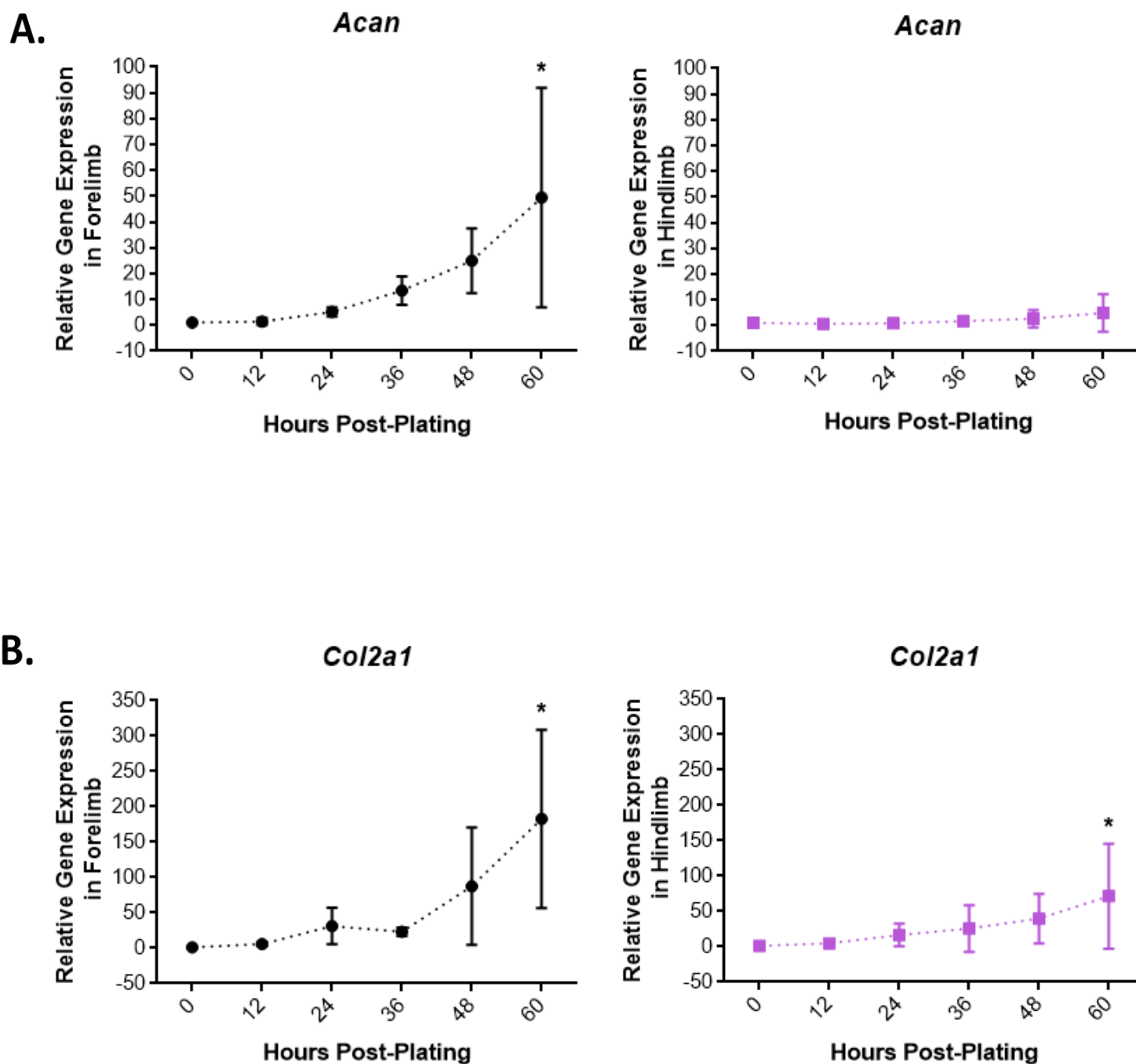
CTCF binding sites identified by us (Bush *et al.*, in prep). In forelimb micromass cultures, *BC006965* expression showed a trend of increasing transcript levels until 36 hours post-plating, then a slight decrease in expression between 36-48 hours **(Figure 3.3A)**. Conversely, transcript levels in the hindlimb micromass cultures appeared to show a slight but steady increase over time, although the fold-change is not statistically significant **(Figure 3.3A)**. Interestingly, a comparison of the expression patterns of *Sox9* and *BC006965* in hindlimb micromass cultures revealed that both transcripts are up-regulated over the time course, with similar relative expression levels at each time point **(Figure 3.3B)**. These results indicate that *BC006965* expression may be regulated in a similar manner to *Sox9* gene expression in the developing hindlimb.

Figure 3.3 Expression of the long non-coding RNA *BC006965* in wild-type forelimb and hindlimb micromass cultures.

Micromass cultures from E10.5 forelimb buds and hindlimb buds were plated and collected at 12-hour intervals. RNA from the cultures was used to perform qRT-PCR reactions to examine gene expression of *BC006965,* a long non-coding RNA proximal to the *Sox9* locus. **A.** *BC006965* expression did not show a significant increase in either forelimb or hindlimb micromass cultures, however trends indicate a slight increase in expression over the time course. **B.** The trend in steadily increasing gene expression levels of *BC006965* in hindlimb micromass cultures is similar to the expression of *Sox9* in hindlimb micromass cultures across the 60 hour time course. All data represented are mean ± SD; * = P < 0.05, N=3 for forelimb, N=6 for hindlimb.

A.

B.
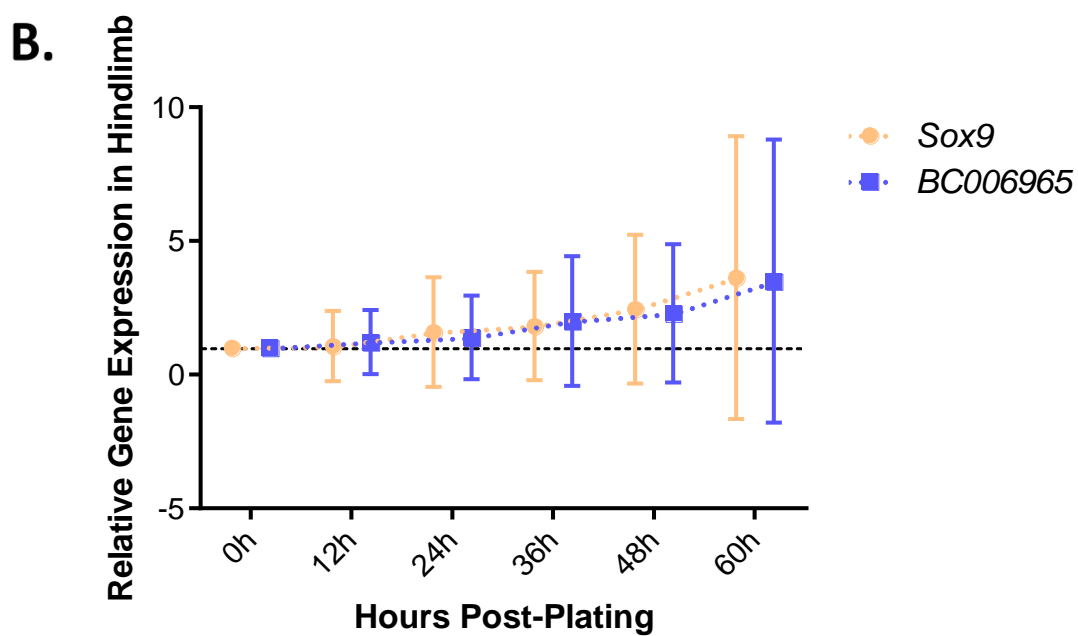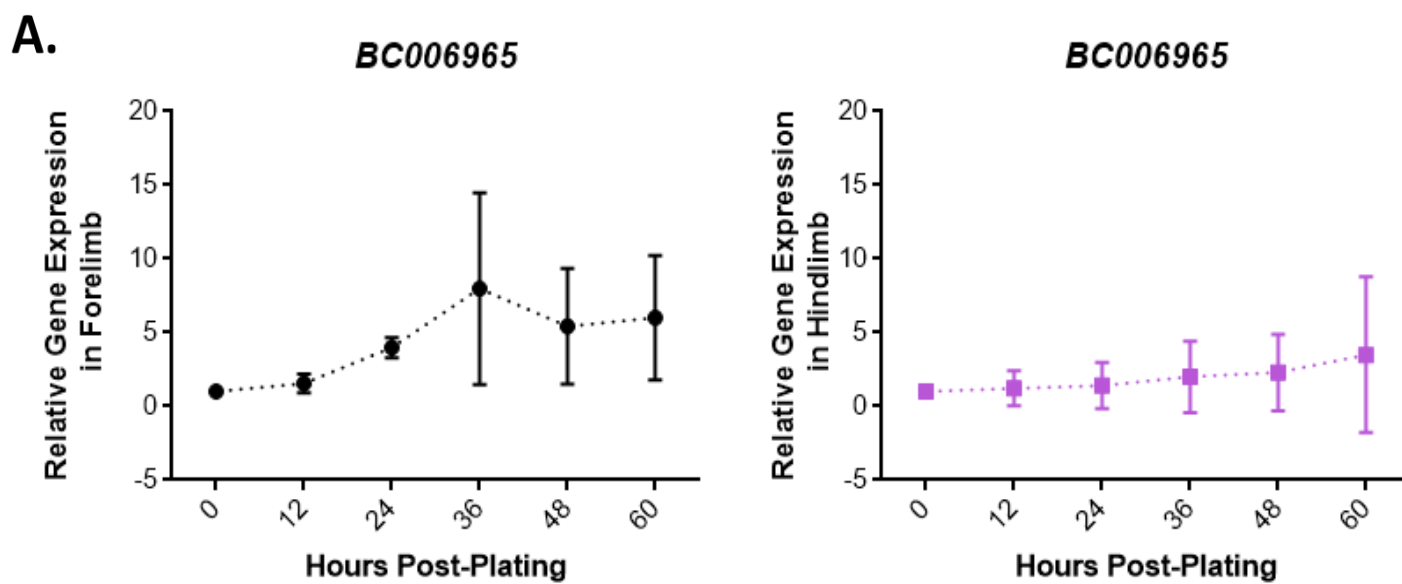
3.2 Validation of *Ctcf* inactivation in hindlimb buds of E12.5 *Ctcf^{Fl/Fl};Prx1Cre* embryos and the published phenotype.

To validate the *Ctcf^{Fl/Fl};Prx1Cre* mouse published by Soshnikova *et al*., I began by confirming the loss of CTCF protein and *Ctcf* transcript levels through immunostaining and qRT-PCR on hindlimb buds at age E12.5. The previous study had focused on the developing forelimb and reported a 90% loss of *Ctcf* mRNA in mutant forelimbs at E10.75, but had not examined the hindlimb. To confirm the loss of CTCF protein, immunofluorescent staining for CTCF was performed on cryosections from *Ctcf*-null and control hindlimb buds. Control hindlimb buds showed the ubiquitous expression of CTCF protein and knockout hindlimb buds showed a reduction in CTCF protein in the mesoderm, with normal CTCF protein expression in the surrounding ectodermal tissue (**Figure 3.4A,B**). *Ctcf* gene expression was also examined and revealed a significant 70% reduction in mRNA in the *Ctcf*-null hindlimb bud (**Figure 3.4C**). These results confirm that CTCF expression is decreased in the hindlimb buds of *Ctcf^{Fl/Fl};Prx1Cre* compared to controls.

The published phenotype of the *Ctcf^{Fl/Fl};Prx1Cre* mice was then validated at various developmental time points. At E15.5, *Ctcf*-null embryos had truncated forelimbs and shortened hindlimbs with oligodactyly, features that were also present at P0 (**Figure 3.5A,B**). The mutant embryos also presented with a brain protrusion above their skull at E15.5, which was still apparent at E18.5, but absent after birth, likely due to shearing during delivery (**Figures 3.5A,B, 3.6A,B**). Furthermore, the knockout mice were dead at birth and displayed holes of various sizes in the skull (**Figure 3.6B**). Interestingly, the *Ctcf*-null mice appeared to have looser skin than their control counterparts, as evidenced by the wrinkled skin around their necks (**Figure 3.5B**). Thus, the phenotypes of the *Ctcf^{Fl/Fl};Prx1Cre* mice are in accordance with those previously

described by Soshnikova *et al*., although this is the first report on the skull defect and potential skin abnormalities.

Figure 3.4 *Ctcf* **gene expression and CTCF protein distribution in E12.5** *Ctcf*$^{Fl/Fl}$*;Prx1Cre* **hindlimb buds.**

A. Immunofluorescent staining for CTCF in the hindlimb bud at E12.5 from control animals demonstrated uniform expression of CTCF protein throughout the developing limb. **B.** *Ctcf*-null hindlimb buds displayed a noticeable reduction in CTCF protein at E12.5 when compared to littermate controls. **C.** qRT-PCR results from whole E12.5 hindlimb buds showed a significant reduction in *Ctcf* gene expression in knockout animals when compared to littermate controls. Data represented are mean $\pm$ SD; * = P < 0.05, N=3. Scale bar = 200 μm at 10x, 100 μm at 20x zoom.

A.

DAPI   CTCF   overlay

control

10x

20x

B.

KO

10x

20x

C.
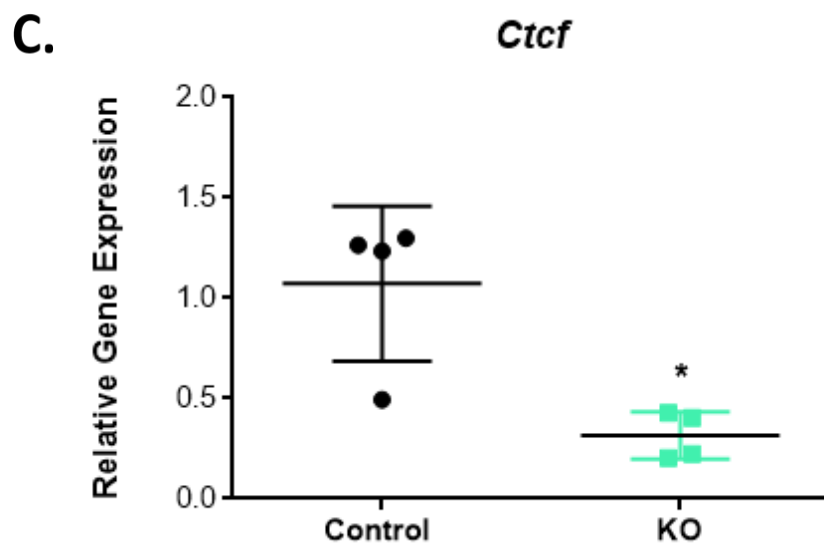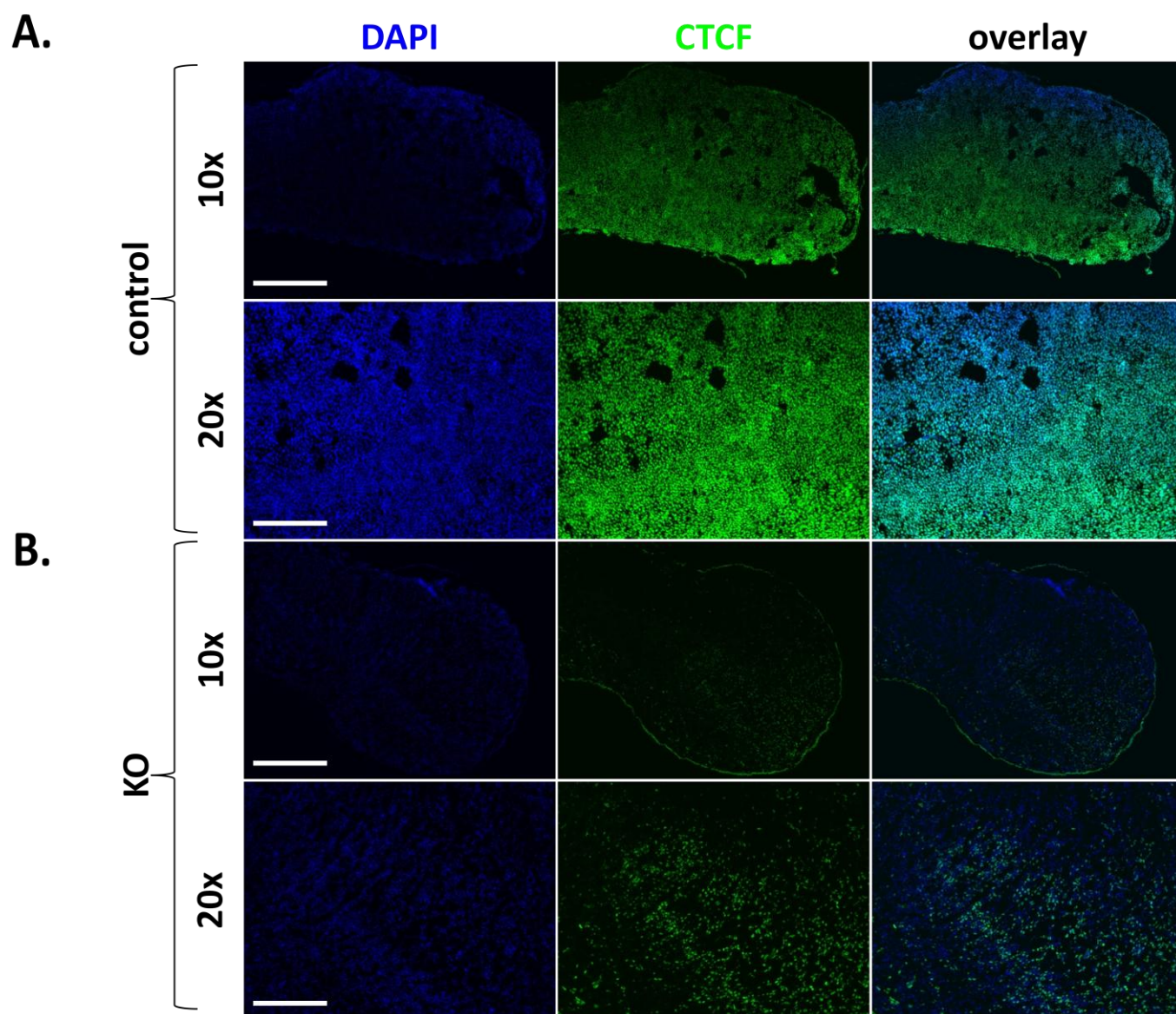
Ctcf

Figure 3.5 Gross examination of *Ctcf^Fl/Fl*;*Prx1Cre* animals and littermate controls at E15.5 and P0.

A. Whole body inspection of *Ctcf*-null animals showed a severely shortened forelimb, hindlimb abnormalities, and a protrusion above the skull at E15.5. **B.** At P0, *Ctcf*-null animals showed severe limb defects and display an open skull vault. Scale bar = 5 mm

A.

| control | KO |

E15.5

B.

P0
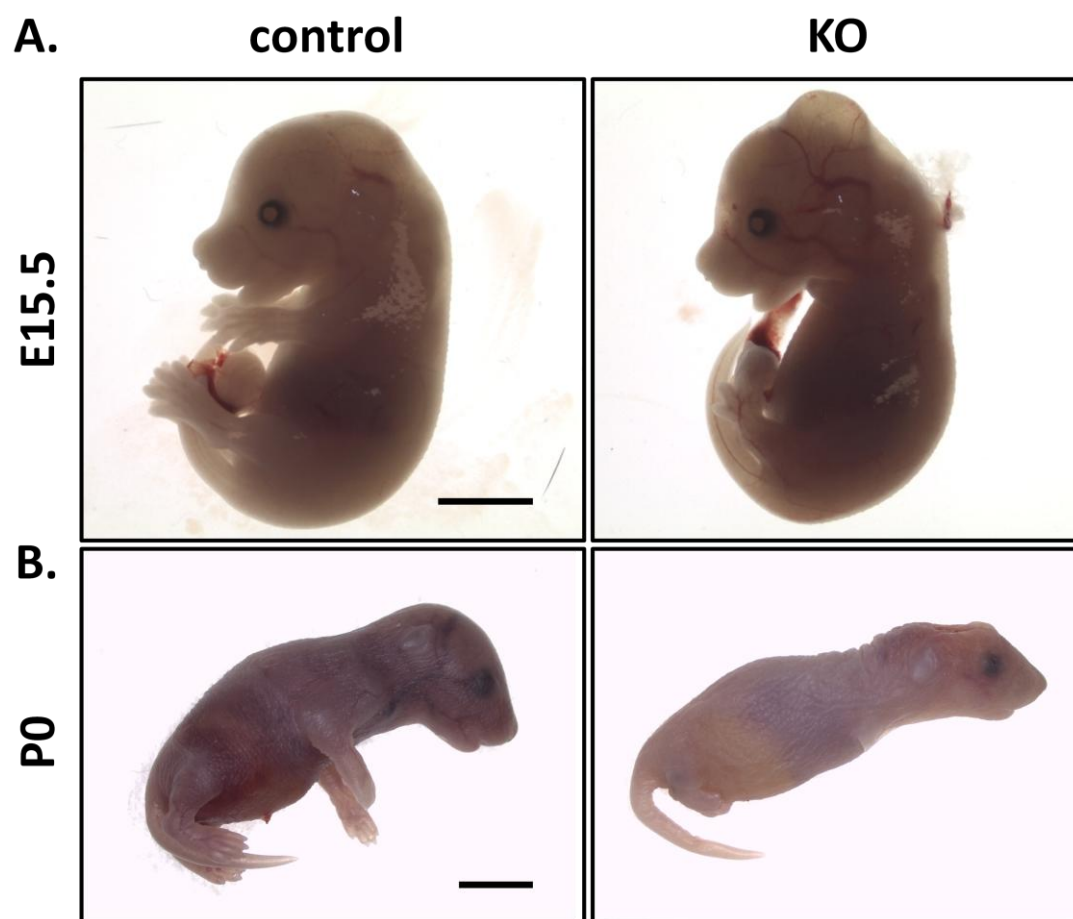
Figure 3.6 Gross examination of the skulls of *Ctcf^{Fl/Fl};Prx1Cre* mice and littermate controls at E18.5 and P0.

A. Gross examination of the heads of E18.5 pups just prior to birth indicated that tissue still covers the protruding brain in *Ctcf*-null animals. **B.** Examination of the heads after birth, however, revealed one knockout mouse with an intact brain protrusion (left), and holes of variable sizes in the skull vault of other *Ctcf*-null pups. Scale bar = 3 mm

A.

B.
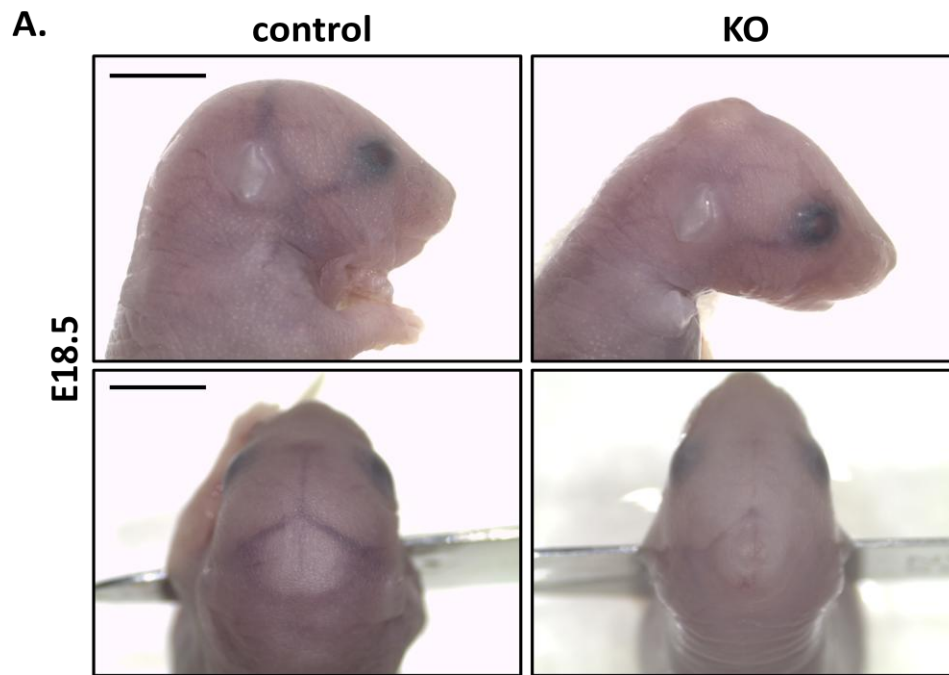
3.3 *Ctcf^{Fl/Fl};Prx1Cre* hindlimbs had significantly higher levels of apoptosis than littermate controls at E12.5, but no differences in proliferation.

Soshnikova *et al.* previously reported that *Ctcf^{Fl/Fl};Prx1Cre* mice had significantly higher levels of apoptosis in their forelimb buds at E11.5, but did not investigate cell death in the hindlimb.   To validate this finding and investigate potential apoptosis in the hindlimb, a fluorescent TUNEL stain was used in forelimb and hindlimb cryosections from E12.5 *Ctcf^{Fl/Fl};Prx1Cre* and control embryos.   As previously reported, the mutant forelimb showed significantly more apoptosis in a representative area when compared to control forelimbs **(Figure 3.7A, B)**.   Mutant hindlimbs also showed higher levels of apoptosis than corresponding littermate controls, but significantly less than mutant forelimbs **(Figure 3.7A, B)**.

A reduction in proliferation in the *Ctcf^{Fl/Fl};Prx1Cre* hindlimb could also contribute to the shortened limb phenotype.   To address this possibility, E12.5 hindlimb cryosections were fluorescently stained for proliferating cell nuclear antigen (PCNA), a marker of cellular proliferation.   Both control and *Ctcf*-null hindlimbs showed a relatively uniform distribution of PCNA protein across the entire limb bud, although the intensity of staining did appear to be variable **(Figure 3.8A)**.   Additionally, no differences were seen in protein localization at the cellular level between mutant hindlimbs and controls, and quantification of PCNA-positive cells indicated no significant difference between genotypes **(Figure 3.8B, C)**.   These results indicate that the shortened hindlimb phenotype may be caused, in part, by increased apoptosis in the early limb bud.

Figure 3.7   Fluorescent TUNEL staining for apoptosis in E12.5 limb bud sections from *Ctcf$^{Fl/Fl}$;Prx1Cre* **mice and control littermates.**

A. Fluorescent TUNEL staining of forelimb and hindlimb revealed cells positively stained for apoptosis in frozen sections from E12.5 knockout mice. **B.** Quantification of TUNEL-positive cells in a representative area (white box) showed a significant increase in apoptosis in the *Ctcf*-null animals when compared to controls, and significantly increased apoptosis in the knockout forelimb when compared to the knockout hindlimb. All data represented are mean ± SD; a, b, c = $P < 0.05$ using a two-way ANOVA, columns with different letters are significantly different from one another; N=3. Scale bar = 250 μm

A.

control KO

forelimb

TUNEL/DAPI

hindlimb

B.
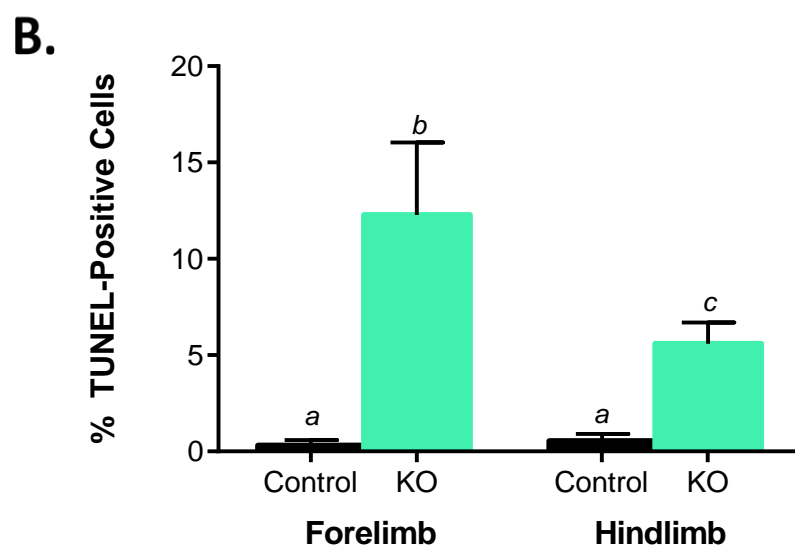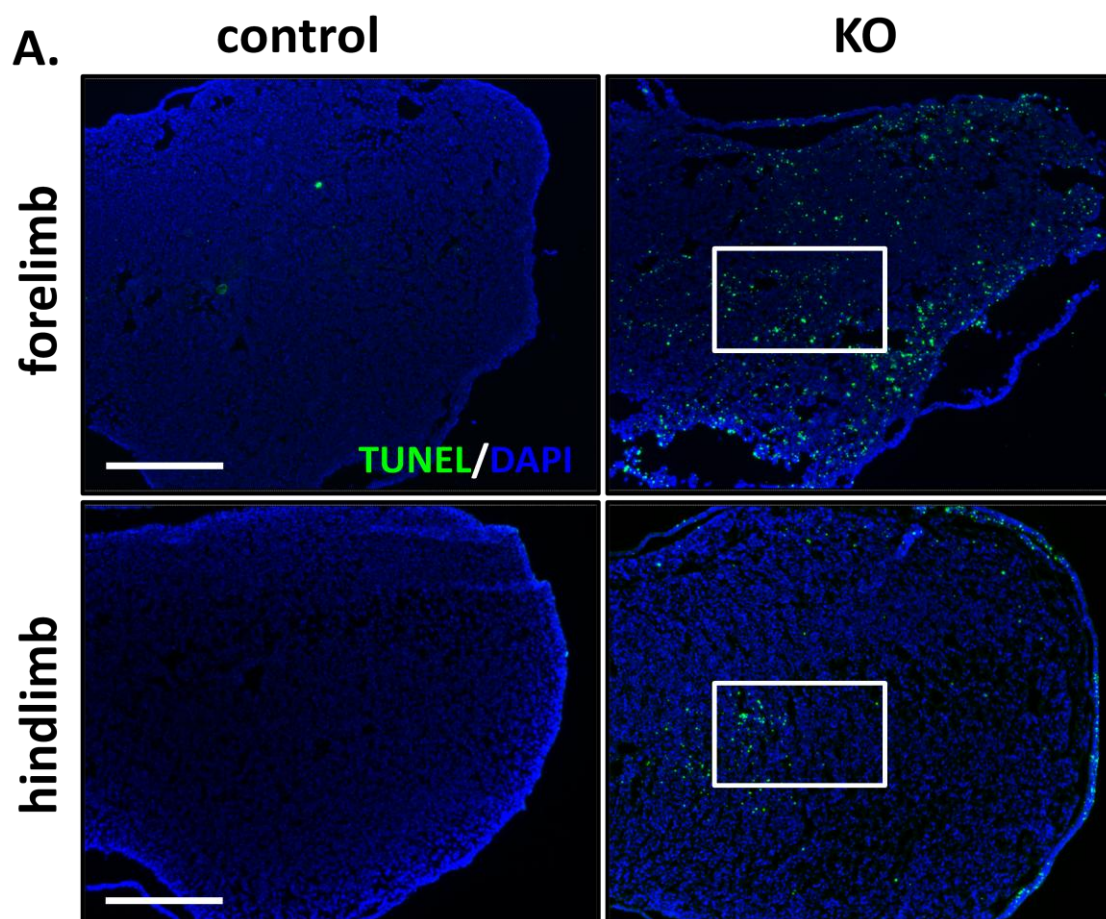
Figure 3.8 Immunofluorescent staining for proliferating cell nuclear antigen (PCNA) in E12.5 hindlimb bud sections from control and *Ctcf^{Fl/Fl};Prx1Cre* mice.

Representative images demonstrating the immunolocalization of PCNA within the E12.5 hindlimb of *Ctcf*-null animals and control littermates. **A.** 10x magnification showed an even distribution of the protein throughout the hindlimb bud. **B.** 20x magnification showed no differences between control and knockout animals. **C.** No differences were seen in the percentage of PCNA-positive cells in a representative area from *Ctcf*-null animals and control littermates. N=3, scale bar = 250 μm

A.

DAPI | PCNA | overlay

control

KO

B.

control

KO

PCNA/DAPI

C.

% PCNA-Positive Cells
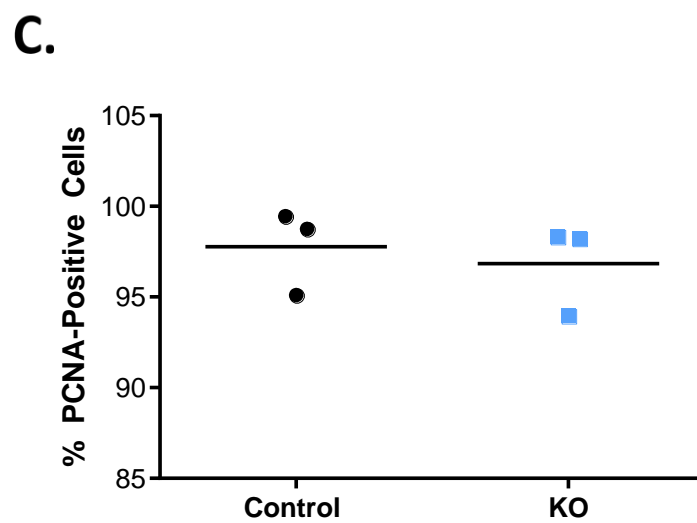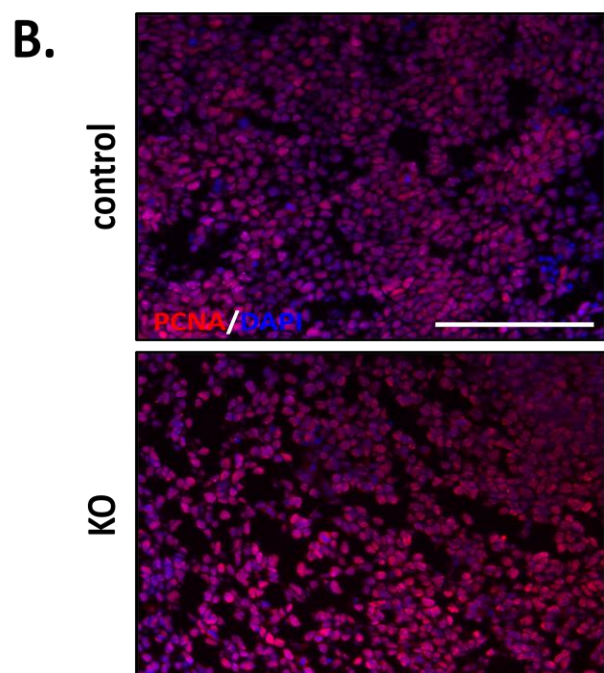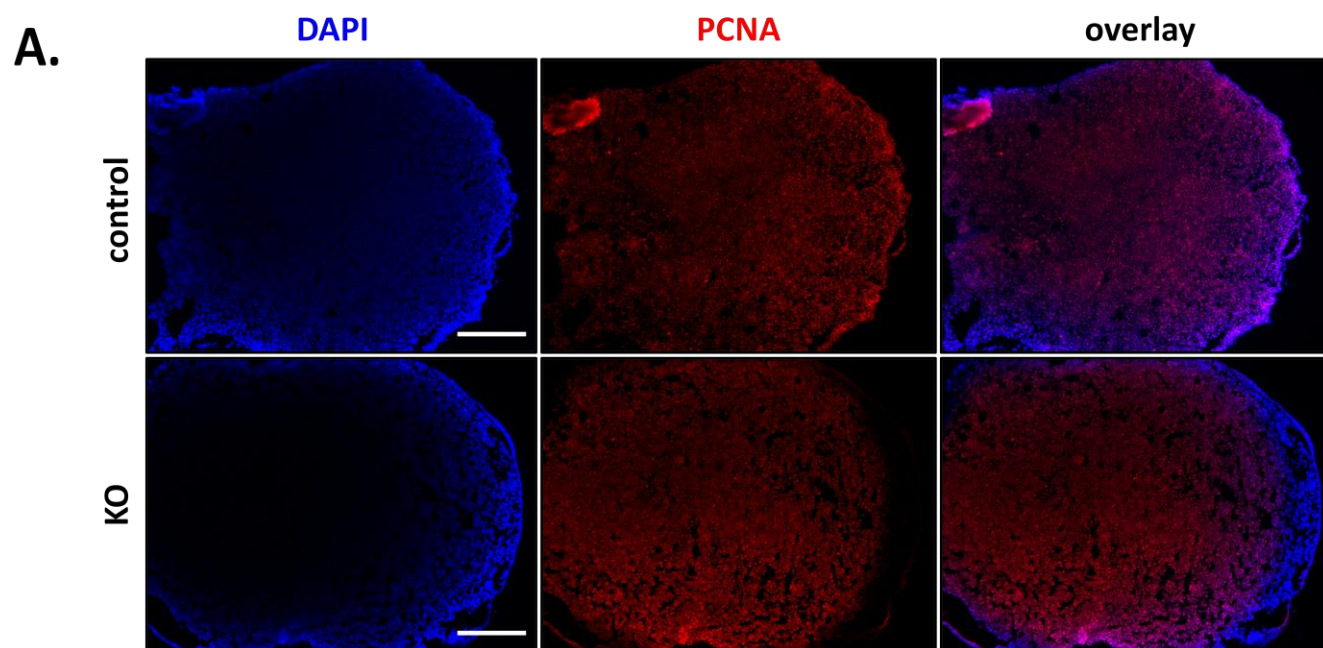
3.4 *Ctcf$^{Fl/Fl}$;Prx1Cre* **hindlimbs showed no differences in SOX9 localization when compared to littermate controls at E12.5, and no differences in relative *Sox9* transcript levels at E12.5 or E13.5.**

Our unpublished data indicate an important role for CTCF in maintaining expression of the *Sox9* gene, therefore examining *Sox9* transcript and SOX9 protein levels in *Ctcf$^{Fl/Fl}$;Prx1Cre* mice was important. To investigate possible alterations in SOX9 protein localization in *Ctcf$^{Fl/Fl}$;Prx1Cre* animals, E12.5 hindlimb cryosections were fluorescently stained for SOX9. Both control and *Ctcf*-null hindlimb buds showed strong localization of SOX9 protein to the developing digit rays **(Figure 3.9A)**. Furthermore, no significant differences were observed in protein localization at the cellular level between mutant hindlimbs and controls, and this observation was further underscored by quantification of SOX9-positive cells in a representative area, indicating no significant difference between genotypes **(Figure 3.9B, C)**.

To confirm the immunohistochemical results, qRT-PCR was performed on RNA from whole *Ctcf*-null and control hindlimb buds at E12.5 and E13.5. An examination of *Sox9* gene expression confirmed no significant difference in expression levels between mutant and control limb buds at either E12.5 or E13.5 **(Figure 3.10A)**. Based on these data, I conclude that at this time point, CTCF does not appear to play a role in regulating *Sox9* transcript or *SOX9* protein levels.

Figure 3.9   Immunofluorescent staining for SOX9 in E12.5 hindlimb bud sections from *Ctcf^{Fl/Fl}*;*Prx1Cre* **animals and control littermates.**

Representative images demonstrating the immunolocalization of SOX9 within the E12.5 hindlimb of *Ctcf*-null animals and control littermates. **A.** 10x magnification showed protein localization to the developing digit rays. **B.** 20x magnification showed no noticeable differences in a representative area from *Ctcf*-null animals and control littermates. **C.** No differences were seen in the percentage of SOX9-positive cells in a representative area from *Ctcf*-null animals and control littermates. N=3, scale bar = 250 μm

A.

DAPI   SOX9   overlay

control

KO

B.

control

KO

SOX9/DAPI

C.

% SOX9-Positive Cells
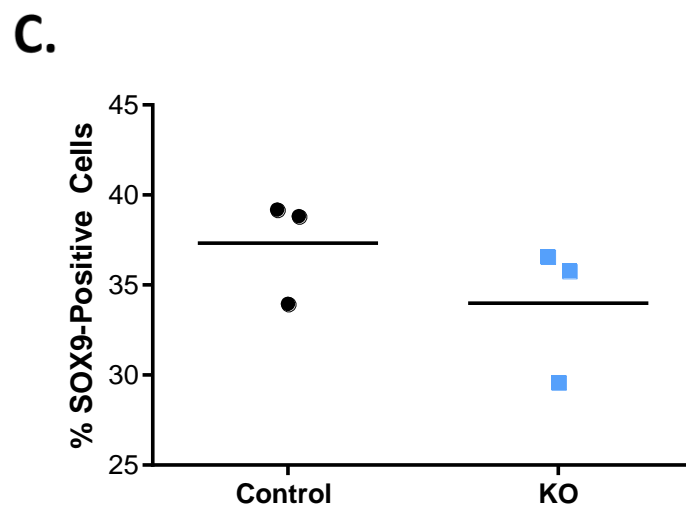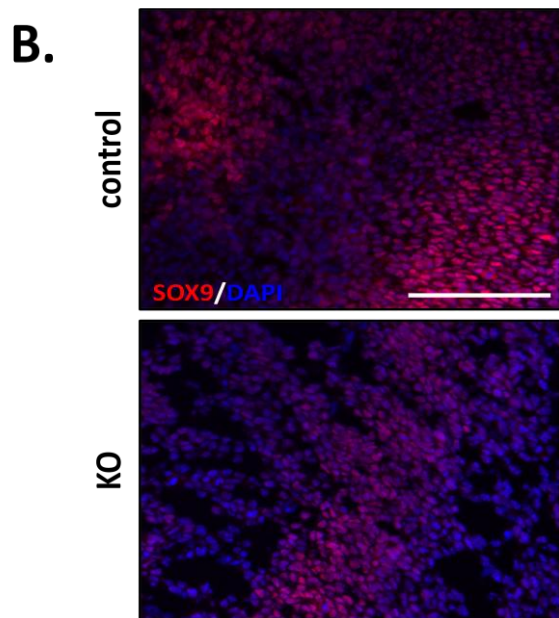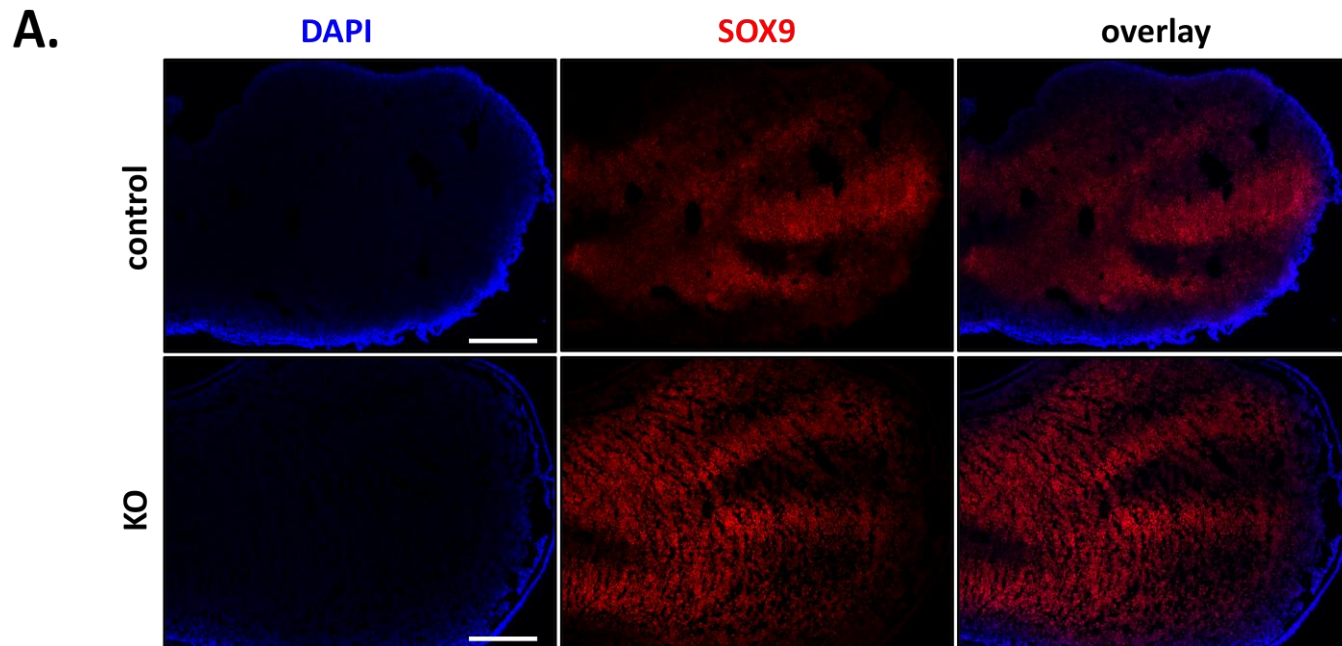
Control   KO

Figure 3.10   Relative gene expression of *Sox9, Sox5* and *Sox6* in *Ctcf$^{Fl/Fl}$;Prx1Cre* and control hindlimb buds at E12.5 and E13.5.

Whole hindlimb buds were removed from *Ctcf*-null and control animals at ages E12.5 and E13.5. RNA was collected and qRT-PCR was utilized to examine *Sox* trio gene expression. **A.** No significant difference in *Sox9* expression was seen between control and mutant hindlimb buds at either time point. **B.**   *Sox5* expression was significantly reduced in mutant hindlimb buds at E13.5 when compared to control hindlimb buds at E12.5. **C.** No significant difference in *Sox6* expression was seen between control and mutant hindlimb buds at either time point.   All data represented are mean $\pm$ SD; * = P < 0.05 using a two-way ANOVA; N=4.

A.

B.

C.
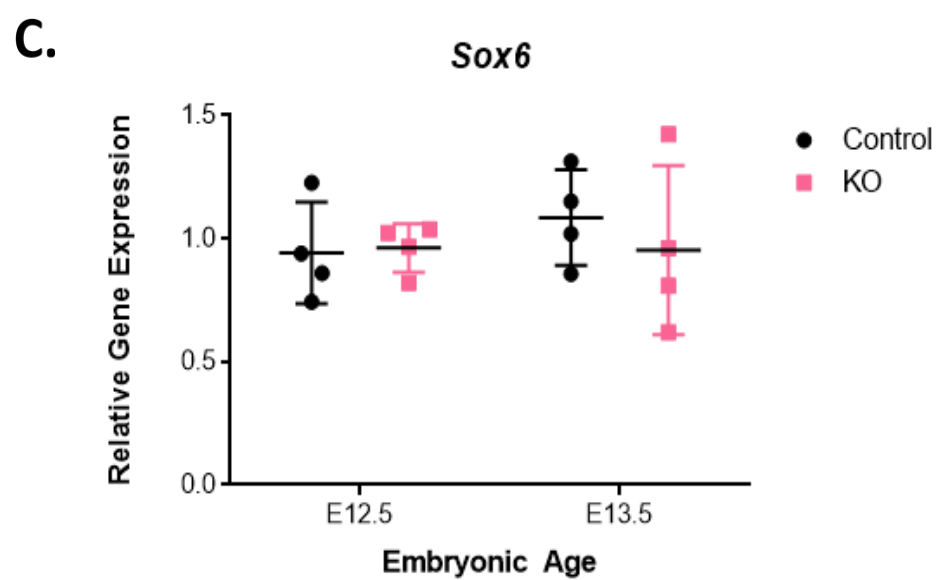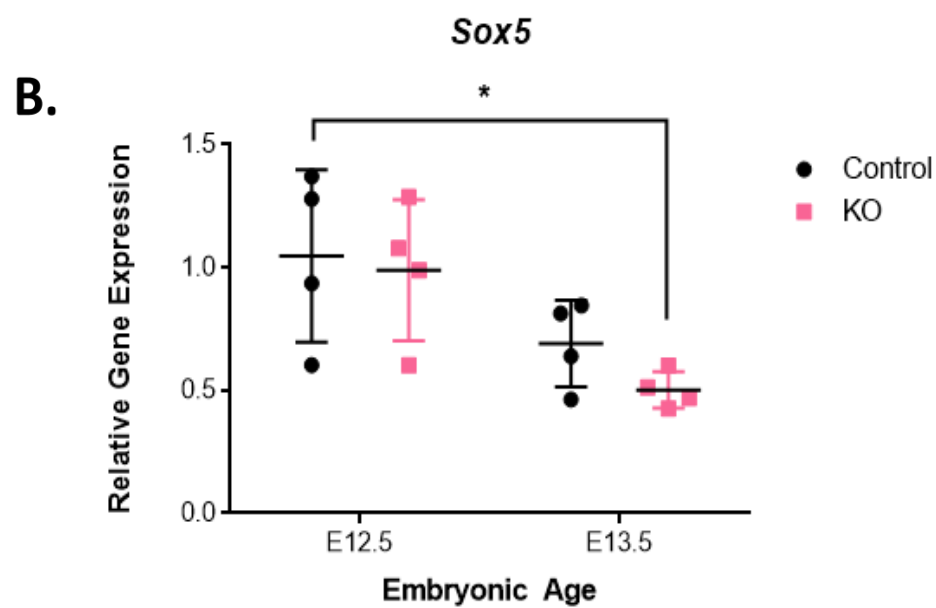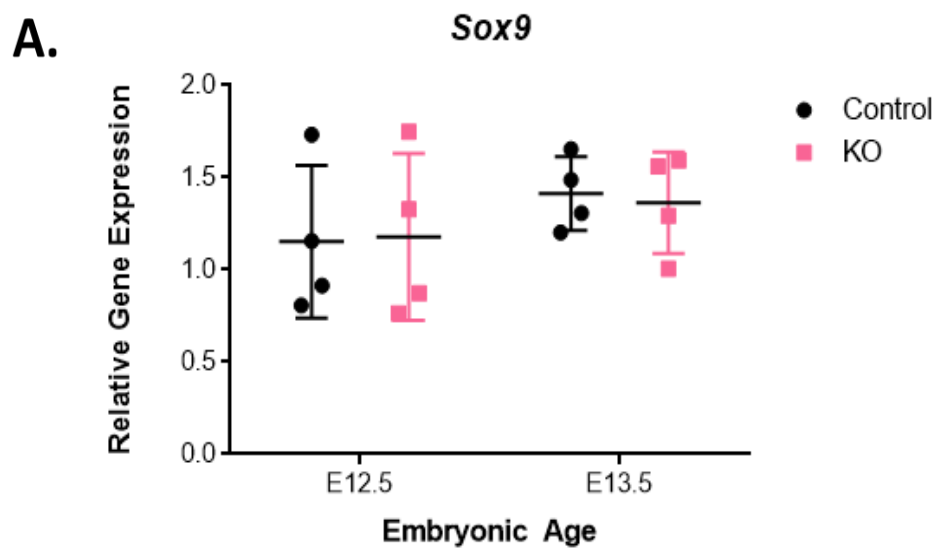
3.5 Relative gene expression levels of *Sox5*, *Sox6*, and *Col2a1* were unchanged between *Ctcf$^{Fl/Fl}$;Prx1Cre* hindlimb buds and controls at E12.5 and E13.5, while *Acan* transcript levels increased in control limb buds over time.

To follow up on potential changes in chondrogenic differentiation and ECM genes expressed downstream of *Sox9*, transcript levels of *Sox5*, *Sox6*, *Col2a1*, and *Acan* were evaluated in control and *Ctcf$^{Fl/Fl}$;Prx1Cre* hindlimb buds at E12.5 and E13.5. *Sox5* expression was unchanged between control and *Ctcf*-null hindlimb buds at E12.5 and E13.5 (**Figure 3.10B**). *Sox5* expression also showed a trend towards slightly reduced expression in E13.5 control hindlimbs compared to E12.5 controls, however this trend was not statistically significant (**Figure 3.10B**). Finally, *Sox6* expression appeared unchanged between *Ctcf*-null and control hindlimb buds at both E12.5 and E13.5 time points (**Figure 3.10C**). Additionally, no significant differences were noted in relative *Col2a1* expression between knockout and control hindlimb buds at either E12.5 or E13.5 time points (**Figure 3.11A**). However, there was a significant increase in *Acan* expression in control hindlimb buds from E12.5 to E13.5 (**Figure 3.11B**). The mutant hindlimb buds failed to show this same increase in expression across time, instead maintaining almost identical *Acan* expression levels at both E12.5 and E13.5 (**Figure 3.11B**), suggesting that CTCF may have a role in regulating *Acan* expression at this time point. Results also suggested, however, that the loss of CTCF did not affect expression of *Sox5, Sox6*, and *Col2a1* at this embryonic stage.

Figure 3.11 Relative transcript levels of *Col2a1* and *Acan* in E12.5 and E13.5 control and *Ctcf$^{Fl/Fl}$;Prx1Cre* hindlimbs.

Whole hindlimb buds were removed from *Ctcf*-null and control animals at E12.5 and E13.5. RNA was collected and qRT-PCR was utilized to examine *Col2a1* and *Acan* chondrocyte marker gene expression. **A.** No significant difference in *Col2a1* expression was seen between control and mutant hindlimb buds at either time point, although there appeared to be a trend showing reduced *Col2a1* expression in mutant hindlimb buds at E13.5. **B.** *Acan* expression was increased significantly from E12.5 to E13.5 in control hindlimb buds, however there was no significant increase in *Acan* expression in the mutant hindlimb buds at E13.5 when compared with E12.5 control hindlimbs. All data represented are mean ± SD; * = P < 0.05 using a two-way ANOVA; N=4.

A.
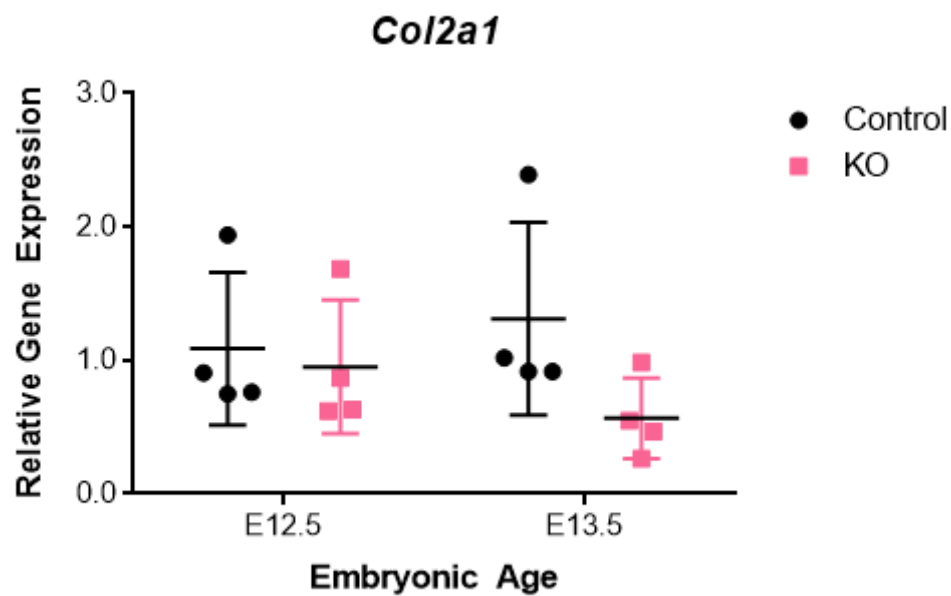
B.
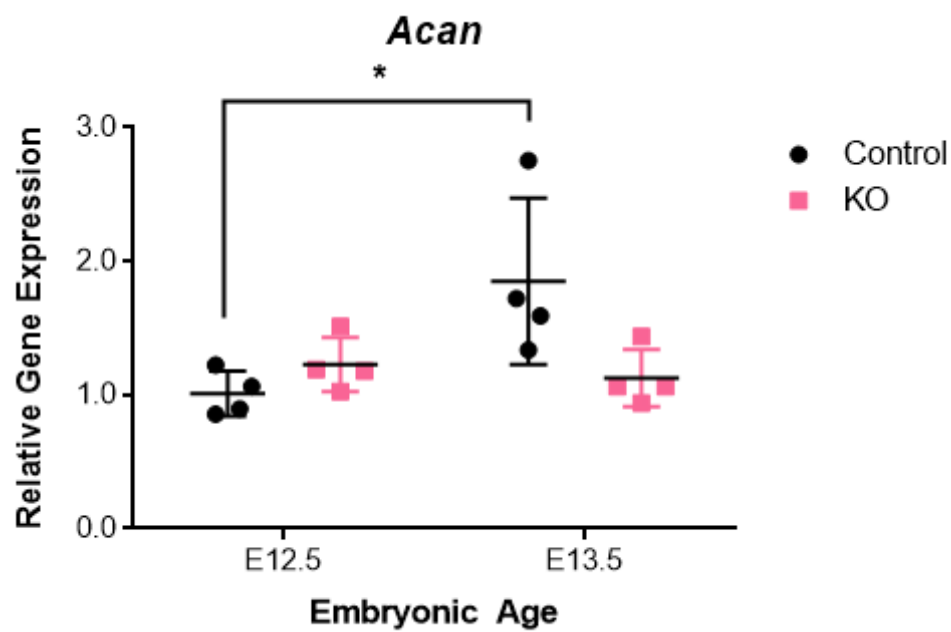
3.6 Long non-coding RNAs at the *Sox9* gene locus, *BC006965* and *D17Rik,* showed relative expression changes between genotypes or developmental stages in the hindlimb bud, while expression levels of *Kcnj2* and *Slc39a11*, genes bordering the *Sox9* locus, did not change.

To follow up on potential expression changes in the two long non-coding RNAs present at the *Sox9* locus, *BC006965* and *D17Rik* transcript levels were examined in *Ctcf^{Fl/Fl};Prx1Cre* and control hindlimbs at E12.5 and E13.5. *BC006965* showed no difference in expression between *Ctcf*-null hindlimb buds and control at each time point examined; however, both control and mutant hindlimb buds showed significantly increased gene expression at E13.5 when compared to E12.5 (**Figure 3.12A**). Furthermore, *D17Rik* expression showed no significant changes between genotypes at either E12.5 or E13.5 (**Figure 3.12B**). Furthermore, I examined potential expression changes in genes bordering the *Sox9* locus, *Kcnj2* and *Slc39a11*. While there were no significant differences in relative *Kcnj2* expression between *Ctcf*-null and control hindlimbs at both time points, there was a trend towards a slight reduction in gene expression in mutant hindlimbs at E13.5 (**Figure 3.13A**). No significant changes were observed in *Slc39a11* expression levels between either genotypes or developmental stages (**Figure 3.13B**). Taken together, these results suggest that CTCF does not appear to play a critical role in regulating either lncRNAs at the *Sox9* gene locus, or neighbouring genes.

Figure 3.12 Relative gene expression of long non-coding RNAs *BC006965* and *D17Rik* in *Ctcf^{Fl/Fl}*;*Prx1Cre* and control hindlimb buds at ages E12.5 and E13.5.

Whole hindlimb buds were removed from *Ctcf*-null and control animals at E12.5 and E13.5. RNA was collected and qRT-PCR was utilized to examine gene expression of the long non-coding RNAs *BC006965* and *D17Rik*. **A.** While *BC006965* expression did not differ between genotype at either time point, both control and knockout hindlimb buds showed significantly increased expression at E13.5 when compared to E12.5. **B.** *D17Rik* expression was significantly higher in the mutant hindlimb bud at E12.5 when compared to control hindlimb buds at E13.5. All data represented are mean $\pm$ SD; *, a, b = $P < 0.05$ using a two-way ANOVA, columns with different letter labels are significantly different; N=4.

A.
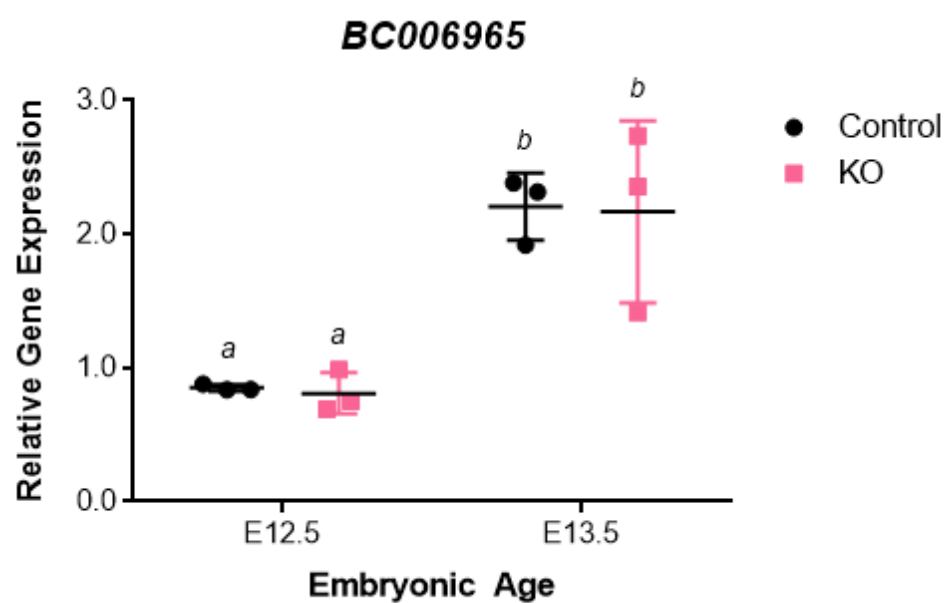
B.
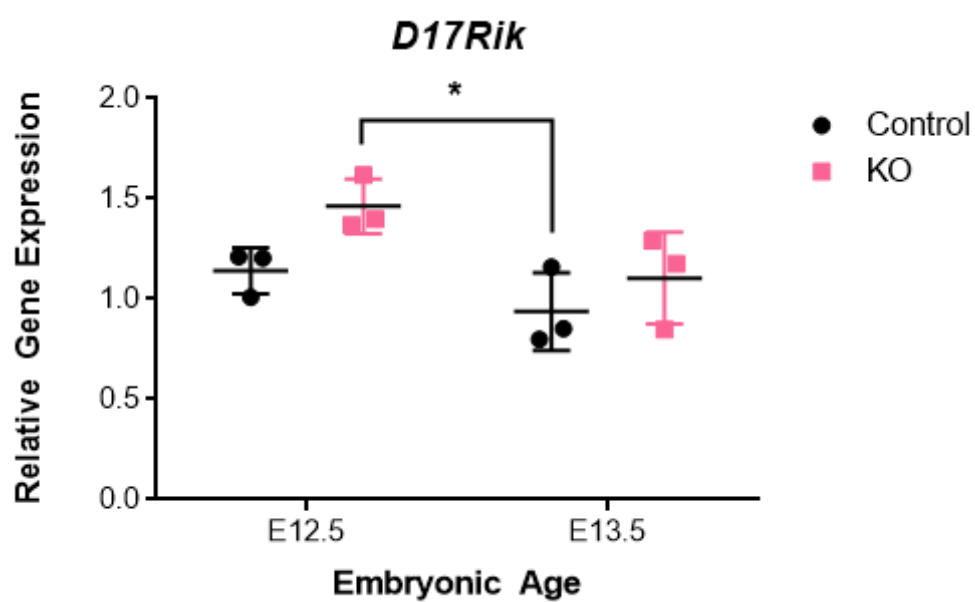
Figure 3.13 Relative transcript levels of the genes bordering the *Sox9* gene locus, *Kcnj2* and *Slc39a11*, in E12.5 and E13.5 *Ctcf*$^{Fl/Fl}$;*Prx1Cre* and control hindlimb buds.

Whole hindlimb buds were removed from *Ctcf*-null and control animals at E12.5 and E13.5. RNA was collected and qRT-PCR was utilized to examine *Kcnj2* and *Slc39a11* gene expression. **A.** No significant difference in *Kcnj2* expression was seen between control and mutant hindlimb buds at either time point, although there appeared to be a trend showing reduced *Kcnj2* expression in mutant hindlimb buds at E13.5. **B.** No significant difference in *Slc39a11* expression was seen between control and mutant hindlimb buds at either time point. All data represented are mean ± SD; * = P < 0.05 using a two-way ANOVA; N=3.

A.

Kcnj2

B.

Slc39a11
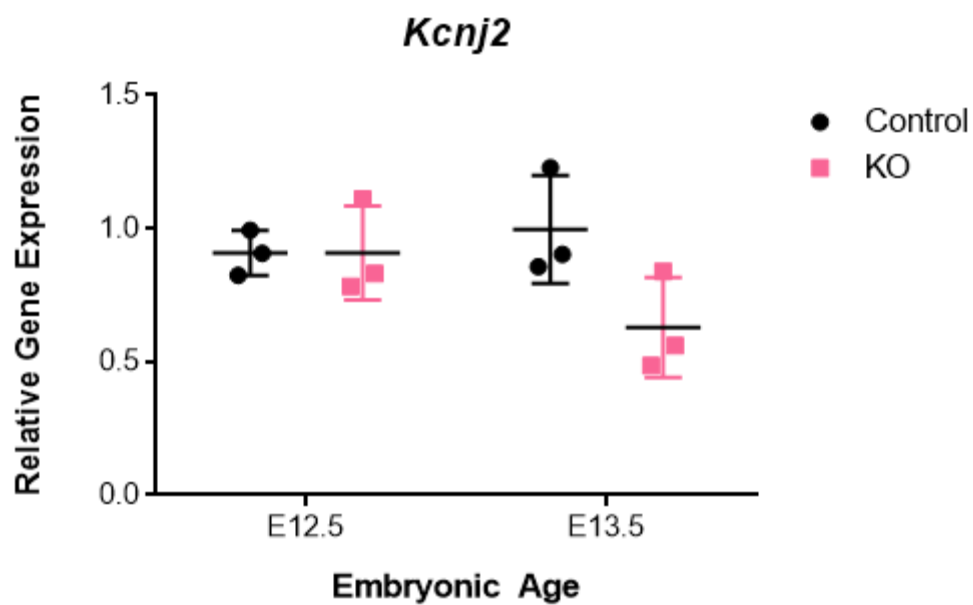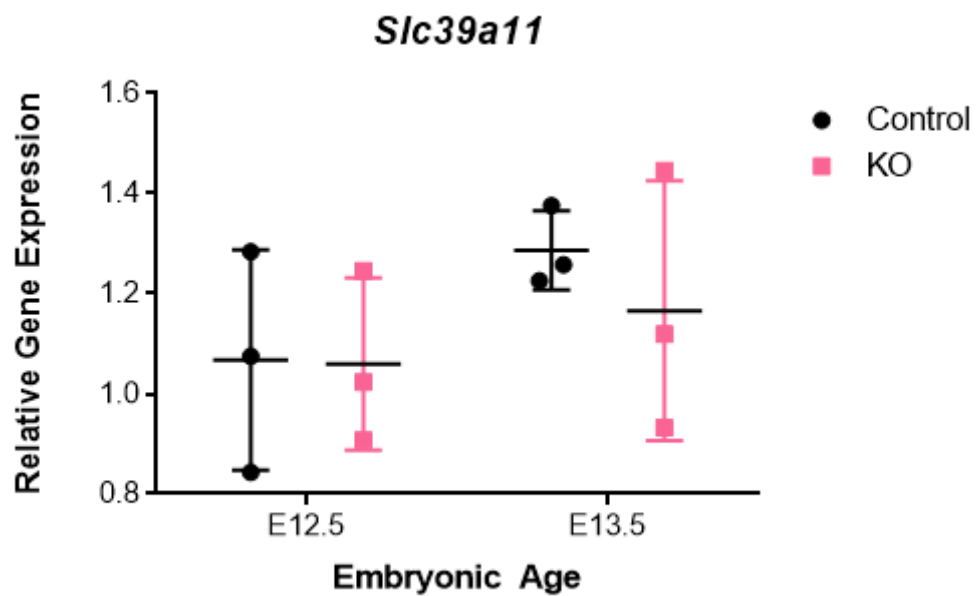
3.7 No gene expression changes were seen in *Cdh-2* or *Cdh-11* in hindlimb buds of *Ctcf*-null or control animals at E12.5 or E13.5.

Proper cell-cell adhesion is critical to mesenchymal condensations and chondrogenesis and involves the expression of cell-cell adhesion molecules Cadherin-2 and Cadherin-11. To investigate potential aberrations in cell-cell adhesion within the $Ctcf^{Fl/Fl}$;*Prx1Cre* hindlimb, transcript levels of *Cdh-2* and *Cdh-11* were evaluated E12.5 and E13.5 in mutant and control hindlimb buds. No discernible trends or significant differences were discovered in relative expression levels for both genes when examining *Ctcf*-null and control hindlimb buds at either time point (**Figure 3.14A, B**). Therefore, these findings suggest that CTCF does not appear to play a significant role in regulating cadherin-mediated cell-cell adhesion in the developing hindlimb at this time point.

Figure 3.14 Relative gene expression of *Cdh-2* and *Cdh-11* in control and *Ctcf^{Fl/Fl};Prx1Cre*

hindlimb buds at E12.5 and E13.5.

Whole hindlimb buds were removed from *Ctcf*-null and control animals at E12.5 and E13.5.
RNA was collected and qRT-PCR was utilized to examine *Cdh-2* and *Cdh-11* gene expression.
A. No significant difference in *Cdh-2* expression was seen between control and mutant hindlimb
buds at either time point. **B.** No significant difference was seen in *Cdh-11* expression between
control and mutant hindlimb buds at either time point. All data represented are mean ± SD; * =
$P < 0.05$ using a two-way ANOVA; N=4.

A.
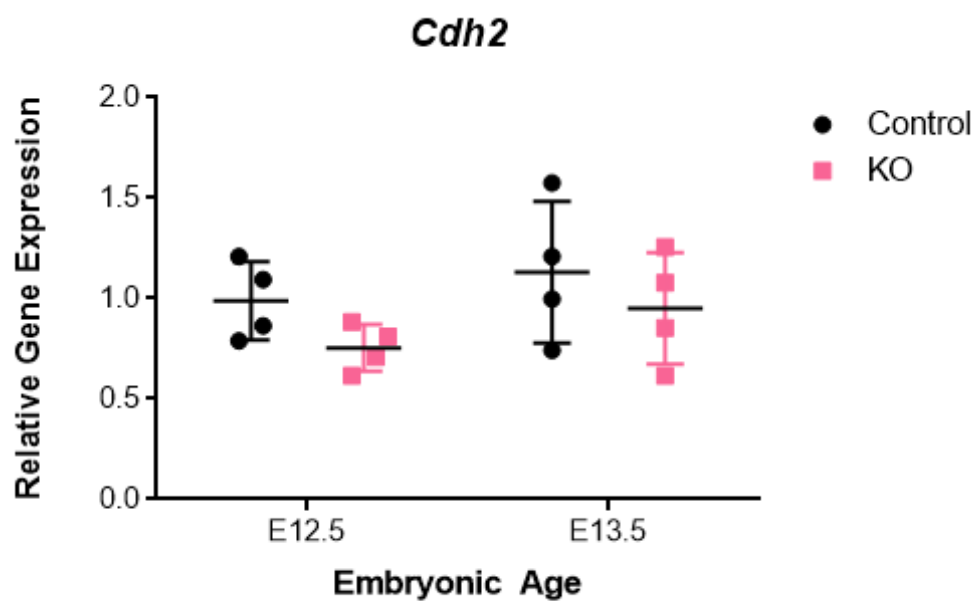
B.
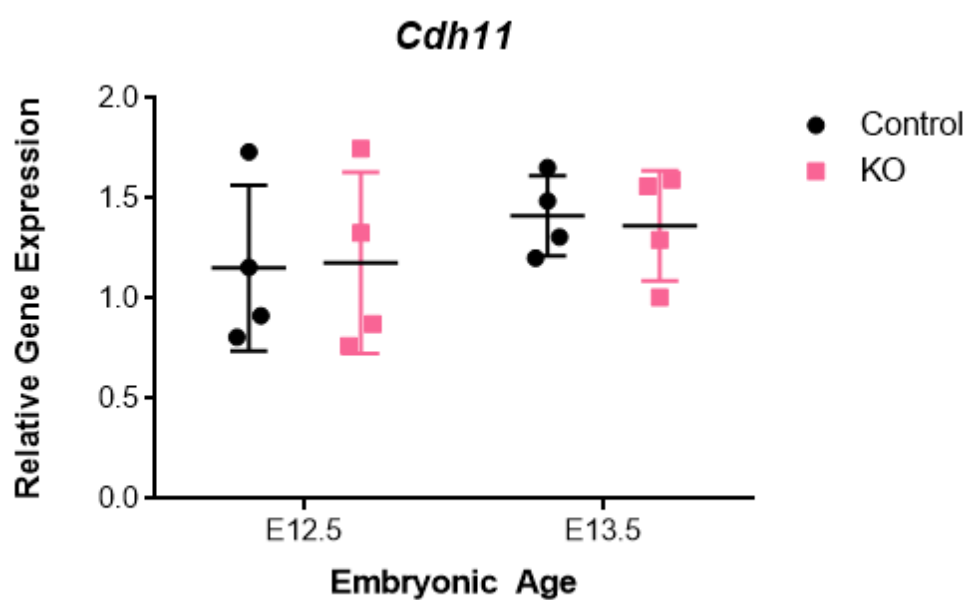
3.8   Tibiae from E15.5 *Ctcf^{Fl/Fl};Prx1Cre* mice displayed severe growth plate and mineralization defects.

To gain a better understanding of growth plate structure and development in the *Ctcf^{Fl/Fl};Prx1Cre* long bones, mutant and control tibiae were collected at E15.5 then sectioned and stained with Safranin-O/Fast Green, Von Kossa, or p57 antibody that detected cartilaginous proteoglycans, cartilage mineralization, and terminally differentiated cells, respectively. Safranin-O/Fast Green staining confirmed that mutant tibiae were severely shortened at E15.5, and had few hypertrophic chondrocytes **(Figure 3.15)**. When stained by Von Kossa, *Ctcf*-null tibiae also showed no mineralized cartilage when compared to control littermates **(Figure 3.16A)**.   Finally, immunostaining was performed for p57, a marker of cell cycle exit and prehypertrophic chondrocyte differentiation. Mutant tibiae showed a shortened region of cells positively-stained for p57 **(Figure 3.16B)**. The resting and proliferating zones of the growth plate, which did not show p57 staining, were then measured and showed significantly shorter zone length than control littermates **(Figure 3.16C)**. Notably, the tissue surrounding the tibia also stained positively for p57. These results indicate that *Ctcf*-null mice have delayed chondrocyte differentiation, as well as shorter proliferative and hypertrophic zones, which likely contributes to the shortened hindlimb length.

Figure 3.15 Safranin-O/Fast Green staining of *Ctcf^{Fl/Fl};Prx1Cre* and control tibiae at E15.5.

Sections from E15.5 tibiae were stained with Safranin-O/Fast Green and morphology was examined. Representative images demonstrate tibiae from *Ctcf*-null animals (outlined in yellow rectangle) were shorter than control littermates and possess shorter resting, proliferative, and hypertrophic zones. Scale bar = 100 μm
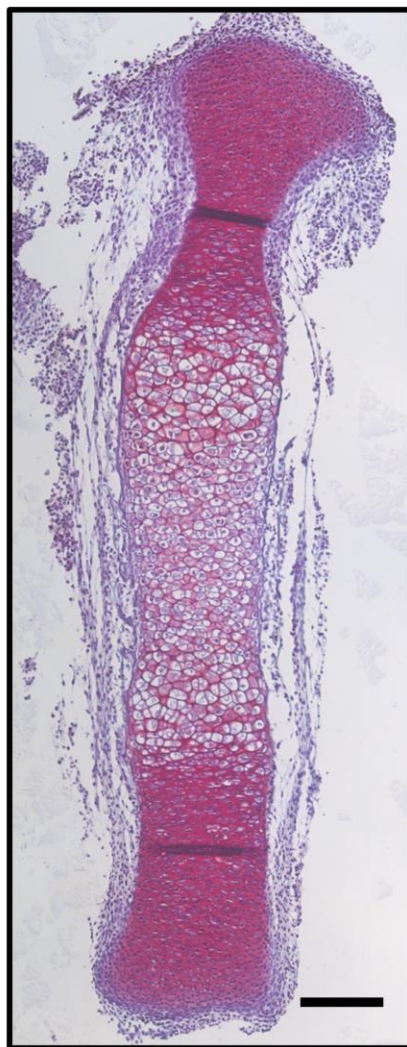
control   **KO**

Safranin-O
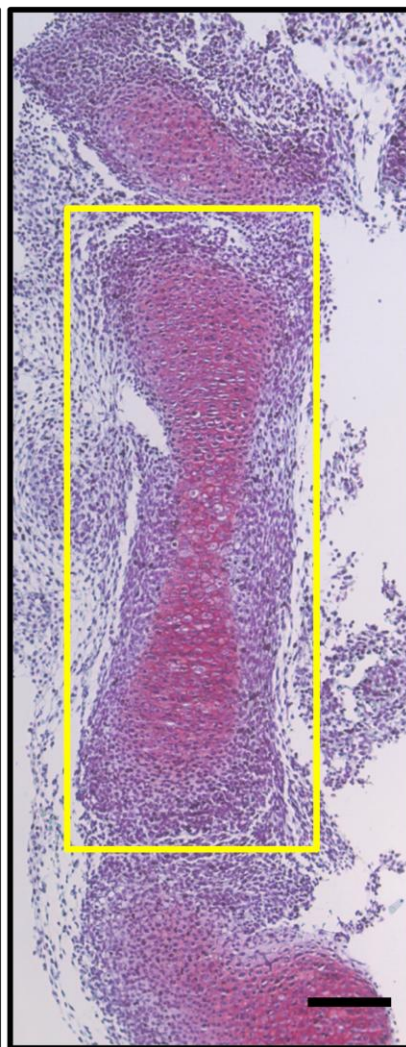
Figure 3.16   Von Kossa staining and immunostaining for p57 in *Ctcf^{Fl/Fl};Prx1Cre* and control littermate tibiae at E15.5.

Sections of E15.5 *Ctcf*-null and control tibiae were stained with Von Kossa for mineralized cartilage, and terminal differentiation marker p57. **A.** Von Kossa staining demonstrated that mutant tibiae lack all mineralization (brown staining) at E15.5. **B.** Immunostaining for p57 in the prehypertrophic and hypertrophic chondrocytes showed reduced staining in mutant tibiae when compared to control littermates. Resting and proliferating zones are indicated by a yellow bar. **C.** Quantification of the resting and proliferating zones demonstrated a significant decrease in zone length in mutant tibiae, when compared with controls. Data represented are mean $\pm$ SD; $*$ = $P < 0.05$ using an unpaired T-test; N=3. Scale bar = 100 μm

A.   **control**   **KO**

Von Kossa
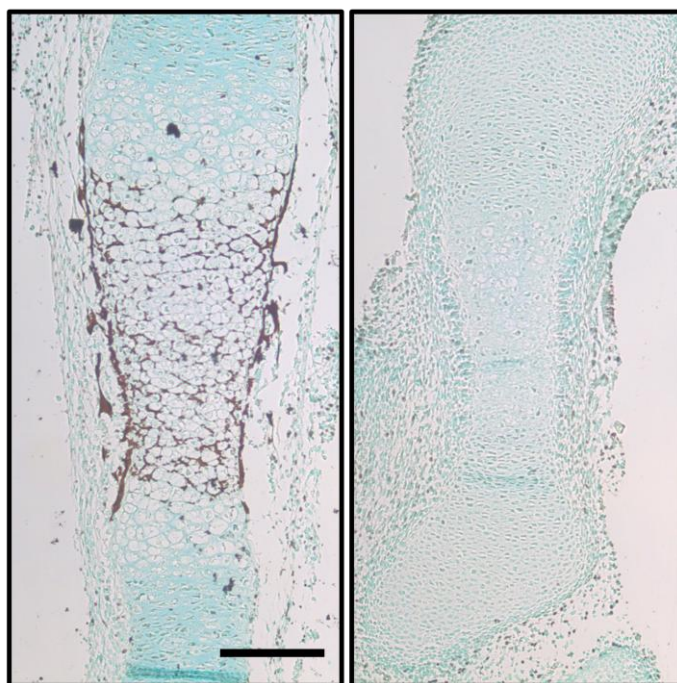
B.   **control**   **KO**

p57
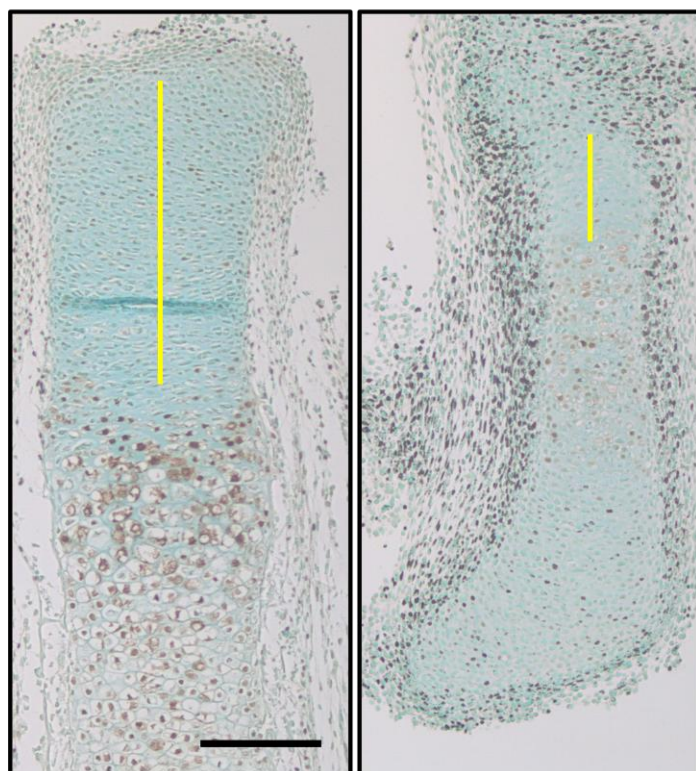
C.

Length of Resting and Proliferative Zones

Control
KO
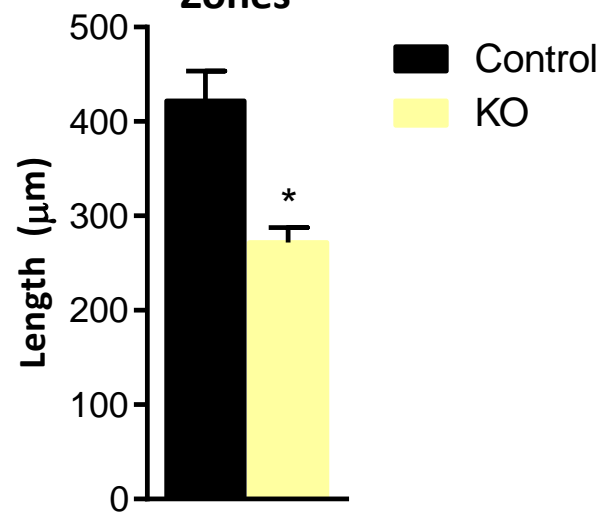
3.9 *Ctcf^{Fl/Fl};Prx1Cre* skeletons showed severely malformed hindlimbs with oligodactyly and reduced mineralization in the long bones, and calvarial defects at P0.

To examine the skeletal defects in more detail, whole skeletons from *Ctcf^{Fl/Fl};Prx1Cre* and control animals were collected at P0 and stained with Alcian blue/Alizarin red for cartilage and mineralized bone, respectively. The *Ctcf*-null skeletons confirmed the truncated forelimbs and severely shortened hindlimbs with oligodactyly **(Figure 3.17A, B)**. The total length of each of the long bones was measured and results indicated that the femur, tibia, and fibula are significantly shorter in *Ctcf*-null animals than in control littermates **(Figure 3.17C)**. Measurements of the mineralized zone as a percentage of total bone length also indicated that the mutant tibia and fibula have significantly less mineralization than controls, even after normalization to total length **(Figure 3.17D)**. An examination of the skull also showed severe calvarial defects. *Ctcf*-null mice were missing portions of the interparietal (IP), parietal (P), frontal (F), and nasal (N) skull plates, which are labeled with corresponding letters on the control skull **(Figure 3.18A)**. Both the palate and jaw of the mutant animals, however, appeared morphologically normal when compared to controls **(Figure 3.18B, C)**. Therefore, these results suggest a role for CTCF in both endochondral and intramembranous ossification, and *Ctcf^{Fl/Fl};Prx1Cre* mice appear to have delayed chondrocyte differentiation and cartilage mineralization.

Figure 3.17 Skeletal preparations of *Ctcf^{Fl/Fl};Prx1Cre* animals and littermate controls at P0, double stained with Alcian blue and Alizarin red.

Skeletons from *Ctcf*-null animals and control littermates were stained with Alcian blue and Alizarin red, then examined and measured for morphological differences in long bone length and mineralized zone. **A.** Whole skeletons of the *Ctcf*-null animals had severely truncated forelimbs and shortened hindlimbs. **B.** Hindlimbs of mutant animals were shorter than control littermates and also presented with oligodactyly. **C.** Mutant femurs, tibiae, and fibulae were significantly shorter than in littermate controls. **D.** The tibia and fibula in mutant hindlimbs had significantly shorter mineralized zones, as a proportion of total bone length, when compared to littermate controls. All data represented are mean ± SD, * = P < 0.05 using an unpaired T-test; N=3. Scale bar = 5 mm for whole body and 3 mm for hindlimbs

A. control   KO

whole body

B.

hindlimb

C.

D.
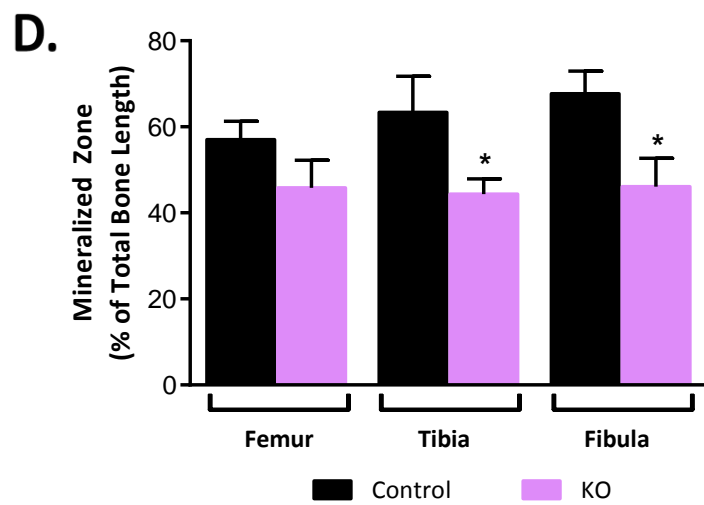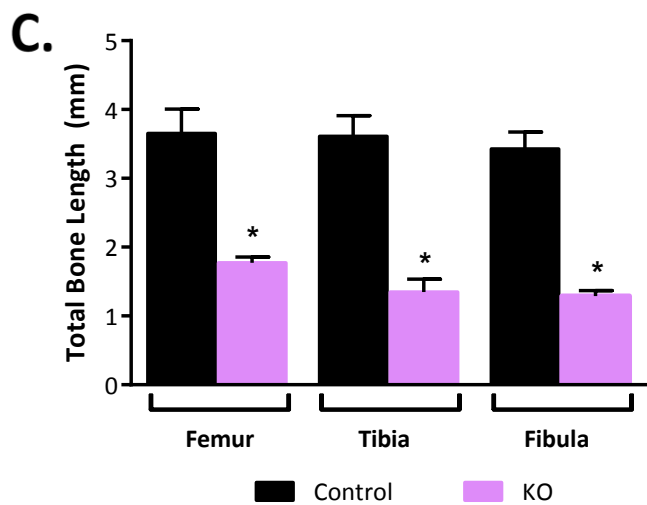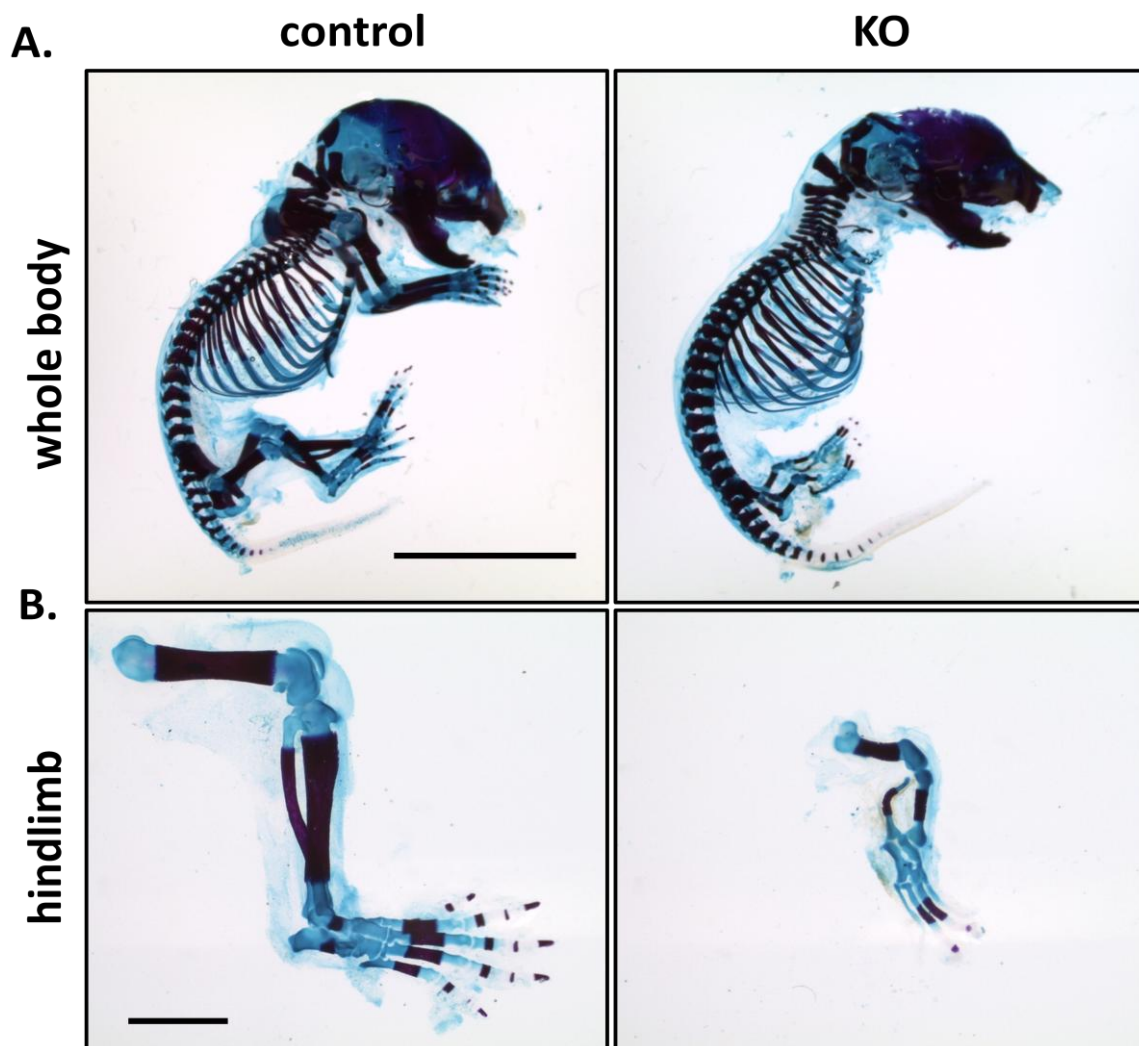
Figure 3.18 Comparison of the skull vault, palate, and jaw between *Ctcf^{Fl/Fl};Prx1Cre* mice and control littermates at P0.

Skeletons from *Ctcf*-null animals and control littermates were stained with Alcian blue and Alizarin red, then examined for morphological differences. **A.** *Ctcf*-null animals displayed severe skull defects and an open skull vault missing portions of the interparietal (IP), parietal (P), frontal (F) and nasal (N) skull plates, labeled with the corresponding letter on the control skull, and outlined in yellow in the mutant skull. **B.** No differences were noted in the palates of mutant animals and controls. **C.** No differences were noted in jaw size or morphology of mutant animals and controls. N=3, scale bar = 3 mm
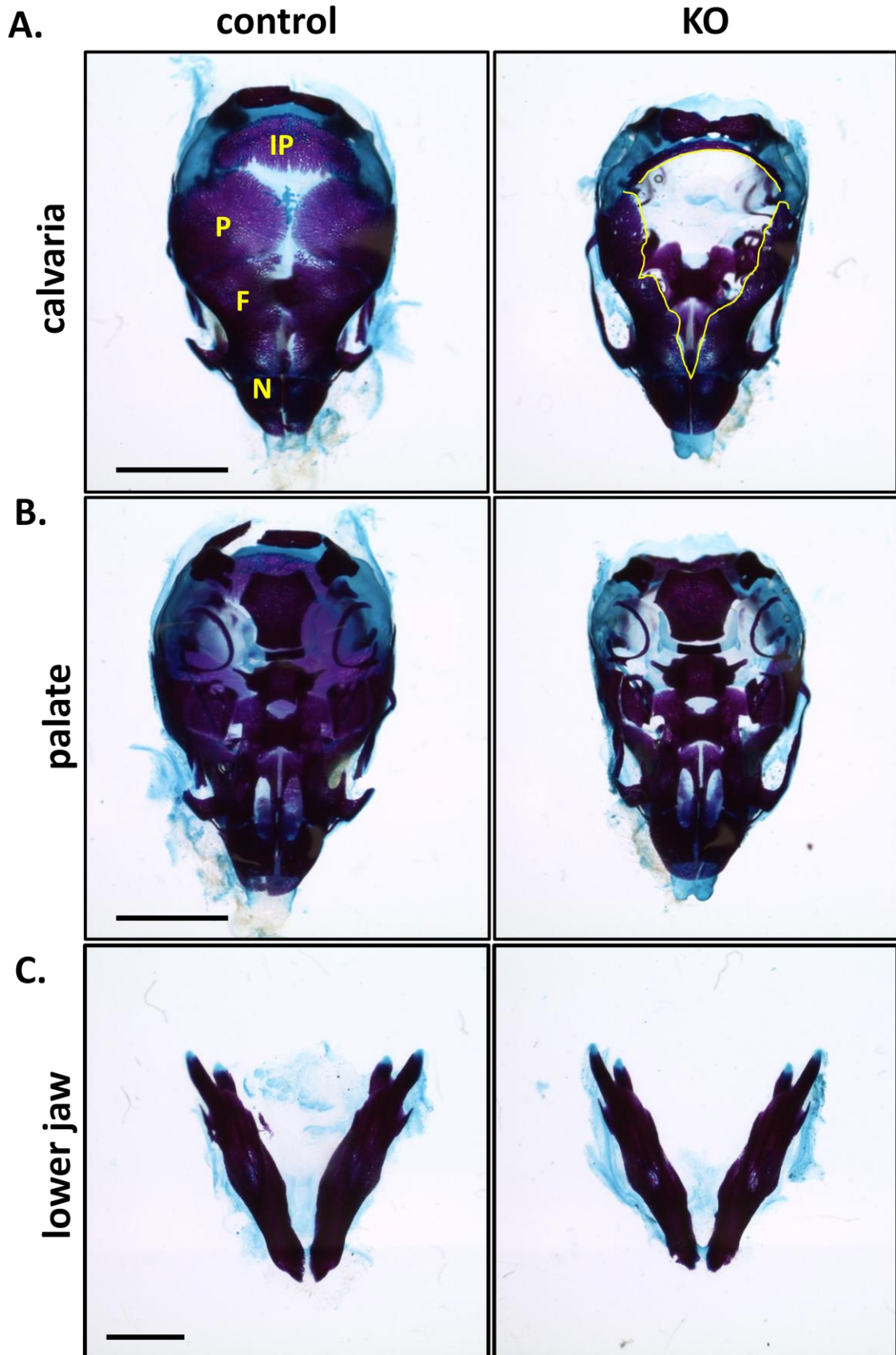
4.0 DISCUSSION

4.1   Summary of Results

The relationship between epigenetic regulation and developmental biology is becoming increasingly complex and exciting. However, the role of chromatin organizers, such as CTCF, in the development of the hindlimb and skeleton is currently unknown. Previous studies by Soshnikova *et al.* demonstrated the importance of CTCF in cell survival in the developing forelimb of *Ctcf^{Fl/Fl};Prx1Cre* mice[83]. Moreover, unpublished studies from our lab using *Ctcf^{Fl/Fl};Col2Cre* mice (which lack CTCF in developing cartilage) indicate an important role for CTCF in maintaining *Sox9* expression in cartilage (Bush *et al.*, in prep.). These mice present with a slight, but significant reduction in both *Sox9* gene and SOX9 protein expression, altered growth plates with fewer and smaller hypertrophic chondrocytes, and campomelia - a phenotype that resembles the human disease Campomelic Dysplasia. The *Ctcf^{Fl/Fl};Col2Cre* mouse model, however, involves *Ctcf* deletion after the onset of *Sox9* expression. Therefore, both these CTCF-deficient animal models, as well as *de novo CTCF* mutations in humans, suggest a role for CTCF in regulating limb and cartilage development. I used the published model of CTCF deficiency in the developing limb, as presented by Soshnikova *et al*., to examine the effects of *Ctcf* deletion in the developing hindlimb[83]. My objective was to investigate the effects of CTCF deletion on chondrogenesis and skeletal development in the hindlimb of *Ctcf^{Fl/Fl};Prx1Cre* mice, which presents an intermediate phenotype between the severely malformed *Ctcf^{Fl/Fl};Prx1Cre* forelimb and the mildly disfigured *Ctcf^{Fl/Fl};Col2Cre* hindlimb.

Micromass cultures from wild-type forelimbs and hindlimbs were utilized to explore the possibility of differential chondrogenic gene expression between limbs as a contributor to phenotypic activity. Gene expression analysis was performed by qRT-PCR on key chondrogenic genes, and the long non-coding RNA encoded at the *Sox9* locus, *BC006965*. Results revealed a

statistically significant 3.5-fold increase in *Sox9* expression in the developing forelimb 48 hours after plating, and 4-fold increase at 60 hours post-plating, while expression in the hindlimb appeared to increase over time, but these results were not statistically significant. *Sox5* expression differed between the limbs, showing an increase in expression in the forelimb immediately after plating, then maintenance of expression levels from 24 to 36h before the transcript levels returned to baseline at 60 hours post-plating. The hindlimb, however, showed a steady increase in *Sox5* transcript levels over the time course, and reached a higher transcript level after 60 hours than the forelimb. *Sox6* expression also showed a trend towards increasing expression in both the forelimb and hindlimb over the time course. Additionally, both *Col2a1* and *Acan* show steadily increasing expression in both forelimb and hindlimb cultures across all time points. *Col2a1* expression is significantly higher at 60 hours post-plating in both forelimbs and hindlimbs, while *Acan* expression is significantly higher only in the forelimb at 60 hours. Finally, I investigated expression levels of the long non-coding RNA *BC006965* to examine a potential relationship with the regulation of *Sox9*. Transcript levels also show trends towards increasing expression over time in both forelimb and hindlimb micromass cultures. Interestingly, when expression patterns of *Sox9* and *BC006965* are compared in hindlimb micromass cultures, they reveal almost identical changes in transcript levels at each time point. Taken together, these results suggests that chondrogenesis appears to occur more rapidly in developing forelimbs, and expression of the *Sox9* and *BC006965* genes may be regulated in the same manner. These phenotypic differences between forelimbs and hindlimbs, provide a further rationale for examining the development of the hindlimb in *Ctcf^{Fl/Fl};Prx1Cre* mice.

Loss of CTCF in *Ctcf^{Fl/Fl};Prx1Cre* mice was validated through immunostaining and qRT-PCR. *Ctcf*-null hindlimbs at age E12.5 revealed a 70% decrease in *Ctcf* mRNA, and a reduction

of CTCF protein in the limb bud mesoderm. An examination of gross morphology revealed the severe limb malformations previously published, as well as a novel skull phenotype, discussed below. Apoptosis in the developing hindlimb was then examined using a fluorescent TUNEL kit on E12.5 limb cryosections, which demonstrated that the mutant hindlimb has significantly more apoptosis than littermate controls, but significantly less apoptosis than corresponding mutant forelimbs. The levels of cell death in the forelimb and hindlimb appear to correlate with the severity of the overall limb phenotype, suggesting that it may contribute to the phenotypic differences seen between limbs. Another possible cause of limb shortening is a defect in proliferation, which I examined in the E12.5 hindlimb. Staining for PCNA revealed no significant differences in proliferation at that time point; thus it does not appear that defects in cell proliferation are contributing to the phenotype at this embryonic stage.

Given our unpublished data (Bush *et al.*, in prep) indicating a role for CTCF in maintaining *Sox9* gene expression, investigating *Sox9* transcript and SOX9 protein levels in $Ctcf^{Fl/Fl};Prx1Cre$ hindlimbs was important. Immunofluorescent staining for SOX9 protein at E12.5 revealed no significant differences in SOX9 protein distribution between control and mutant animals at that time. *Sox9* transcripts also showed no differences between genotypes at E12.5 and E13.5.

To investigate potential changes in chondrogenic marker genes, ECM genes, and genes related to the *Sox9* locus, transcript levels of *Sox5, Sox6, Col2a1, Acan, BC006965, D17Rik, Kcnj2,* and *Slc39a11* were analyzed in control and *Ctcf*-null animals at ages E12.5 and E13.5. No changes in *Sox5* or *Sox6* transcript levels were seen between genotypes at either time point. *Col2a1* expression is also not different between genotypes or time, although mutant hindlimbs at E13.5 do appear to show a trend toward lower expression. In contrast, *Acan* expression is

significantly higher in the E13.5 control limb bud, compared to E12.5 controls, but there is no corresponding increase in expression in the mutant hindlimb at E13.5. Both *BC006965* and *D17Rik* demonstrate no significant difference across time or genotype in expression, although there is a marked trend towards increased *BC006965* expression in both control and mutant hindlimbs at E13.5. The two genes bordering the Sox9 locus, *Kcnj2* and *Slc39a11*, were also examined, but showed no significant changes, suggesting they are regulated independently of *Sox9*. Finally, gene expression changes for *Cdh-2* and *Cdh-11* were also examined to rule out potential defects in cell-cell adhesion in early mesenchymal condensations, but no significant differences were seen. Taken together, these results suggest that CTCF may have a role in regulating *Acan* expression in early limb development, however it does not contribute to regulation of other cartilage and ECM markers, as well as *Sox9* locus-related genes and cell-cell adhesion markers examined.

To gain a better understanding of the role of CTCF in growth plate structure and development, *Ctcf^{Fl/Fl};Prx1Cre* long bones were examined via histology at E15.5. Tibial sections were stained with Safranin-O/Fast Green, and Von Kossa, and immunohistochemistry was performed for cell cycle exit marker p57. Safranin-O staining revealed disorganized growth plates with fewer hypertrophic chondrocytes in the mutant tibia. Mutant tibiae also failed to mineralize at E15.5, although control counterparts demonstrated significant mineralization. p57 staining and measurements of the resting and proliferating zones also revealed that each growth plate zone is significantly shorter in *Ctcf*-null animals. Therefore, *Ctcf^{Fl/Fl};Prx1Cre* mice appear to have a delay in chondrocyte differentiation and severe growth plate defects.

Finally, the skeletons were examined at P0 using Alcian blue/Alizarin red double staining for cartilage and mineralized bone. After birth, *Ctcf*-null mice show severe hindlimb defects and

oligodactyly, and the femur, tibia, and fibula are all significantly shorter than control counterparts. Interestingly, P0 tibiae show mineralization, however the amount of mineralization as a proportion of total bone length is significantly reduced in the tibia and fibula of *Ctcf*-null mice. Furthermore, mutant mice are missing portions of each of the interparietal, parietal, frontal, and nasal skull plates. These findings suggest that CTCF is critical for proper chondrogenesis and hindlimb development, as well as skull development.

4.2 Contribution to the Current State of Knowledge of CTCF in Hindlimb Development and Potential Future Studies

The role of CTCF in limb development was first described by Soshnikova *et al.* in 2010 through analysis of the developing forelimb in *Ctcf^{Fl/Fl};Prx1Cre* mice. *Ctcf*-null forelimbs were described as undergoing massive amounts of apoptosis, which was correlated to up-regulation of the pro-apoptotic gene *Puma* (p53 up-regulated modulator of apoptosis), contributing to the severe defect and total abrogation of limb growth. Additionally, although genome-wide studies identified CTCF binding sites within and surrounding the *HOXD* cluster, Soshnikova *et al*. found that the *Hoxd* genes were not regulated by CTCF. These studies, however, did not investigate the effects of CTCF inactivation in the developing hindlimb, which presented with a less severe phenotype. Moreover, unpublished data from our lab suggest a role of CTCF in maintaining *Sox9* expression, however the effects of deletion of *Ctcf* prior to the onset of chondrogenesis have not yet been investigated. Therefore, the studies presented in this thesis are the first to examine the hindlimb of *Ctcf^{Fl/Fl};Prx1Cre* mice in detail at the molecular level.

I confirmed that, as presented by Soshnikova *et al.*, loss of CTCF in the developing forelimb leads to an increase in apoptosis, which we also observe in the mutant hindlimb[83]. However, the reduced amount of apoptosis in the *Ctcf*-null hindlimb (compared to the mutant

forelimb) might account for its less severe phenotype. I speculate that the reduced level of apoptosis seen in the hindlimb is correlated with reduced Cre expression in the hindlimb compared to the forelimb[83,90,91]. The population of cells that escape Cre inactivation and are not *Ctcf*-null in the hindlimb is therefore greater that in the corresponding forelimb, which likely contributes to the less severe phenotype. I speculate that the increased cell death in the hindlimb may also be correlated to up-regulation of the p53 effector PUMA, as seen in the mutant forelimb. CTCF is a known repressor of *PUMA*, and has been shown to bind with cohesin intragenically at the *PUMA* locus to dampen expression of *PUMA*[92]. Moreover, PUMA was also up-regulated in the *Ctcf*-null developing forebrain studied by Watson *et al.*, and deletion of both *Ctcf* and *Puma* in the embryonic brain rescued *Ctcf*-null neuroprogenitor apoptosis[84]. Taken together these results suggest that loss of CTCF in the hindlimb may lead to PUMA up-regulation, thereby causing apoptosis. Further investigations into *Puma* expression and function in the *Ctcf*-null hindlimb would be needed to confirm this hypothesis.

My investigation into proliferation also confirmed results reported by Soshnikova *et al.* where *Ctcf* mutant forelimbs showed normal cell proliferation at E11.5[83]. The PCNA-stained hindlimbs at age E12.5 showed no differences in proliferation between control and *Ctcf*-null hindlimbs, as we expected. This finding also provides insight into the phenotypic differences between the developing forelimb and hindlimb in *Ctcf*^*Fl/Fl*^*;Prx1Cre* mice, suggesting that cell proliferation does not contribute to the differences witnessed, and that CTCF is not critical for regulating proliferation at this stage of development. It is important to note, however, that immunostaining analysis of proliferation is not as sensitive as detection of DNA synthesis with BrdU or EdU, and future experiments confirming proliferation using a thymidine analogue method would be appropriate.

During the mesenchymal condensation stage at E12.5 immediately preceding chondrogenic differentiation, CTCF does not appear to be important in regulating the onset of *Sox9* transcript expression or SOX9 protein localization. These data are in agreement with the absence of changes in levels of *Sox5* and *Sox6* transcripts between control and *Ctcf*-null mice at these time points. This finding was somewhat unexpected given our lab's data on CTCF binding to the *Sox9* locus and its critical role in maintaining *Sox9* expression in cartilage (Bush *et al.*, in prep.). Thus, the absence of changes in the expression of most other examined genes was not surprising, since most of them are regulated by SOX9. Our data suggest that CTCF plays different roles in the regulation of *Sox9* expression at different developmental stages; the molecular basis of this interesting phenomenon is unknown, but should be examined in the future. For such studies, it will be essential to determine how CTCF regulates DNA looping and epigenetic events (DNA methylation, histone modifications etc.) in the *Sox9* locus.

CTCF loss did not affect the expression of the critical cartilage ECM gene *Col2a1* at either E12.5 or E13.5 in the hindlimb bud, however *Acan* expression failed to increase in the mutant hindlimb at E13.5. Since *Sox9* does not appear affected in the mutants at this stage, these data suggest that CTCF regulates *Acan* expression through other mechanisms. Deletion of *Ctcf* leads to a disrupted growth plate with shorter resting and proliferative zones, as well as fewer hypertrophic chondrocytes. Interestingly, the shortened hypertrophic zone seen in *Ctcf^{Fl/Fl};Prx1Cre* mice is similar to the growth plates in humans with CCD, caused by haploinsufficiency of RUNX2[46]. Additionally, mutant tibiae fail to mineralize at E15.5, but have some mineralization by birth, although significantly less than controls. The mineralization defects suggest that CTCF may, in part, regulate cartilage mineralization in the long bones. Taken together, these results provide strong evidence for CTCF as a regulator of chondrocyte

differentiation and progression through the chondrocyte life cycle, perhaps through regulation of *Runx2*. These results also suggest a potential explanation for the short stature seen in human patients with heterozygous mutations in *CTCF*.

In contrast to long bone development, the skull is formed through intramembranous ossification. The murine skull is composed largely of parietal and frontal skull plates, which are derived from cephalic mesoderm and cranial neural crest cells, respectively. Here I show that CTCF is important for normal development of the cranial vault. The *Ctcf^{Fl/Fl};Prx1Cre* mice are born with large holes in their skull, and lack portions of each of the parietal, frontal, nasal, and interparietal calvariae, or skull plates. No previous studies have implicated CTCF in skull development or intramembranous ossification, thus the novelty of this result should be underscored. Interestingly, the poorly developed skull is remarkably similar to, but slightly less severe than that described for conditional knockout mice for transforming growth factor beta (TGFβ) reported by Seo and Serra in 2009. The *Tgfb2^{Fl/Fl};Prx1Cre* mice are also neonatal lethal and are born with an open skull. Their studies demonstrate that while slightly reduced proliferation in the developing skull vault may contribute to the phenotype, there is a significant down-regulation of both *Runx2* and *Osterix (OSX)* expression in the mutant embryos, suggesting altered osteoblast differentiation. Given the similarity of the phenotypes, one possibility is that CTCF may play a role in regulating *RUNX2*, *OSX*, or both, potentially through TGFβ, and future studies should consider investigating these factors.

It is also possible that CTCF function in tissues surrounding the developing skeleton contributes to the phenotype seen in the *Ctcf^{Fl/Fl};Prx1Cre* mice. Both paracrine or biomechanical mechanisms should be considered, and tendons are a potential candidate tissue to investigate further. The *Prx1* enhancer used to drive Cre expression in *Ctcf^{Fl/Fl};Prx1Cre* mice is expressed

in the tendons of the forelimb and hindlimb buds by E15.5[90]. CTCF function has not yet been investigated in tenogenic cells, yet it seems critical for all tissues in which it has been examined, therefore we speculate that the deficiency of CTCF in tendons could lead to chemical or physical force alterations, or both. Generation and analysis of a mouse with the conditional deletion of CTCF in tendons using a *Scleraxis* Cre driver would be a reasonable way to approach these postulations.

Finally, my studies suggest subtle differences in chondrogenesis between forelimbs and hindlimbs. It is well established that development proceeds from cranial to caudal; thus, a slight delay in development of the hindlimb is expected. However, my data also suggest some variances in the patterns of chondrogenic gene induction between the limbs. On the other hand, some of the experimental limitations discussed below resulted in large variability between trials, especially for the hindlimb; thus, further investigations are required to characterize the differences between forelimb and hindlimb.

4.3   Limitations of Research and Alternative Approaches

In the studies presented, an *in vitro* micromass culture system was utilized. This culture method allows investigators to examine chondrogenic tissue formation in a controlled environment without artificial materials and is well-established in the field of skeletal biology[88,89,93]. However, mesenchymal cells are pluripotent and can differentiate into other non-cartilaginous tissues, such as adipose tissue, muscle, and bone. Although previous studies in our lab demonstrated an increase in cartilage-specific markers and gene expression over time, in conjunction with a decrease in gene expression for markers of other cell types, the differentiation of these cells into chondrocytes is density-dependent. Cells on the periphery of these micromass cultures are subject to slightly different conditions, and therefore the potential exists for

additional cell types to be present within these cultures. This results in increased variability in gene expression analyses, which we did observe, especially in the hindlimb micromass cultures. Another cause of this variability is the exact time between fertilization and harvest of embryos that can vary from litter to litter (as discussed further below). This will particularly affect the hindlimb as it is developmentally delayed compared to the forelimb.

The *Ctcf^{Fl/Fl};Prx1Cre* mouse model used in these studies was originally published in 2010 by Soshnikova *et al*[83]. This mouse model involves the conditional loss of CTCF in early limb mesenchyme, prior to the onset of chondrogenesis. The *Prx1* Cre driver is well-established in the limb development field for examining limb-specific effects of a certain gene, however there are certain limitations to this mouse model use of this model[90,91]. First, *Prx1* is not as robustly expressed in the developing hindlimb as in the forelimb, and Cre expression is therefore considered "leaky". Because a number of cells escape Cre inactivation, there is still CTCF protein present in the mutant mouse hindlimb. The presence of any amount of CTCF is a confounding factor when considering results, particularly differences between the forelimb and hindlimb phenotype in these mice. Second, a mesenchyme-specific Cre driver leads to deletion of *Ctcf* in chondrogenic precursor cells, as well as progenitors for other cell types such as tendons and osteoblasts[90,91,94,95]. This consideration is important because of the large number of interactions between tissue types during development. Furthermore, the deletion of *Ctcf* in developing tissue and tissue surrounding the cartilage elements may contribute to the limb defects witnessed and the severity of the phenotype in *Ctcf^{Fl/Fl};Prx1* mice compared to *Ctcf^{Fl/Fl};Col2* mice with *Ctcf*-null cartilage. The loss of CTCF in multiple tissues therefore makes it difficult to pinpoint a specific role for the protein in one individual tissue. This model is, however, beneficial when examining a more global role for CTCF in a developing body part.

Third, *Prx1* expression is not just limited to the developing limb mesenchyme. *Ctcf* is therefore conditionally deleted in other tissues including the skull mesenchyme, forebrain, and developing heart valves. The loss of CTCF in multiple tissues leads to difficulty in discerning the cause for the neonatal lethality of the mutant mice.

Beyond limitations of the mouse model utilized, there are technical limitations to these studies as well. Mice were mated in a timed process, as described in methods, and all dissections took place at 10 am to reduce variability. However, timed matings do not guarantee that all embryos are the same age at the time of dissection. Both the time of mating and fertilization contributes to variability between embryonic age; therefore, although the hindlimb tissue taken from mutant and control mice for RNA isolation and gene expression analyses were assumed to be E12.5, there is some variability between litters. These studies would thus benefit from increasing the number of trials to ensure the studies have enough power. Additionally, the whole hindlimb bud was taken from mutant and control embryos, including the ectoderm, in which *Ctcf* was not deleted. Inclusion of the CTCF-rich ectoderm in the samples taken for qRT-PCR analyses may have confounded the results, and future studies should involve microdissection of just mesenchymal tissue. Another significant limitation to these studies involved mouse breeding issues. Although the colonies were closely monitored and taken care of in accordance with all animal breeding protocols at Western University, I encountered difficulty when breeding mice for experiments and was limited by the small number of litters containing both mutant and control animals. This lack of animals for use in experiments led to the decision of examining only E12.5, E15.5, and P0 animals. Although these three time points have led to a wealth of information on the role of CTCF in the developing hindlimb, examining additional time points is advisable to produce a more complete time course. Future studies should examine histology and

immunofluorescence at E13.5, and histology at E14.5, E16.5, and E17.5 to pinpoint the earliest onset of the phenotype, and when mineralization occurs in mutant tibiae.

Finally, my findings raised multiple interesting questions that should be followed up with additional experiments. First, previous studies in our lab have examined CTCF binding to genomic DNA in developing wild-type cartilage at E15.5. Performing RNA sequencing (RNA-seq) on cartilage from *Ctcf^{Fl/Fl};Prx1Cre* tibiae at E15.5 to detect key target genes would be an appropriate follow-up. Genes identified by RNA-seq as having altered transcription in *Ctcf*-null hindlimbs could then be compared to CTCF-binding in normal cartilage, and a list of target genes could be compiled. This experiment would help narrow the focus to the specific role of CTCF in developing cartilage. Once target genes have been identified, performing circularized chromosome conformation capture (4C) and chromosome conformation capture (3C) may be of interest to detect chromosomal interactions at target gene loci and provide more insight into the mechanism of CTCF-mediated gene regulation. Moreover, performing ChIP-seq for cohesin binding and other epigenetic markers (e.g. histone modifications) in the wild type and *Ctcf*-null hindlimb would provide mechanistic insights into how CTCF controls DNA looping and gene expression.

Additionally, my studies have shown growth plate abnormalities in *Ctcf*-null tibia, and a failure or delay of chondrocytes to become hypertrophic. Use of a *Ctcf^{Fl/Fl};Col10Cre* mouse line to conditionally delete CTCF in hypertrophic chondrocytes would undoubtedly provide more insight into this interesting phenotype and the role of CTCF in chondrocyte differentiation. Furthermore, evidence indicates the importance of CTCF in proper cartilage and long bone development, however both the *Ctcf^{Fl/Fl};Prx1Cre* and *Ctcf^{Fl/Fl};Col2Cre* mice are neonatal lethal. Using the tamoxifen-inducible *Ctcf^{Fl/Fl};Aggrecan-CreER(T2)* mouse model would allow the

depletion of CTCF in developing or adult cartilage at various time points. In particular, this mouse model would allow an investigation into the role of CTCF in adult cartilage and a potential role for CTCF in age-related cartilage diseases such as osteoarthritis. Finally, these studies have provided evidence for a role of CTCF in the developing skull. This result is novel and given the severity of the calvarial defects, an investigation into the role of CTCF in intramembranous ossification and specifically skull development is advised. These studies should include histology to examine proliferation and apoptosis in the developing skull vault, as well as investigation of osteoblast differentiation markers.

4.4   Significance

Human limb malformations are a type of congenital anomaly with a major burden on individuals, families and the public health system. The 2013 Congenital Anomalies in Canada Report by the Public Health Agency stated that Limb Deficiency Defects are characterized by total or partial absence of a limb, or a smaller portion, and occur in three to eight infants per 10,000 live births. Limb defects, however, are a heterogeneous group of malformations and limb development is a highly complex process that is not yet completely understood. Knowledge of the regulation of chondrogenesis and skeletal development in the hindlimb is critical for understanding both normal and pathological limb development. Particularly, elucidating the role of chromatin organizers such as CTCF will shed light on the regulation of key genes involved in chondrogenesis and help provide a more global understanding of severe chondrodysplasias. The studies in this thesis have underscored the importance of CTCF in proper hindlimb development and endochondral ossification, and provided insight into the phenotype seen in human patients with mutations in *CTCF*. My work suggests that CTCF is an important regulator of the cartilage

growth plate and proper mineralization of developing long bones, and is critical for preventing apoptosis in the developing limb. In conclusion, these studies have contributed valuable insights into chondrogenesis and hindlimb development, and may ultimately lead to improved detection and treatments of limb and skeletal malformations.

5.0 REFERENCES

1.   Lefebvre, V. & Bhattaram, P. Vertebrate skeletogenesis. *Curr. Top. Dev. Biol.* **90,** 291–317 (2010).

2.   Olsen, B. R., Reginato, A. M. & Wang, W. Bone Development. *Annu. Rev. Cell. Dev. Biol.* 191–220 (2000).

3.   Kronenberg, H. M. & Kronenberg, H. M. Developmental regulation of the growth plate. *Nature* **423,** 332–6 (2003).

4.   Jiang, X., Iseki, S., Maxson, R. E., Sucov, H. M. & Morriss-Kay, G. M. Tissue origins and interactions in the mammalian skull vault. *Dev. Biol.* **241,** 106–16 (2002).

5.   Gilbert, S. F. *Developmental Biology*. (2010).

6.   Solomon, L. A., Be, N. G. & Beier, F. Transcriptional Regulators of Chondrocyte Hypertrophy. **130,** 123–130 (2008).

7.   Deutsch, U., Dressler, G. R. & Gruss, P. Pax 1, a member of a paired box homologous murine gene family, is expressed in segmented structures during development. *Cell* **53,** 617–625 (1988).

8.   Cserjesi, P. *et al.* Scleraxis: a basic helix-loop-helix protein that prefigures skeletal formation during mouse embryogenesis. *Development* **121,** 1099–1110 (1995).

9.   Karaplis, A. C. *Principles of Bone Biology*. (2002).

10. Hall, B. K. & Miyake, T. All for one and one for all: Condensations and the initiation of skeletal development. *BioEssays* **22,** 138–147 (2000).

11. DeLise, a. M., Fischer, L. & Tuan, R. S. Cellular interactions and signaling in cartilage development. *Osteoarthr. Cartil.* **8,** 309–334 (2000).

12. Ballock, R. T. & O'Keefe, R. J. Physiology and pathophysiology of the growth plate. *Birth Defects Res. Part C - Embryo Today Rev.* **69,** 123–143 (2003).

13. Mori-Akiyama, Y., Akiyama, H., Rowitch, D. H. & de Crombrugghe, B. Sox9 is required for determination of the chondrogenic cell lineage in the cranial neural crest. *Proc. Natl. Acad. Sci. U. S. A.* **100,** 9360–5 (2003).

14. Smits, P. *et al.* The Transcription Factors L-Sox5 and Sox6 Are Essential for Cartilage Formation. *Dev. Cell* **1,** 277–290 (2001).

15. Smits, P., Dy, P., Mitra, S. & Lefebvre, V. Sox5 and Sox6 are needed to develop and maintain source, columnar, and hypertrophic chondrocytes in the cartilage growth plate. *J. Cell Biol.* **164,** 747–758 (2004).

16.   De Crombrugghe, B. *et al.* Transcriptional mechanisms of chondrocyte differentiation. *Matrix Biol.* **19,** 389–394 (2000).

17.   Akiyama, H., Chaboissier, M. C., Martin, J. F., Schedl, A. & De Crombrugghe, B. The transcription factor Sox9 has essential roles in successive steps of the chondrocyte differentiation pathway and is required for expression of Sox5 and Sox6. *Genes Dev.* **16,** 2813–2828 (2002).

18.   Beier, F. Cell-cycle control and the cartilage growth plate. *J. Cell. Physiol.* **202,** 1–8 (2005).

19.   Abad, V. *et al.* The role of the resting zone in growth plate chondrogenesis. *Endocrinology* **143,** 1851–1857 (2002).

20.   Hunziker, E. B. Mechanism of longitudinal bone growth and its regulation by growth plate chondrocytes. *Microsc. Res. Tech.* **15,** 505–19 (1994).

21.   St-Jacques, B., Hammerschmidt, M. & McMahon, a P. Indian hedgehog signaling regulates proliferation and differentiation of chondrocytes and is essential for bone formation. *Genes Dev.* **13,** 2072–2086 (1999).

22.   Koziel, L., Wuelling, M., Schneider, S. & Vortkamp, A. Gli3 acts as a repressor downstream of Ihh in regulating two distinct steps of chondrocyte differentiation. *Development* **132,** 5249–5260 (2005).

23.   Mak, K. K., Kronenberg, H. M., Chuang, P.-T., Mackem, S. & Yang, Y. Indian hedgehog signals independently of PTHrP to promote chondrocyte hypertrophy. *Development* **135,** 1947–1956 (2008).

24.   Hojo, H., Ohba, S., Yano, F. & Chung, U. Il. Coordination of chondrogenesis and osteogenesis by hypertrophic chondrocytes in endochondral bone development. *J. Bone Miner. Metab.* **28,** 489–502 (2010).

25.   Inada, M. *et al.* Critical roles for collagenase-3 (Mmp13) in development of growth plate cartilage and in endochondral ossification. *Proc. Natl. Acad. Sci. U. S. A.* **101,** 17192–17197 (2004).

26.   Stickens, D. *et al.* Altered endochondral bone development in matrix metalloproteinase 13-deficient mice. *Development* **131,** 5883–5895 (2004).

27.   Lin, E. a. & Liu, C. J. The role of ADAMTSs in arthritis. *Protein Cell* **1,** 33–47 (2010).

28.   Caplan, A. I. & Pechak, D. G. in *Bone and Mineral Research* 117–183 (Elsevier, 1987).

29.   Pest, M. a & Beier, F. Developmental biology: Is there such a thing as a cartilage-specific knockout mouse? *Nat. Rev. Rheumatol.* 1–2 (2014). doi:10.1038/nrrheum.2014.168

30. Gerber, H. P. *et al.* VEGF couples hypertrophic cartilage remodeling, ossification and angiogenesis during endochondral bone formation. *Nat. Med.* **5,** 623–628 (1999).

31. Lefebvre, V., Li, P. & De Crombrugghe, B. A new long form of Sox5 (L-Sox5), Sox6 and Sox9 are coexpressed in chondrogenesis and cooperatively activate the type II collagen gene. *EMBO J.* **17,** 5718–5733 (1998).

32. Bi, W., Deng, J. M., Zhang, Z., Behringer, R. R. & de Crombrugghe, B. Sox9 is required for cartilage formation. *Nat. Genet.* **22,** 85–89 (1999).

33. Gordon, C. T. *et al.* Long-range regulation at the SOX9 locus in development and disease. *J. Med. Genet.* **46,** 649–56 (2009).

34. Wagner, T. *et al.* Autosomal Sex Reversal and Campomelic Dysplasia Are Caused by Mutations and around the SRY-Related Gene SOX9. **79,** (1994).

35. Yao, B. *et al.* The SOX9 upstream region prone to chromosomal aberrations causing campomelic dysplasia contains multiple cartilage enhancers. *Nucleic Acids Res.* **43,** 5394–5408 (2015).

36. Ducy, P., Zhang, R., Geoffroy, V., Ridall, a L. & Karsenty, G. Osf2/Cbfa1: a transcriptional activator of osteoblast differentiation. *Cell* **89,** 747–754 (1997).

37. Komori, T. *et al.* Targeted disruption of Cbfa1 results in a complete lack of bone formation owing to maturational arrest of osteoblasts. *Cell* **89,** 755–764 (1997).

38. Zhang, P. *et al.* Altered cell differentiation and proliferation in mice lacking p57KIP2 indicates a role in Beckwith-Wiedemann syndrome. *Nature* **387,** 151–158 (1997).

39. Rousseau, F., Bonaventure, J. & Legeai-Mallet, L. Mutations in the gene encoding fibroblast growth factor receptor-3 in achondroplasia. *Nature* (1994). at <http://www.nature.com/nature/journal/v371/n6494/abs/371252a0.html>

40. Jain, V. & Sen, B. Campomelic dysplasia. *J. Pediatr. Orthop. B* **23,** 485–8 (2014).

41. Kwok, C. *et al.* Mutations in SOX9, the gene responsible for Campomelic dysplasia and autosomal sex reversal. *Am. J. Hum. Genet.* **57,** 1028–1036 (1995).

42. Wagner, T. *et al.* Autosomal sex reversal and campomelic dysplasia are caused by mutations in and around the SRY-related gene SOX9. *Cell* **79,** 1111–1120 (1994).

43. Mansour, S., Hall, C. M., Pembrey, M. E. & Young, I. D. Original articles A clinical and genetic study of campomelic dysplasia. 415–420 (1995).

44. Yap, S. P. *et al.* Generation of mice with a novel conditional null allele of the Sox9 gene. *Biotechnol. Lett.* **33,** 1551–8 (2011).

45.   Warman, M. L. *et al.* A type X collagen mutation causes Schmid metaphyseal chondrodysplasia. *Nat. Genet.* **5,** 79–82 (1993).

46.   Zheng, Q. *et al.* Dysregulation of chondrogenesis in human cleidocranial dysplasia. *Am. J. Hum. Genet.* **77,** 305–312 (2005).

47.   Phillips, J. E. & Corces, V. G. CTCF: master weaver of the genome. *Cell* **137,** 1194–211 (2009).

48.   Bacher, C. P. *et al.* Transient colocalization of X-inactivation centres accompanies the initiation of X inactivation. *Nat. Cell Biol.* **8,** 293–299 (2006).

49.   Apostolou, E. & Thanos, D. Virus Infection Induces NF-??B-Dependent Interchromosomal Associations Mediating Monoallelic IFN-?? Gene Expression. *Cell* **134,** 85–96 (2008).

50.   Spilianakis, C. G., Lalioti, M. D., Town, T., Lee, G. R. & Flavell, R. a. Interchromosomal associations between alternatively expressed loci. *Nature* **435,** 637–645 (2005).

51.   Johannes, S., Holwerda, B. & Laat, W. De. their chromatin loops CTCF : the protein , the binding partners , the binding sites and their chromatin loops. (2013).

52.   Lobanenkov, V. V *et al.* A novel sequence-specific DNA binding protein which interacts with three regularly spaced direct repeats of the CCCTC-motif in the 5'-flanking sequence of the chicken c-myc gene. *Oncogene* **5,** 1743–1753 (1990).

53.   Lobanenkov, V. V, Adler, V. V, Klenova, E. M., Nicolas, R. H. & Goodwin, G. H. *Gene regulation and AIDS: transcriptional activation, retroviruses and pathogenesis.* (Portfolio Publishing Corporation, 1989).

54.   Klenova, E. M. *et al.* CTCF , a Conserved Nuclear Factor Required for Optimal Transcriptional Activity of the Chicken c-myc Gene , Is an 11-Zn-Finger Protein Differentially Expressed in Multiple Forms. **13,** 7612–7624 (1993).

55.   Filippova, G. N. *et al.* An exceptionally conserved transcriptional repressor, CTCF, employs different combinations of zinc fingers to bind diverged promoter sequences of avian and mammalian c-myc oncogenes. *Mol. Cell. Biol.* **16,** 2802–2813 (1996).

56.   Heger, P., Marin, B., Bartkuhn, M., Schierenberg, E. & Wiehe, T. The chromatin insulator CTCF and the emergence of metazoan diversity. *Proc. Natl. Acad. Sci.* **109,** 17507–17512 (2012).

57.   Klenova, E. M. *et al.* Functional phosphorylation sites in the C-terminal region of the multivalent multifunctional transcriptional factor CTCF. *Mol. Cell. Biol.* **21,** 2221–2234 (2001).

58.   El-Kady, A. & Klenova, E. Regulation of the transcription factor, CTCF, by phosphorylation with protein kinase CK2. *FEBS Lett.* **579,** 1424–1434 (2005).

59.   Yu, W. *et al.* Poly(ADP-ribosyl)ation regulates CTCF-dependent chromatin insulation. *Nat. Genet.* **36,** 1105–1110 (2004).

60.   Witcher, M. & Emerson, B. M. Epigenetic Silencing of the p16INK4a Tumor Suppressor Is Associated with Loss of CTCF Binding and a Chromatin Boundary. *Mol. Cell* **34,** 271–284 (2009).

61.   MacPherson, M. J., Beatty, L. G., Zhou, W., Du, M. & Sadowski, P. D. The CTCF insulator protein is posttranslationally modified by SUMO. *Mol. Cell. Biol.* **29,** 714–725 (2009).

62.   Wang, H. *et al.* Widespread plasticity in CTCF occupancy linked to DNA methylation. *Genome Res.* **22,** 1680–1688 (2012).

63.   Murrell, A., Heeson, S. & Reik, W. Interaction between differentially methylated regions partitions the imprinted genes Igf2 and H19 into parent-specific chromatin loops. *Nat. Genet.* **36,** 889–93 (2004).

64.   Guastafierro, T. *et al.* CCCTC-binding factor activates PARP-1 affecting DNA methylation machinery. *J. Biol. Chem.* **283,** 21873–21880 (2008).

65.   Nasmyth, K. & Haering, C. H. Cohesin: its roles and mechanisms. *Annu. Rev. Genet.* **43,** 525–558 (2009).

66.   Hadjur, S. *et al.* Cohesins form chromosomal cis-interactions at the developmentally regulated IFNG locus. *Nature* **460,** 410–413 (2009).

67.   Hou, C., Dale, R. & Dean, A. Cell type speci fi city of chromatin organization mediated by CTCF and cohesin. **107,** 3651–3656 (2010).

68.   Nativio, R. *et al.* Cohesin is required for higher-order chromatin conformation at the imprinted IGF2-H19 locus. *PLoS Genet.* **5,** (2009).

69.   Gosalia, N., Neems, D., Kerschner, J. L., Kosak, S. T. & Harris, A. Architectural proteins CTCF and cohesin have distinct roles in modulating the higher order structure and expression of the CFTR locus. *Nucleic Acids Res.* **42,** 1–11 (2014).

70.   Wendt, K. S. *et al.* Cohesin mediates transcriptional insulation by CCCTC-binding factor. *Nature* **451,** 796–801 (2008).

71.   Yao, H. *et al.* Mediation of CTCF transcriptional insulation by DEAD-box RNA-binding protein p68 and steroid receptor RNA activator SRA. *Genes Dev.* **24,** 2543–2555 (2010).

72. Chen, H., Tian, Y., Shu, W., Bo, X. & Wang, S. Comprehensive identification and annotation of cell type-specific and ubiquitous CTCF-binding sites in the human genome. *PLoS One* **7,** (2012).

73. Schmidt, D. *et al.* Waves of retrotransposon expansion remodel genome organization and CTCF binding in multiple mammalian lineages. *Cell* **148,** 335–348 (2012).

74. Chen, X. *et al.* Integration of External Signaling Pathways with the Core Transcriptional Network in Embryonic Stem Cells. *Cell* **133,** 1106–1117 (2008).

75. Ong, C.-T. & Corces, V. G. CTCF: an architectural protein bridging genome topology and function. *Nat. Rev. Genet.* **15,** 234–46 (2014).

76. Heath, H. *et al.* CTCF regulates cell cycle progression of alphabeta T cells in the thymus. *EMBO J.* **27,** 2839–50 (2008).

77. Chung, J. H., Bell, a C. & Felsenfeld, G. Characterization of the chicken beta-globin insulator. *Proc. Natl. Acad. Sci. U. S. A.* **94,** 575–580 (1997).

78. Splinter, E. *et al.* CTCF mediates long-range chromatin looping and local histone modification in the beta-globin locus. *Genes Dev.* **20,** 2349–54 (2006).

79. Vostrov, a a & Quitschke, W. W. The zinc finger protein CTCF binds to the APBbeta domain of the amyloid beta-protein precursor promoter. Evidence for a role in transcriptional activation. *J. Biol. Chem.* **272,** 33353–33359 (1997).

80. Ferraiuolo, M. a. *et al.* The three-dimensional architecture of Hox cluster silencing. *Nucleic Acids Res.* **38,** 7472–7484 (2010).

81. Narendra, V. *et al.* Transcription. CTCF establishes discrete functional chromatin domains at the Hox clusters during differentiation. *Science* **347,** 1017–21 (2015).

82. Kim, T. H. *et al.* Analysis of the Vertebrate Insulator Protein CTCF-Binding Sites in the Human Genome. *Cell* **128,** 1231–1245 (2007).

83. Soshnikova, N., Montavon, T., Leleu, M., Galjart, N. & Duboule, D. Functional analysis of CTCF during mammalian limb development. *Dev. Cell* **19,** 819–30 (2010).

84. Watson, L. A. *et al.* Dual Effect of CTCF Loss on Neuroprogenitor Differentiation and Survival. *J. Neurosci.* **34,** 2860–70 (2014).

85. Schaub, M. a, Boyle, A. P., Kundaje, A. & Frazer, K. a. Linking disease associations with regulatory information in the human genome Toward mapping the biology of the genome. 1748–1759 (2012). doi:10.1101/gr.136127.111

86. Gregor, A. *et al.* De novo mutations in the genome organizer CTCF cause intellectual disability. *Am. J. Hum. Genet.* **93,** 124–31 (2013).

87. Barbero, J. L. Genetic basis of cohesinopathies. *Appl. Clin. Genet.* **6,** 15–23 (2013).

88. Ahrens, P. B., Solursh, M. & Reiter, R. S. Stage-related capacity for limb chondrogenesis in cell culture. *Dev. Biol.* **60,** 69–82 (1977).

89. Stanton, L.-A., Sabari, S., Sampaio, A. V, Underhill, T. M. & Beier, F. p38 MAP kinase signalling is required for hypertrophic chondrocyte differentiation. *Biochem. J.* **378,** 53–62 (2004).

90. Martin, J. F. & Olson, E. N. Identification of a prx1 limb enhancer. *Genesis* **26,** 225–9 (2000).

91. Logan, M. *et al.* Expression of Cre Recombinase in the developing mouse limb bud driven by a Prxl enhancer. *Genesis* **33,** 77–80 (2002).

92. Gomes, N. P. & Espinosa, J. M. Gene-specific repression of the p53 target gene PUMA via intragenic CTCF-Cohesin binding. *Genes Dev.* **24,** 1022–34 (2010).

93. De Lise, A. M., Stringa, E., Woodward, W. A., Mello, M. A. & Tuan, R. S. in *Developmental Biology Protocols, Volume III* 359–375 (2000).

94. Leussinka, B. *et al.* Expression patterns of the paired-related homeobox genes MHoxlPrxl and WPrx2 suggest roles in development of the heart and the forebrain. **52,** (1995).

95. Martin, J. F., Bradley, a & Olson, E. N. The paired-like homeo box gene MHox is required for early events of skeletogenesis in multiple lineages. *Genes Dev.* **9,** 1237–1249 (1995).

APPENDIX

Animal Use Protocol

Western

2007-045-06::7:

AUP Number: 2007-045-06

AUP Title: Regulation of Endochondral Bone Growth by Hormones

Yearly Renewal Date: 08/01/2014

The YEARLY RENEWAL to Animal Use Protocol (AUP) 2007-045-06 has been approved, and will be approved for one year following the above review date.

1. This AUP number must be indicated when ordering animals for this project.
2. Animals for other projects may not be ordered under this AUP number.
3. Purchases of animals other than through this system must be cleared through the ACVS office.
   Health certificates will be required.

REQUIREMENTS/COMMENTS

Please ensure that individual(s) performing procedures on live animals, as described in this protocol, are familiar with the contents of this document.

The holder of this Animal Use Protocol is responsible to ensure that all associated safety components (biosafety, radiation safety, general laboratory safety) comply with institutional safety standards and have received all necessary approvals. Please consult directly with your institutional safety officers.

Submitted by: Kinchlea, Will D

on behalf of the Animal Use Subcommittee

CURRICULUM VITAE

Katherine Lee Rabicki

UNIVERSITY EDUCATION

2013-2015	MSc Candidate in Physiology & Pharmacology
	Collaborative Program in Developmental Biology
	Dr. Frank Beier's Laboratory
	Co-Supervised by Dr. Nathalie Bérubé
	Schulich School of Medicine & Dentistry
	Western University
	London, Ontario
2009-2013	BSc Biology, Honours Specialization in Genetics
	Western University
	London, Ontario

TEACHING & SUPERVISORY EXPERIENCE

2014	Lecturer for Cardiac Physiology Unit
	First Year Human Physiology - Physiology 1021
	Department of Physiology & Pharmacology
	Western University
2013-2015	Teaching Assistant
	Second Year Human Physiology - Physiology 2130
	Department of Physiology & Pharmacology
	Western University
2013-2014	Co-Supervised 4th-Year Honours Thesis Student, Beier Laboratory
	"The role of DOT1L, a histone methyltransferase, in chondrogenesis"
	Departments of Physiology & Pharmacology, and Biology
	Western University

HONOURS, SCHOLARSHIPS & AWARDS

2015	Teaching Assistant Award
	Society of Graduate Students, PSAC 610
	Western University
	$500
2015	Best Poster Award
	London Health Research Day
	London, Ontario, Canada
	$500

2014-2015	Ontario Graduate Scholarship Western University *$15000*
2014	George W. Stavraky Teaching Scholarship Department of Physiology & Pharmacology Western University *$1000*
2014	Teaching Assistant Award Society of Graduate Students, PSAC 610 Western University *$500*
2013-2015	Western Graduate Research Scholarship Department of Physiology & Pharmacology Western University *$9000*
2013	Best Thesis Presentation Department of Biology Western University *$50*
2011-2013	Dean's Honour List Western University
2012	Educational Grant The Davey Tree Expert Company *$1000*
2009	Western Scholarship of Excellence Western University *$2000*
2009	Queen Elizabeth II Aiming for the Top Scholarship Ontario Student Assistance Program *$3500*
2009	Optimist Club Scholarship Optimist Club of Waterdown *$1000*

CONFERENCES & MEETINGS

1. Developmental Biology Research Day
Western University, June 5th, 2015
"The Chromatin Organizer CTCF is Necessary for Hindlimb Development"
Oral Presentation

2. Department of Paediatrics Research Day
London, Ontario, May 27th, 2015
"The Chromatin Organizer CTCF is Necessary for Hindlimb Development"
Poster Presentation

3. Annual Bone and Joint Retreat
London, Ontario, May 6th, 2015
"The Chromatin Organizer CTCF is Necessary for Hindlimb Development"
Poster Presentation

4. London Health Research Day
London, Ontario, April 1st, 2015
"The Chromatin Organizer CTCF is Necessary for Hindlimb Development"
Poster Presentation *Award Winner*

5. Canadian Conference on Epigenetics: Epigenetics, Eh!
London, Ontario, June 24-27, 2014
"CTCF is Necessary for Hindlimb Development"
Poster Presentation

6. Canadian Connective Tissue Conference
London, Ontario, June 8-10, 2014
"CTCF is Necessary for Hindlimb Development"
Poster Presentation

7. Developmental Biology Research Day
Western University, May 30th, 2014
"CTCF is Necessary for Hindlimb Development"
Poster Presentation

8. Canadian Developmental Biology Conference
Mont Tremblant, Quebec, March 17-20, 2014
"CTCF is Necessary for Hindlimb Development"
Poster Presentation

9. Bone and Joint Injury and Repair Conference
London, Ontario, January 16-17, 2014
"CTCF is Necessary for Hindlimb Development"
Oral Presentation

10. Physiology & Pharmacology Research Day
        Western University, November 4th, 2014
        "CTCF is Necessary for Hindlimb Development"
        Poster Presentation

11. Ontario Biology Day
        Hamilton, Ontario, March 16-17, 2013
        "CTCF in Chondrocyte Differentiation"
        Oral Presentation